UNIVERSIDADE
BEIRA INTERIOR

Validation of LoggerOne system's 5-lead ECG

Versão final após defesa

Lisana Moniz de Sousa Daniel

Dissertação para obtenção do Grau de Mestre em
Bioengenharia
(2º ciclo de estudos)

Orientador: Prof. Doutor Nuno Manuel Garcia dos Santos
Co-orientadora: Prof.ª Doutora Virginie dos Santos Felizardo

Dezembro de 2023.

Declaração de Integridade

Eu, Lisana Moniz de Sousa Daniel, que abaixo assino, estudante com o número de inscrição M11819 de Bioengenharia da Faculdade de Engenharia, declaro ter desenvolvido o presente trabalho e elaborado o presente texto em total consonância com o **Código de Integridades da Universidade da Beira Interior**.

Mais concretamente afirmo não ter incorrido em qualquer das variedades de Fraude Académica, e que aqui declaro conhecer, que em particular atendi à exigida referenciação de frases, extratos, imagens e outras formas de trabalho intelectual, e assumindo assim na íntegra as responsabilidades da autoria.

Universidade da Beira Interior, Covilhã 11 /12 /2023

Dedication

Ao Midas.

Acknowledgements

Quero agradecer ao meu orientador e à minha coorientadora, ao Professor Doutor Nuno Garcia, Faculdade de Ciências da Universidade de Lisboa e à Doutora Virginie Felizardo, Universidade da Beira interior. Agradeço todo o apoio e disponibilidade prestado ao longo destes dois anos. Obrigada pela ajuda a superar muitos do obstáculos com que me deparei durante esta dissertação.

Agradeço também à equipa da Dynasys que me prestou apoio durante o desenvolvimento do trabalho. Agradeço também o empréstimo do equipamento usado.

Agradeço ao CHUCB pelo empréstimo do equipamento usado assim como pelo apoio e disponibilidade em fornecer um espaço onde pude trabalhar.

Agradeço aos meus pais e aos meus irmãos por todo o apoio que me deram durante a minha vida até agora e pelo apoio que sei que ainda vou ter no futuro. A pessoa que foi capaz de escrever este trabalho foi criada por vocês e ao vosso lado.

Agradeço também ao meu primo David que me convenceu a sair para relaxar sempre que precisei, mas que também compreendeu e respeitou quando eu não podia.

Agradeço aos meus amigos, aos da minha terra e aos da minha terra honorária, com quem partilhei desgostos e vitórias.

Por último, mas não menos importante agradeço à Sara, na tua presença consigo verdadeiramente descansar.

Resumo

Estudos de validação tornam-se cada vez mais importantes com os avanços na tecnologia e o aumento considerativo de *wearables* para eletrocardiografia (ECG). No entanto, os estudos de validação existentes são limitados ao objetivo de validação do estudo em questão. Normalmente, poucos parâmetros do ECG são analisados e o métodos utilizados não são normalizados. O objetivo principal desta dissertação é o desenvolvimento de uma metodologia que possa ser aplicada a uma grande variedade de estudos de validação. Para efeito, o dispositivo LoggerOne vai ser comparado com um dispositivo já validado, o sistema COMEN.

Sinais de ECG de um simulador vão ser adquiridos simultaneamente pelos dois dispositivos em questão. O simulador usado tem marcação CE e permite a simulação de sinais tanto pediátricos como de adultos, para além disso, permite ainda simular diferentes tipos de arritmias. Os sinais adquiridos vão ser processados com o apoio de diversas bibliotecas para Python que permitem a manipulação dos dados recolhidos para análise. Antes do processo de validação, os sinais dos dois dispositivos vão ser normalizados e vários conjuntos de filtros e algoritmos vão ser testados. Os algoritmos otimizados vão então ser aplicados para extraír intervalos e segmentos relevantes tais como: as ondas P e T, o complexo QRS, os intervalos RR, PR, ST e QT, e os segmentos ST e PR. Para a validação, estes intervalos e segmentos vão ser comparados através do uso de diferentes métodos estatísticos tais como, *Bland-Altman limits of agreement* (LoA), *intraclass correlation coefficient* (ICC) e através de uma comparação morfológica dos sinais.

Os resultados do trabalho desenvolvido dividem-se em duas componentes: resultados da otimização de algoritmos e resultados da validação. Em relação aos resultados dos algoritmos, apenas algumas derivações apresentaram pontos da onda P e T *onsets* com valores abaixo de 95% de sensibilidade (Se) e valor preditivo positivo (+P), enquanto a maioria dos resultados apresenta valores acima de 98%. Os valores do desvio padrão (SD) para P *onset*, P *offset* e QRS *onset* excederam os valores de referência em algumas derivações, ao contrário dos restantes valores que permaneceram dentro dos valores de referência. Adicionalmente, os valores da média permaneceram abaixo do valor de referência estipulado. Em relação aos resultados de validação, quase todos os resultados para cada derivação apresentam boa concordância e confiabilidade, exceto para intervalos e segmentos calculados usando o T *onset*.

Palavras-chave

ECG; 5 derivações; Validação; Processamento de sinal; Extração de características de ECG.

Resumo Alargado

0.1 Introdução

Neste capítulo faz-se uma introdução ao tema da dissertação. É apresentada contextualização e motivação da dissertação assim como as contribuições do trabalho. Por fim, dá-se a conhecer a organização da dissertação que se divide em:

- Introdução;
- Estado da arte onde se resume o ECG, as técnicas de segmentação de ECG e as técnicas de validação utilizadas para dispositivos de ECG;
- Métodos usados para a segmentação do ECG e para a validação;
- Conclusão do trabalho realizado e possíveis trabalhos futuros.

0.2 Estado da arte

O estado da arte feito aborda os 3 temas relevantes à dissertação: ECG, processamento de ECG, e validação de ECG.

Na primeira secção, é explicado que um ECG é um sinal que representa o potencial elétrico do coração. Adicionalmente, são explicadas as características de um sinal de ECG normal e indicados os intervalos e segmentos pelos quais um ECG é composto. Estes são: Onda P, complexo QRS, onda T, onda U, segmento PR ou PQ segmento, intervalo PR ou PQ, segmento ST, intervalo ST, e intervalo QT. Por fim, é também explicada a recolha de sinais ECG, ou seja, como se aplicam os elétrodos, e como são calculadas as 12 derivações de um ECG.

Na segunda secção explica-se como se procede o processamento de sinal de um ECG, começando por explicar os passos necessários durante o pré-processamento. Explica-se os diversos tipos de ruído existentes e que técnicas para remover esses ruídos existem na literatura. Menciona-se a importância da normalização do sinal e é mostrada uma das técnicas usadas na literatura. Após o pré-processamento fala-se nas diversas técnicas de extração de características de um ECG. Neste caso, aborda-se a extração de características relativas aos intervalos e segmentos do ECG, ou seja, os pontos fiduciais. Por fim, são abordadas a formas de avaliação da performance de algoritmos de segmentação de ECG e os *standards* utilizados nessa avaliação.

Na última secção abordam-se as técnicas de validação usadas em dispositivos de ECG. Como contexto, são apresentadas as definições de correlação, concordância e confiabil-

idade, assim como a relevância destas em termos de validação. No final apresenta-se um pequeno estudo de literatura onde é feita uma revisão a diferentes metodologias usadas na validação. Para isso, consideram-se fatores como: dispositivos usados, população, condições do exame, características comparadas e respetivos métodos de extração e métodos de validação usados.

0.3 Métodos

Neste capítulo são descritos os métodos usados tanto para a extração dos pontos fiduciais como também os métodos usados na validação. Para a extração dos pontos fiduciais foram usadas bibliotecas de *Python* para o processamento dos sinais e também para a validação dos dados adquiridos.

No desenvolvimento dos algoritmos a ser utilizados na segunda parte do trabalho foram usados sinais de uma base de dados online. Esta base de dados contém sinais de ECGs de 12 derivações e as respetivas localizações dos pontos fiduciais. Os algoritmos *R peak*, *Peak* e *DWT* da biblioteca Neurokit2 foram utilizados em conjunto com diversos filtros fornecidos pela mesma biblioteca. Na necessidade de melhorar os resultados obtidos, foi feita uma modificação aos algoritmos disponibilizados pela biblioteca e foram testados filtros *Butterworth* considerando passa bandas com um *low-cut* de 0.5 Hz e um *high-cut* que varia entre 16 Hz e 35 Hz, com ordens entre 1 e 80. Na avaliação da performance dos algoritmos usados aplicaram-se vários parâmetros tais como sensibilidade (Se), valor preditivo positivo (+P), média e desvio padrão (SD). Para a média definiu-se um valor absoluto de 15 ms como o máximo aceitável, já para o SD foram considerados os *standards* da *Common Standards in Quantitative Electrocardiography work party* para definir limites aceitáveis.

A validação do dispositivo LoggerOne é feita comparando-o com o dispositivo COMEN. A recolha dos sinais é realizada a 500 Hz e em simultâneo, com recurso a um simulador de sinais ECG com marcação CE. Este simulador permite simular sinais pediátricos, de adultos e sinais com arritmias. Antes da aplicação dos algoritmos desenvolvidos para a localização dos pontos fiduciais, os sinais de ambos os dispositivos são normalizados. Depois dos pontos serem localizados, os intervalos e segmentos que compõe um ECG são calculados. A primeira fase de validação é feita comparando os segmentos e intervalos de cada dispositivo através de métodos estatísticos como LoA e ICC. No final, é feita uma avaliação morfológica onde os sinais de cada derivação são segmentados em batimentos e é calculado o SD. Antes desta análise é necessário alisar os sinais utilizando um filtro *Savitzky-Golay*.

0.4 Resultados e discussão

Este capítulo divide-se em duas partes, sendo que na primeira parte são discutidos os resultados do desenvolvimento dos algoritmos e na segunda os resultados da validação.

De forma a perceber o comportamento dos diferentes algoritmos disponibilizados pela biblioteca utilizada foram feitos testes preliminares na primeira derivação. Estes testes revelaram que dos 3 algoritmos utilizados, *Peak*, *CWT* e *DWT*, apenas os algoritmos *Peak* e *DWT* são viáveis. No entanto, como o algoritmo *Peak* não localiza todos os pontos fiduciais do ECG e o algoritmo DWT não alcançou uma performance aceitável, foi feita uma modificação a estes algoritmos. Na modificação localizam-se os picos P e T com o algoritmo *Peak* que, posteriormente, são fornecidos ao algoritmo *DWT* para encontrar os pontos que o método anterior não consegue. Assim, o algoritmo *DWT-Peak* foi desenvolvido, superando as limitações de usar um ou outro algoritmo em separado.

Após os primeiros testes, os algoritmos Peak e DWT-Peak foram aplicados com os diferentes filtros fornecidos pela biblioteca usada. Nos resultados obtidos, apenas os picos P, T e R e o *offset* da onda T apresentaram resultados aceitáveis. De forma a melhorar este resultado testou-se outro conjunto de filtros:

- Para as ondas P e T foram testados filtros *Butterworth* com passas bandas de 0.5-10 Hz e 0.5-20 Hz com ordens entre 1 e 4;
- Para o complexo QRS foram testados filtros *Butterworth* passa banda com um *low-cut* de 0.5 e um *high-cut* entre 16 e 35 Hz com ordens de 5 a 80.

Nos resultados obtidos verificou-se que para as ondas P filtros com uma passa banda de 0.5-20 Hz têm melhor performance, já na onda T, consoante a derivação em questão, filtros tanto com uma passa banda de 0.5-10 Hz como com uma passa banda de 0.5-20 Hz resultam numa boa performance dos algoritmos. Quanto às melhores ordens para estes filtros, filtros de primeira e segunda ordem foram os que revelaram melhores resultados para ambas as ondas. Nos resultados obtidos para o complexo QRS verificou-se que as melhores passa bandas variam bastante consoante a derivação e o ponto fiducial em questão. No geral, os melhores *high-cuts* encontram-se entre 17 e 27 Hz. No que toca à ordem, filtros de maior ordem (30 ou superior) obtêm melhor performance.

Analisando todos os resultados, apenas o *onset* da onda P nas derivações I, II, V1, V2 e V3 e o *offset* da onda P e o *onset* do complexo QRS nas derivações V1 e V2 excedem os limites definidos anteriormente. Ainda mais, de todas as derivações a V1 é a que apresenta pior performance, no entanto, isto deve-se provavelmente ao número reduzido de sinais usados nessa derivação. Adicionalmente, apesar de não haver um *standard* de limite de SD para o *onset* da onda T, observando a média e a aplicação dos algoritmos aos sinais do simulador reparou-se que estes resultados não são ideais. Apesar de a média se encontrar dentro dos limites estipulados, nota-se que para médias absolutas superiores a 5 ms a

prestação dos algoritmos piora e que para médias superiores a 10 ms, esses resultados são ainda mais notáveis.

De forma a fazer uma pré-análise aos resultados de validação e de identificar possíveis erros de extração, analisaram-se *scatter plots* dos intervalos obtidos de ambos dispositivos. Nesta análise verificou-se que, como esperado, os resultados obtidos estão dependentes da performance dos algoritmos, assim os intervalos que são calculados utilizando o *onset* da onda T apresentam gráficos mais dispersos.

Numa seguinte análise aplicaram-se os métodos LoA e ICC. Destes, o método LoA confirmou o mesmo que as *scatter plots* já tinham confirmado, mais especificamente, todos os intervalos e segmentos que não são calculados com o *onset* da onda T apresentam boa concordância. Quanto ao segundo método, os resultados das ondas P e T e do intervalo QT não estão em concordância com a análise anterior. Em primeiro lugar, o intervalo da onda P apresenta pior concordância do que o intervalo da onda T. Já o intervalo QT apenas apresenta excelente confiabilidade na derivação I quando, segundo os resultados anteriores, seria de esperar que apresentasse excelente confiabilidade em todas as derivações. Depois de estudar estes resultados verificou-se que se devem a uma limitação do método ICC. Este método depende da variedade dos dados utilizados e os intervalos P e os intervalos QT nas derivações II, V1, V2, V3, V4, V5 e V6 apresentam uma variedade limitada de intervalos, enquanto os intervalos da onda T e o intervalo QT na primeira derivação apresentam gamas mais lagas de intervalos.

Por fim, os resultados obtidos durante a avaliação morfológica mostram que o SD entre ambos os dispositivos é baixo(<0.02), no entanto, estes resultados acrescentam pouco à validação.

Analisando todos os resultados obtidos verificaram-se 4 fatores relevantes:

- A validação de um dispositivo de ECG vai estar dependente dos algoritmos utilizados;
- Scatter plots e LoA plots são bons médotos para avaliar a prestação do dispositivo a ser validado, no entanto, não há standards delineados para a validação de ECG utilizando estes métodos;
- O método ICC deve ser utilizado com caução, analisando a variedade dos dados testados;
- A análise morfológica não acrescenta muito ao que ja se tive verificado com as análises anteriores.

0.5 Conclusão e Trabalho futuro

Neste trabalho não só foram desenvolvidas e estudadas metodologias de segmentação de ECG como também foi feita a validação de um dispositivo de ECG. Os algoritmos desenvolvidos apresentam bons resultados de uma forma geral, exceto para a derivação V1. No entanto, os resultados da extração dos pontos da onda P e do *onset* da onda T ainda têm de ser otimizados. No que toca aos valores de referência utilizados, o valor da média deve ser reduzido em avaliações futuras.

Quanto aos resultados da validação, estes estão altamente dependentes dos algoritmos utilizados na extração dos pontos fiduciais. As falhas na performance dos algoritmos influenciaram os resultados de validação, sendo que os intervalos que são calculados com a *onset* da onda T (segmento ST e onda T) revelaram resultados ambíguos. Adicionalmente, os métodos utilizados apresentam limitações. Quando ao método LoA, não há *standards* definidos para o que são considerados limites de concordância bons na validação de ECG. Por outro lado, o método ICC apresenta guidelines que distinguem bons de maus resultados de confiabilidade, no entanto, estes resultados ficam dependentes da variedade da gama de intervalos utilizados. Por fim, a avaliação morfológica não adicionou mais informação à já obtida.

Concluindo, o trabalho desenvolvido não pode garantir que o dispositivo em questão está validado devido a 2 razões: os algoritmos utilizados não estão validados e os sinais utilizados não são de pacientes reais. No entanto, o objetivo deste trabalho é fazer apenas uma primeira validação deste dispositivo de forma a perceber se esta pronto para uma validação clínica. Tendo em conta este objetivo, é possível afirmar que está apto para uma próxima fase de validação. Numa próxima fase de validação, o dispositivo deverá ser testado numa população humana validada. Além disso, a utilização de algoritmos de segmentação já validados será um fator importante para considerar estes dispositivos validados. A utilização de algoritmos já validados irá permitir superar os problemas derivados principalmente da baixa performance na localização dos *onsets* da onda T. Por fim, todo o trabalho desenvolvido pode ser aplicado a confirgurações diferentes de ECG, incluíndo ECG de 12 derivações

Abstract

Validation studies are becoming increasingly crucial as technology advances and the number of electrocardiography (ECG) wearables grows. Existing validation studies, however, are limited and particular to the approach in question. The primary purpose of this dissertation is to provide a standard validation method that can be used for a wide range of validation studies. To that purpose, the LoggerOne system will be compared against the COMEN system, an established gold standard.

ECG signals will be recorded using both devices at the same time, with the assistance of an ECG signal simulator. The simulator used is a CE certified device that can simulate both pediatric and adult ECG signals, as well as different types of arrhythmia's. The recorded signals will be processed using Python's ECG and data manipulation toolboxes. Prior to validation, signals from both devices will be normalized, and a number of filters and algorithms for feature extraction for each lead will be tested. The optimized algorithms will then extract relevant signal properties such as the P and T wave, QRS complex, RR, PR, ST, and QT intervals, and ST and PR segments. This intervals and segments from each device will be analyzed using statistical analysis methods such as Bland-Altman limits of agreement (LoA), intraclass correlation coefficient (ICC), and morphological comparison to validate the device.

This work results can be divided into two components: algorithm optimization results and validation results. Regarding algorithm results, only some leads presented P wave bounds and the T onset with values of sensitivity (Se) and positive predictive value (+P) below 95% , whereas most results present values above 98%. Standard deviation (SD) values for P bounds and QRS onset exceeded the reference values in some leads, whereas all other values remained within the range of reference. The mean values remained below the reference value imposed. Regarding validation results, almost all results for each lead show good agreement and reliability, except for intervals and segments computed using the T onset.

Keywords

ECG; 5-lead; Validation; Signal processing; ECG feature extraction.

Contents

List of Figures

List of Tables

Acronyms and Abbreviations

+P	Positive predictive value
Acc	Accuracy
ANN	Artificial neural networks
Ca^{2+}	Calcium
CSE	Common Standards in Quantitative Electrocardiography
CVDs	Cardiovascular diseases
CWT	Continuous wavelet transform
DWT	Discontinuous wavelet transform
ECG	Electrocardiography
ELA	Left arm electrode
ELL	Left leg electrode
ERA	Right arm electrode
FN	False negatives
FP	False positives
GT	Goldberger terminal
HR	Heart rate
HRV	Heart rate variability
ICC	Interclass correlation coefficient
Na^{+}	Sodium
K^{+}	Potassium
NK	Neurokit2
LoA	Bland-Altman limits of agreement
LUDB	Lobachevsky University Electrocardiography Database
PCC	Pearson's correlation coefficient
PSO	Particle swan optimization
PTA	Pan and Tompkins algorithm
QTc	Corrected QT
SA	Sinoatrial
Se	Sensitivity
SD	Standard deviation
SWT	Stationary wavelet transform
TP	True positive
WCT	Wilson central terminal
WHO	World Health Organization
WT	Wavelet transform

Chapter 1

Introduction

This chapter presents an introduction to the dissertation entitled "Validation of LoggerOne system's 5-lead ECG.". This dissertation aims to validate a medical device's electrocardiogram (ECG) signal for 5-lead placements. This validation study will be accomplished using an algorithm to extract relevant features from the medical device's ECG signal. The remaining chapter presents the following topics:

- the context and motivation of this study;
- the problem definition and objectives of the research;
- the main contributions of this study, and,
- the thesis organization.

1.1 Context and motivation

The ECG signal is the most significant physiological signal in terms of clinical significance [1], as the World Health Organization (WHO) reports that cardiovascular diseases (CVDs) are the leading cause of death worldwide every year [2]. Additionally, it is anticipated that around 23.6 million individuals will die from CVDs by 2030 [3]. However, there are several CVDs that can be successfully treated if the anomaly is recognized early [1].

The 12-lead ECG continues to be the industry standard for CVDs evaluation. However, it can only be used stationary in a clinical setting by qualified professionals. Due to these restrictions, this device cannot be used at home or in environments where moving around is necessary [4, 5]. Ambulatory ECG monitoring with the Holter is a clinically accepted method that can get beyond these restrictions. The Holter can collect ECG data for 24 to 72 hours while allowing the patient to continue daily activities. Longer recordings allow for the identification of arrhythmic abnormalities that the standard 12-lead cannot [6].

Nowadays, Holter devices are no longer the only option for ambulatory monitoring. There has been a rise in interest in wearables due to recent advancements in wireless data transmission and battery technologies. With these advancements, other ECG monitoring devices have been created in an effort to surpass the Holter and its limitations. The validation of handheld devices in comparison to the standard 12-lead ECG, however, has not been adequately studied [7, 8].

With all the factors stated above taken into consideration, the main motivation for this dissertation is to propose a validation method that can be translated to validate any ECG device against a 12-lead ECG gold standard, standardizing the validation process for different applications.

1.2 Problem statement and objectives

The dissertation focuses on validating the ECG medical device LoggerOne for 5-lead ECG signals against a gold standard, the COMEN system. For validation, the ECG signals will be recorded using both devices simultaneously and alternating between precordial leads to validate all possible leads. To acquire the signal, an ECG simulator will be used, simulating 51 different signals. Python will be used to process the captured ECG signal. Artifact removal, normalization, and feature extraction will be among the processing steps. Measure comparison techniques such as BA and ICC will be used to compare the features obtained from the device and the gold standard.

The dissertation objective is to use ECG segmentation algorithms to extract ECG fiducial points and compute ECG characteristic intervals and segments for both devices. The comparison results between both devices will determine if the device in question is ready for the next phase of validation using real ECG signals. Additionally, the results analysis will be done by comparing each lead individually in addition to the overall results.

1.3 Main contributions

The conclusion of this validation study achieved the following main contributions:

- a literature study to identify methodologies for ECG validation;
- a study of different filters for ECG feature extraction;
- the modification and study of an open source ECG segmentation toolbox for Python and the respective application to ECG leads I, II, V1, V2, V3, V4, V5, and V6;
- the development of algorithms for ECG validation that can be reused for other studies.

1.4 Dissertation organization

This dissertation is organized in the following chapters:

- Chapter 1: This chapter includes an introduction, contextualization of the dissertation, and identification of the dissertation's main contributions;
- Chapter 2: This chapter discusses the state of the art and basic concepts in ECG feature extraction and validation, as well as current approaches to these elements;
- Chapter 3: This chapter discusses the approaches implemented for both ECG feature extraction and validation.
- Chapter 4: This chapter contains the final results and discussion. The results are separated into two major components: feature extraction results and validation results;
- Chapter 5: This chapter discusses the dissertation's conclusion and possible improvements for future work.

Chapter 2

State of the art and basic concepts

This chapter presents and discusses concepts of the state-of-the-art of ECG waveform validation, giving a background on the topic and a literature review covering the approaches and methods both for ECG processing and validation. In subsection 2.3.6, a review of ECG validation approaches present in the literature is made.

2.1 Electrocardiography

The heart is a muscular organ that pumps blood via four chambers: the right atrium, the left atrium, the right ventricle, and the left ventricle. The cardiac conduction system begins when an electrical impulse exits the sinoatrial (SA) node and travels across both atria, stimulating the muscles to contract. The SA node is the heart's natural pacemaker; it starts every heartbeat and regulates heart rhythm. The electrical impulse then passes to the AV node, where a conduction delay guarantees that the atria have emptied all of the blood into the ventricles before they contract. After passing through the AV node, the electrical impulse travels swiftly through the His bundle, as well as the left and right bundles, to activate the ventricles almost simultaneously via the Purkinje system [9, 10].

2.1.1 Action potential

When at rest, heart muscle cells are polarized, which means that the net charge density of the fluid within and outside the cells differs due to differences in ion concentrations, primarily sodium (Na^+), potassium (K^+), and calcium (Ca^{2+}) on either side of the cell membranes. While potassium concentrations are greater inside the cell, those of sodium and calcium are more concentrated outside the cell. Cellular membranes have voltage-sensitive ion channels that allow these ions to travel more easily. The potential within the cell is around -90 mV at rest; however, with consecutive changes in the state of the ion channels, the potential inside the cell shifts from negative to positive in relation to the potential outside the cell membrane before returning to the initial -90 mV value. A phase is the name given to these changes in state, and each cycle of a phase begins when the potential of the cell membranes reaches a certain threshold. For pacemaker cells and cardiomyocytes, the threshold potential is different. The action potential is the resulting voltage pulse for every cell in a cycle. The ECG, as you can see in Fig. 2.1, is a representation of the sum of all action potentials from the heart [11, 12].

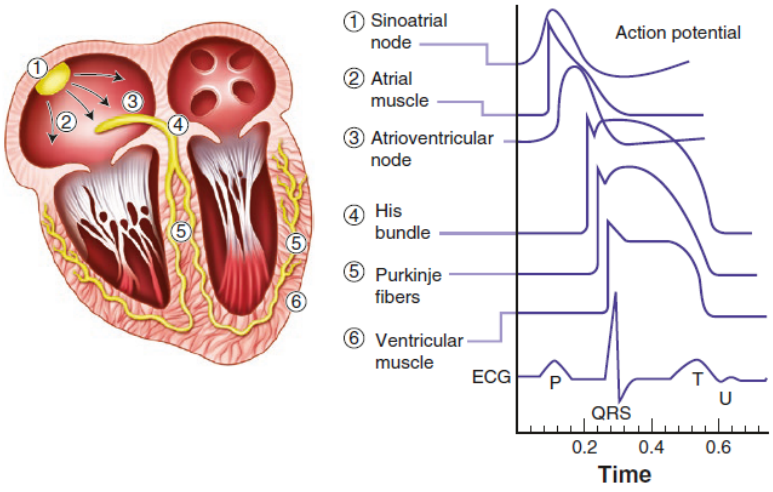

Figure 2.1: Heart action potentials (adapted from [9]).

2.1.1.1 SA action potential

The pacemaker action potential (Fig. 2.2) is divided into three stages: zero, three, and four. Due to the absence of phases one and two in pacemaker cells, which will be described later, phase zero is followed by phase three. According to [12], each stage is characterized by particular instances:

- **Phase 0:** When the membrane potential hits -40 mV, the depolarization phase begins. Slow Ca^{2+} channels open, allowing Ca^{2+} ions to enter, and membrane potential rises +10 mV as a result of this influx. Because calcium channels are slower than sodium channels, the increase in membrane potential is not as sudden as it is in cardiomyocytes.
- **Phase 3:** repolarization occurs during this phase as Ca^{2+} channels close and K^{+} channels open. The membrane potential rapidly decreases to -60 mV as a result of the efflux of K^{+} ions.
- **Phase 4:** A gradual depolarization that is exclusive to pacemaker cells takes place during this phase. The slow influx of Na^{+} ions changes the membrane potential to the threshold potential of -40 mV. The slope of phase four determines heart rate and varies among pacemaker cells in various areas.

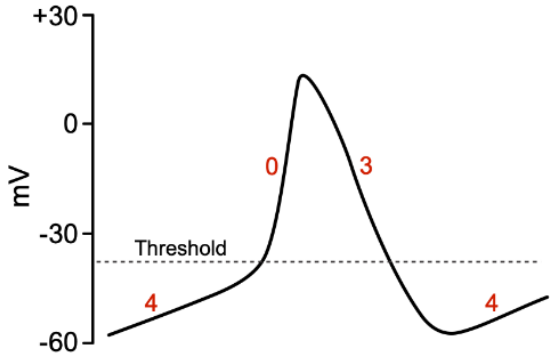

Figure 2.2: SA action potential (adapted from [13]).

2.1.1.2 Myocardiocyte action potential

The myocardiocyte action potential (Fig. 2.3) is different from that of pacemaker cells and has five phases. According to [12], each stage is characterized by particular instances:

- **Phase 0:** is a fast depolarization phase caused by the opening of fast N^+ channels, resulting in a quick influx of Na+ ions. The membrane potential shifts from -70 mV to +50 mV. This rapid shift is caused by sodium channels being faster than calcium channels.
- **Phase 1:** Na^+ channels close and some K+ channels open, resulting in efflux, which leads to initial repolarization and the start of phase two;
- **Phase 2:** Ca^{2+} channels open during this phase, also referred to as the plateau phase, generating an influx of ions. The calcium influx balances the K+ efflux, resulting in a plateau at roughly +50 mV. During this time, no new action potentials may be initiated;
- **Phase 3:** K^+ efflux through the opening of more K^+ channels and the closing of Ca^{2+} channels leads to repolarization;
- **Phase 4:** resting phase with no spontaneous depolarization.

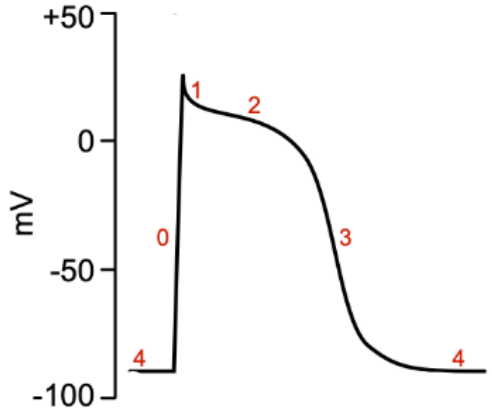

Figure 2.3: Myocardiocyte action potential (adapted from [13]).

2.1.2 Normal ECG

The typical ECG (Fig. 2.4) is composed of various characteristic waves, segments, and intervals, including P wave, QRS complex, T wave, U wave, PR or PQ segment, PR or PQ interval, ST segment, ST interval, the QT interval and the TP segment. The P wave, QRS complex, and T wave, in that order, represent the depolarization of the atria, the depolarization of the ventricles, and the repolarization of the ventricles. Furthermore, R-peak recognition is an important aspect of ECG signal analysis since other ECG signal fiducial points, such as P and T peaks and the QRS complex, can be identified using R-peaks as reference points [14]. The proper ECG evaluation process involves analyzing the heart rate (HR), P, T, and U waves, the QRS complex, the ST segment, the PQ or PR, and QT intervals [15].

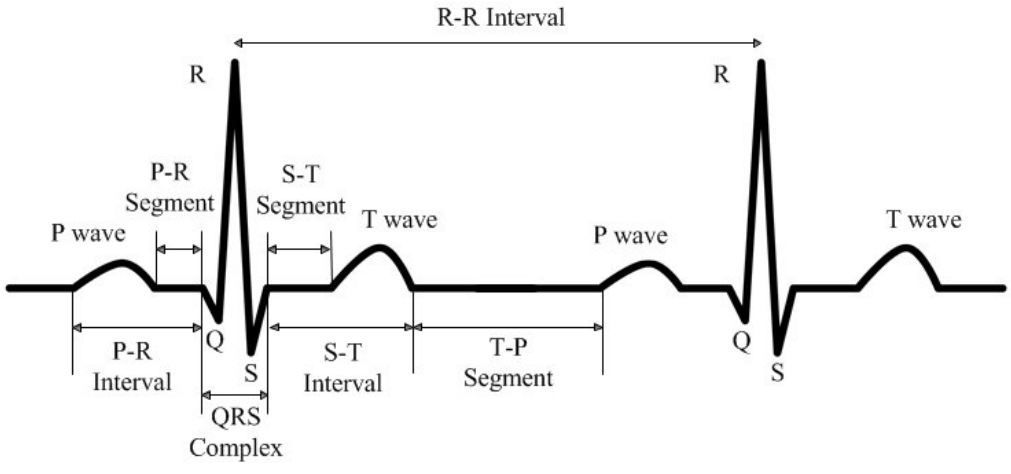

Figure 2.4: ECG wave [16].

2.1.2.1 P wave

The P wave, has a usual duration of 60 ms to 110 ms and a maximum amplitude of 0.25 mV, should be measured in lead I [15]. There is no gender difference in P wave duration and amplitude in both adults and children; however, children have a lower top limit of 100 ms and even a lower 80 ms for children under 1 year [17].

2.1.2.2 PR or PQ interval

If the first wave of the QRS complex is the R wave, this interval is denoted as PR, and if it is the Q wave, it is denoted as PQ. It is measured from the beginning of the P wave to the beginning of the Q or R wave and should be measured in leads I, II, and III where it begins and ends, i.e., in the lead where the P wave and complex QRS occur first. Its duration ranges between 120 and 200 milliseconds [15].

2.1.2.3 QRS complex

The QRS complex should be measured in unipolar leads and has a normal maximum duration of 100 ms [15]. Cardiologists assume the same QRS duration for both genders [17].

2.1.2.4 ST segment

This segment begins at the end of the complex QRS and finishes at the beginning of the T wave. However, the boundary between the ST segment and the T wave is rarely visible. J point indicates the intersection of complex QRS and segment ST [15]. Age and gender have an impact on ST amplitudes. Men's typical ST amplitude limits are greater than those of women, while older men's ST amplitudes are lower than those of younger men. When compared to younger women, older women have similar limits for the typical ST amplitude [17].

2.1.2.5 T wave

The top limits of the normal T waves exhibit significant gender differences; although the upper limit of normal in men is 1.4 mV, the normal upper limit of normal in females is 1.0 mV. Additionally, T wave morphology varies sometimes in females. More often than not, T wave inversion in V2 would be considered typical in females, whereas in a man it would not [17].

2.1.2.6 U wave

This wave, which is not represented in Fig. 2.4, comes after the T wave and has the same polarity as the T wave. This wave is apparent in V2 and V4 leads [15].

2.1.2.7 QT interval

The QT interval begins with a Q wave and concludes at the end of a T wave and should be measured in lead II or lead V2 if lead II is unavailable. It usually lasts between 350 and 420 milliseconds [15]. This interval changes with heart rate, which has given rise to the idea of correcting the QT interval to "account for rate-related T changes". Bazett's formula is the most commonly employed, but it is also the most widely criticized, as it leads to a shorter corrected (QTc) at lower rates and longer QTc at higher rates. (2.1) [17, 18].

$$QTc = \frac{QT}{\sqrt{RR}} \quad (2.1)$$

Other equations, such as the Hodges formula 2.2, which is based on a linear adjustment, and the Fridericia formula 2.3, which is similar to Bazett's and the Framingham formula 2.4, can be employed [17, 18].

$$QTc = QT + 105(\frac{1}{RR - 1}) \quad (2.2)$$

$$QTc = \frac{QT}{\sqrt[3]{RR}} \quad (2.3)$$

$$QTc = QT + 0,154(1 - RR - 1) \quad (2.4)$$

Although none of the four formulas stated have been proved to be clearly superior, Bazett's formula is employed for automated analysis and large clinical investigations, despite its evident flaws [17]. However one study [19], considers this formula the least accurate of all and refers the Fridericia and Framingham formulas as the best for QT correction. This shows that there is controversy when choosing the best approach.

2.1.3 Lead Systems

Each lead used to record an ECG signal consists of the difference between a positive electrode and a negative electrode (the reference electrode). By positioning the electrodes in certain locations on the torso, it is possible to project the electrical heart activity along

several electrical axes, enabling doctors to identify cardiac diseases by spatially correlating ECG events on particular leads. Although noninvasive electrodes are more frequently used, invasive electrodes are nevertheless an option. Non-invasive electrodes are applied with conductive gel to lower the skin-electrode impedance [20].

2.1.3.1 12-lead system

Since the 1940s, the standardized electrode recording system has remained mostly unchanged. Although customized lead recording methods are occasionally employed, an ECG with 12 leads is by far the most frequent. The 12 ECG leads (Fig. 2.5) are split into three bipolar limb leads (I, II, and III), six unipolar chest or precordial leads (V1 to V6), and three augmented unipolar limb leads (aVR, aVL, and aVF) [18]. ECG studies cardiac phenomena in the frontal plane using limb and augmented leads and in the horizontal plane using precordial leads [15]. The 10 electrode positions are represented in the following figure:

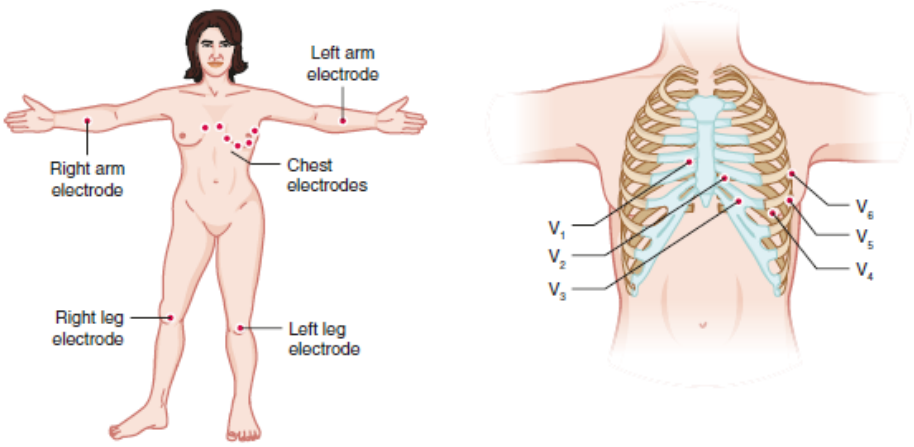

Figure 2.5: 12-lead standard electrode placements (adapted from [18]).

2.1.3.2 Limbs leads

Einthoven's three bipolar limb leads (Fig. 2.6, which he first used in 1950, shows the potential difference between two limbs. The potential difference for lead I can be expressed as Eq. 2.5, where the left arm electrode (ELA) is the positive electrode and the right arm electrode (ERA) is the negative electrode. For lead II and lead III, the left leg electrode (ELL) is the positive electrode, and the right arm (lead II) and left arm (lead III) electrodes are the negative electrodes. Accordingly, the respective potential differences can be expressed as Eq. 2.6 and Eq. 2.7. The relationship between these three paths is established by Einthoven's law (Eq. 2.8). Finally, the right leg electrode is needed to reduce common-mode interference and is conveniently located in the leg. [18, 20].

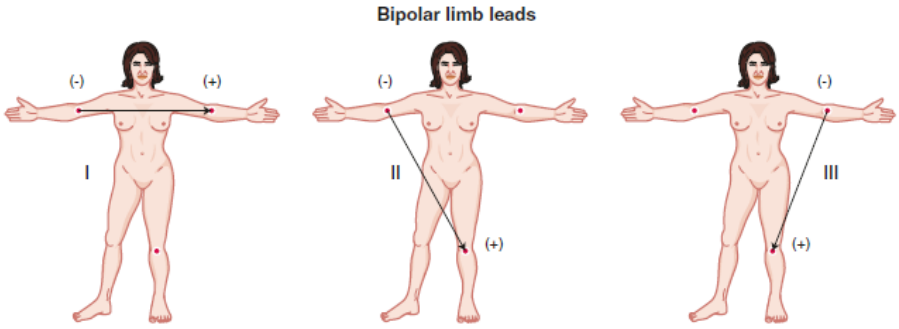

Figure 2.6: Positive and negative electrodes in limb leads (adapted from [18]).

$$I = E_L A - E_R A \quad (2.5)$$

$$II = E_L L - E_R A \quad (2.6)$$

$$III = E_L L - E_L A \quad (2.7)$$

$$II = I + III \quad (2.8)$$

2.1.3.3 Precordial leads

The unipolar chest leads, also known as precordial leads, are made up of six electrodes that are positioned at the thorax: V1 and V2 are located on the right and left sides at the fourth intercostal space, V3 is located between V2 and V4, V4 is located at the fifth intercostal space, V5 is located between V3 and V6, and V6 is located at the midaxillary line. According to Eq. 2.10, each lead (V1-V6) measures the difference in potential between a positive exploratory electrode (E1-E6) and the total potential of the left arm, right arm, and left leg, also known as the Wilson Central Terminal (WTC) reference (Eq. 2.9). Wilson invented this technique in the 1930s for the purpose of observing heart action potential in the horizontal plane as opposed to other leads that only view the heart action potential in the frontal plane [18, 20].

$$WCT = \frac{1}{3} \times (E_{RA} + E_{LA} + E_{LL}) \quad (2.9)$$

$$V_i = E_i – WCT, i = 1...6. \quad (2.10)$$

2.1.3.4 Augmented leads

For unipolar leads, the right arm, left arm, and left leg serve as the positive electrodes, while the negative electrode is a modified WTC called the Golberger Terminal (GT), where the average of the other two limbs is calculated (Fig. 2.7). The letter ”a” signifies the increased voltage amplitudes (also known as ”augmented”) caused by GT as measured by the limbs. Each lead is represented by Eq. 2.11, 2.12 and 2.13 [18, 20].

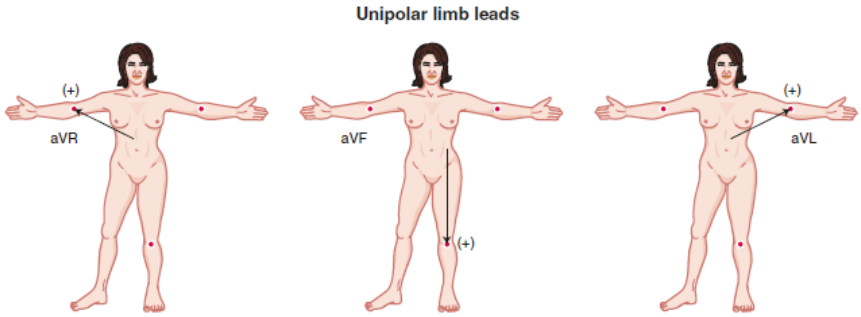

Figure 2.7: Positive and negative electrodes in augmented leads (adapted from [18]).

$$aVR = E_{RA} - GT = E_{RA} - \frac{1}{2} \times (E_{LA} + E_{LL}) \quad (2.11)$$

$$aVL = E_{LA} - GT = E_{RA} - \frac{1}{2} \times (E_{RA} + E_{LL}) \quad (2.12)$$

$$aVF = E_{LL} - GT = E_{LL} - \frac{1}{2} \times (E_{RA} + E_{LA}) \quad (2.13)$$

The augmented unipolar limb leads can also be calculated as a function of the ECG bipolar limb leads since they are a linear combination of the bipolar limb leads (Eq. 2.14, 2.15 and 2.16) [20].

$$aVR = \frac{1}{2} \times (I + II) \quad (2.14)$$

$$aVL = \frac{1}{2} \times (I - II) \quad (2.15)$$

$$aVF = \frac{1}{2} \times (II + III) \quad (2.16)$$

2.2 ECG processing

The ECG may be thoroughly analyzed to find any cardiac anomalies. However, assessing long-term ECG recordings can be difficult and time-consuming. Furthermore, owing to weariness, some personal mistakes may arise during an ECG examination, and signal interpretation necessitates extensive expertise. As a result, computer-assisted approaches for automated ECG analysis are used [21].

2.2.1 Preprocessing

The ECG signal can be filtered during the preprocessing stage to remove artifacts and enhance specific features; additionally, a normalization step may be advantageous. The following are examples of ECG signal artifacts [21]:

- **Power line interference:** noise in the frequency of 50 or 60 Hz;
- **Baseline wander:** a low-frequency noise from 0.15 to 0.3 Hz, generated by the patient's breathing, forcing the ECG signals to shift their baseline;
- **Electrode contact noise:** noise caused by a lack of skin-electrode contact, which effectively disconnects the measuring device from the patient;
- **Electrode motion artifacts:** noise caused by fluctuations in electrode-skin impedance derived from electrode motion;
- **Electromyography noise:** noise caused by the contraction of muscles except the heart;
- **Electrosurgical noise:** frequency noise in a range of 100 Hz to 1 MHz generated by various medical devices, such as a pacemaker;
- **Instrumentation noise:** noise generated by the electrical devices used to measure the ECG;

2.2.1.1 Filtering

Different filtering approaches might be utilized depending on what features we wish to extract from the ECG signal. Furthermore, the main frequencies of P and T waves differ from the main frequencies of the QRS complex. As a result, various filtering algorithms can be employed to enhance or eliminate specific ECG features. Observing the power spectra of a noisy ECG signal (Fig. 2.8), it can be determined that the ideal frequency band for detecting P and T waves is 0.5-10 Hz, and the optimal frequency band for detecting QRS complexes is 0.5-30 Hz [22, 23].

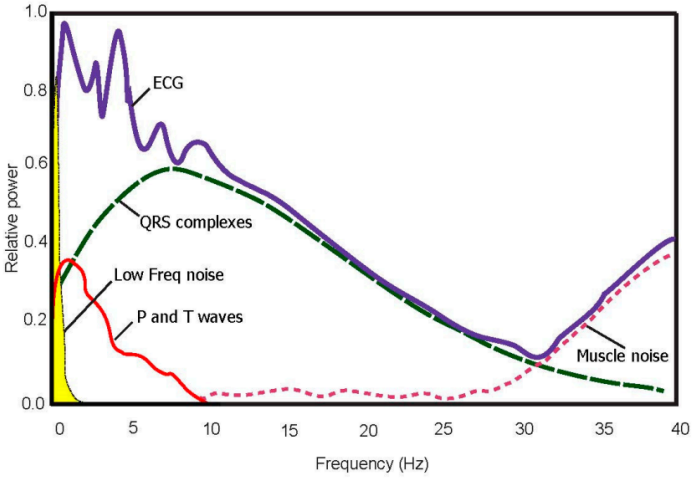

Figure 2.8: Power spectra of a noisy ECG signal [22].

Berkaya *et al.* [21], conducted a survey on the many types of filters that are utilized and their uses. They discovered that bandpass filtering in the frequency range of 0.1–100 Hz is the most extensively utilized of all filters for removing muscle noise, baseline drift, power line interference, minimizing ADC saturation, and avoiding antialiasing. In the literature, low-pass filters were employed to reduce power line interference. To remove baseline drift and the DC offset caused by the electrode-skin contact, high-pass filters were typically used. Notch filters are used to provide a narrow stop band of unwanted frequencies, thereby removing powerline interference and reducing DC components. Although less prevalent, there are other types of filters used for ECG denoising, such as median filters to remove the baseline wander and/or P and T waves; averaging filters to assess the polarity of the P and T waves; Savitsky-Golay filters for smoothing the signals; and adaptive filter to reduce power line interference without distorting the signal. Finally, several types of wavelet transforms (WT) are utilized to remove artifacts. Stationary wavelet transform (SWT), for example, can be utilized to eliminate muscle artifacts and electrode movement artifacts. On the other hand, multiresolution WT can remove baseline drift.

Table 2.1 resumes the frequency ranges applied to ECG signal filtering as per the survey stated above:

Table 2.1: Filters respective frequencies for ECG denoising [21].

Filter	Frequency
Band-pass	0.05-40 Hz; 0.1-100 Hz; 0.4-40 Hz; 0.5-40 Hz; 0.5-50 Hz; 1-30 Hz; 1-40 Hz; 1-100 Hz; 1-120 Hz
Low-pass	11 Hz; 30 Hz; 35 Hz; 50 Hz; 70 Hz; 90 Hz; 100 Hz
High-pass	0.5 Hz; 1 Hz; 2 Hz; 5 Hz
Notch	50 Hz; 60 Hz

2.2.1.2 Normalization

Normalization of the signal, which prevents amplitude and DC offset effects, is one of the initial steps in ECG preprocessing. A normalization step can help prevent false negatives (FN) or false positives (FP) arising from high-amplitude T waves and low-amplitude R peaks in non-normalized ECG data. It can also help when comparing signals visually. In the literature, this preprocessing step can be carried out by dividing each beat's features by the arithmetic mean of the previous eight regular beats [21]. Equation 2.17 describes yet another normalizing procedure utilized in a study with the primary purpose of morphologically comparing ECG signals [24].

$$x_{norm} = \frac{x[k] - \mu_x}{max_x - min_x} \quad (2.17)$$

2.2.2 ECG segmentation

To segment the ECG wave, algorithms must identify each fiducial point on the wave: onsets and offsets of P, QRS, and T waves. Identifying these locations, however, is challenging due to aspects such as the considerable variability in the shape of the QRS complex, the lower amplitude of the P-wave, and smooth transitions between the end of the ST segment and the beginning of the T-wave. Furthermore, the absence of universal agreement on the precise position of the fiducial points complicates the work even further. There are various methods for segmenting the ECG in the literature, although not all approaches detect every fiducial point of the ECG wave [25].

2.2.2.1 Methods in literature

A number of studies have been conducted on QRS complexes. As a result, numerous strategies for locating QRS complexes and their features have been developed, including

particle swan optimization (PSO), artificial neural networks (ANN), principal component analysis, and the widely known Pan and Tompkins algorithm (PTA) [26]. The PTA is one of the popular techniques for QRS complex detection and uses the amplitude thresholding technique and high slope detection to locate the R peak accurately in ECG [27]. On the other hand, P and T waves have been detected using phasor transform [28], debuchies [25], and an algorithm that uses moving window integration along with threshold detection method [28].

P, QRS, and T waves can also be detected using different types of WT, such as multiresolution WT, continuous wavelet transform (CWT), and discontinuous wavelet transform (DWT) [25, 26]. This time-frequency feature extraction technique employs scaled and shifted versions of the mother wave to break down a signal into components that appear at various scales. Simpler high- and low-frequency components are created by breaking down the signal. Since wavelet analysis may be used to temporally localize the spectrum components and provide a time-frequency representation of the signal, the WT has the benefit of maintaining temporal locality [21]. When analyzing a signal, DWT is employed as a more effective transform because CWT increases computing complexity [26].

2.2.3 Evaluation methods

Due to the disparities in methods and databases utilized for algorithm evaluation, a direct comparison of segmentation algorithms used in the literature is challenging [25]. Furthermore, different studies establish distinct evaluation criteria to compare the algorithm results with the manual annotations in the database. Some use merely sensitivity (Se) as a performance parameter [25], some use Se and positive predictive value (+P) [22, 28, 29], and yet others use those two parameters plus accuracy (Acc) [23, 30]. However, the performance indicators provided in equations (2.18), (2.19), and (2.20) only reflect whether or not an algorithm finds a fiducial point and do not show the algorithm's actual performance. As a result, several studies include the mean difference and standard deviation (SD) as performance metrics [23, 25, 29].

$$Se = \frac{TP}{TP + FN} \quad (2.18)$$

$$+P = \frac{TP}{TP + FP} \quad (2.19)$$

$$Acc = \frac{TP + TN}{TP + FP + FN} \quad (2.20)$$

where TP is the true positive i.e. the correctly identified fiducial points, FP is the false

positives i.e. the incorrectly identified fiducial points and FN is the false negatives i.e. the missing identified fiducial points.

2.2.3.1 ECG measurement standards

The Common Standards in Quantitative Electrocardiography (CSE) work party created a framework for algorithm validation in order to standardize automatic fiducial point recognition [31]. As a result, the CSE recommends using the validated CSE database to evaluate P and QRS onsets and offsets, as well as T offsets. Furthermore, it is advised to measure these fiducial points with at least three leads recorded simultaneously, though this framework is equally relevant to single lead measurement.

Table 2.2 indicates the SD values that the method to be verified ought to stick to; these values are ”robust estimators of what can be expected from an expert cardiologist as well as what a panel of experts can achieve.”. The algorithm's SD should not only not exceed these levels, but it should also produce results that are as close to the annotations in the database as possible.

Table 2.2: SD results derived from CSE data sets [31].

Lead group	**P wave**		**QRS wave**		**T wave**:
	Onset	Offset	Onset	Offset	**end**
I-III	8.0	12.8	7.8	12.4	32.8
aVR-aVF	9.2	12.0	7.8	13.4	27.6
V1-V3	12.4	14.4	5.2	9.4	28.6
V4-V6	12.6	13.6	5.2	12.0	28.8
XYZ	8.6	10.8	6.6	10.6	35.2
Average	10.2	12.7	6.5	11.6	30.6

2.3 Validation

2.3.1 Introduction

In several research fields, statistical comparisons are frequently applied to evaluate the efficacy of novel methods or devices. This can be done against a gold standard for validation or to compare two distinct procedures to see which one is the best. To ensure that the results of a new technique or method can be trusted, performance should be assessed to determine agreement and reliability. Knowing what comparison metrics to use and how to interpret the findings for each study case is of utmost importance in this regard. That isn't always the case, though, as some studies don't do that and don't disclose crucial details like confidence intervals [32].

When it comes to ECG, various parameters are frequently compared against a gold standard using comparison measures such as Pearson's correlation coefficient (PCC), inter-

class correlation coefficient (ICC), and Bland-Altman limits of agreement (LoA). When verifying a diagnosis for a specific disease or condition, categorical comparison measures like Cohen's kappa are also employed. Most studies employ multiple measures of comparison rather than just one [7, 33]. The most common validated parameters are HR, heart rate variability (HRV), and RR intervals [4, 5]. Other investigations have been conducted to validate ECG wave parameters such as QTc, QRS complex intervals, and P and T wave intervals [7, 33, 34]. Other, albeit fewer studies, compare the ECG wave's morphology as opposed to specific parameters [24].

2.3.2 Correlation, Agreement and Reliability

Despite their inaccuracy, correlation and linear regression are frequently utilized when assessing the agreement or reliability of two different methods. Measures of agreement actually evaluate how similar the measured values are across two methods, as opposed to correlation, which just serves as an indicator of the strength of the linear relationship between two variables. In contrast, reliability describes how effectively measured values can be discriminated despite measurement error, or more precisely, how well the method can discern subject differences [32, 35].

Additionally, agreement and reliability may be distinguished by stating that the former is relevant when attempting to distinguish between within-subject variation over time and the latter is relevant when attempting to distinguish between between-subject variation. As an illustration for this difference, "consider a scenario where researchers want to evaluate the performance of a new method in measuring heart rate in comparison to the gold standard method. If this new method is used to measure the variation in heart rate of patients over time, the parameter of interest in evaluating this method would be its agreement with the gold standard method, but if it is used to distinguish patients with high heart rate from those with lower heart rate, the parameter of interest in evaluating this method would be reliability" [32].

2.3.3 Validation methods

2.3.3.1 Cohen's Kappa

When calculating inter-rater agreement for categorical items, Cohen's kappa (κ) takes into account the possibility that the agreement could have happened by chance. The κ statistic can accept values in the range of -1 and 1 where [35, 36]:

- 0 - agreement equivalent to chance;
- 0.10–0.20 - poor agreement;
- 0.21–0.40 - fair agreement;

- 0.41–0.60 - moderate agreement;
- 0.61–0.80 - substantial agreement;
- 0.81–0.99 - near-perfect agreement;
- 1.00 - perfect agreement;
- < 0 - compared to what would be predicted by chance, the observed agreement is worse.

According to [36], Cohen's Kappa can be computed as:

$$\kappa = \frac{p_A - p_E}{1 - p_E} \quad (2.21)$$

where $p_A$is the relative observed agreement between raters, and p_E is the chance agreement between raters.

2.3.4 Pearson's correlation

The PCC is one of the most commonly used correlation coefficients in medical research. It measures the linear association between two variables where a change in one variable is correlated with a change in another variable, in either direction, be it positive or negative. Pearson's correlation values are defined between -1 and 1, where r = 0 means there is no linear relationship between the variables, and the relationship becomes stronger as the correlation coefficient increases to either -1 or +1 [37].

2.3.5 Bland-Altman limits of agreement

The erroneous use of correlation coefficients as a measure of agreement is criticized by Martin Bland and Douglas Altman since these approaches don't actually show agreement but rather the relationship between the two methodologies under consideration. As a result, they suggested the LoA approach for evaluating agreement in 1983. This approach is now regarded as a suitable tool to assess how well a new method agrees with an existing gold standard [38].

Although it lacks criteria for ECG parameters, LoA is one of the most used and tested methods for assessing the agreement between two different clinical measurements. The differences between each pair of measurements are plotted against the mean of the differences. Assuming 95% limits of agreement, we can compute the limits of agreement as the mean difference (mean bias) of all pairs of measurements minus 1,96 times the standard deviation of the differences or plus 1,96 times the standard deviation. These limits are

expected to contain 95% of future measurements (2.22) [39].

$$LoA = \overline{d} \pm 1.96 \times SD \quad (2.22)$$

where $\overline{d}$ is the mean difference or bias and SD the standard deviation.

Even if this method is frequently used for clinical validation, there are still issues that need to be taken into account. One is that it is restricted to data sets that conform to the normal distribution assumption. Although continuous measurement variables do not have to be normally distributed, differences should be. This can be verified using the Shapiro-Wilk test, for example, and in the event of failure, data may be converted logarithmically if the normal distribution presumption is not met. A non-normal distribution of differences, on the other hand, is not as critical for the LoA as it may be in other methods because, according to Bland-Altman, "non-normal distributions are still likely to have about 5% of observations within about two standard deviations of the mean". Another issue is that repeated measurements cannot be compared using this type of analysis. As a result, Martin Bland and Douglas Altman later introduced a new approach to the LoA method that considers repeated measurements [38, 39].

2.3.5.1 Intraclass correlation coefficient

ICC is a statistical method for determining measurement reliability that takes into account not just agreement but also correlation. The ICC is calculated using mean squares obtained through analysis of variance, and the calculated reliability value is in the range of 0 to 1, with values nearer 1 indicating higher reliability. The ICC should be reported along with the 95% intervals of confidence[40, 41].

There are ten alternative methods for computing ICC that, when used in the same scenario, may produce a different result. For this reason, it is crucial to choose the best strategy. Shrout and Fleiss first published six types of ICC in 1979, and McGraw and Wong added four more in 1996. McGraw and Wong recognized the need to adjust Shrout's and Fleiss' equations for four different types of studies, making the ICC technique very versatile. The appropriate ICC variant is defined by the type of reliability research of interest, and it is selected by taking three primary factors into account: model, type, and definition (table 2.3). After determining each factor and defining the kind of ICC in question, the ICC is obtained using the formulas shown in table 2.4. Each formula will give a result between 0 and 1 that can be interpreted using one of the two distinct criteria shown in table 2.5 [40, 41].

Table 2.3: Definition of the different factors that affect ICC (adapted from [41]).

Model	
One-way random-effect	Each subject is rated by a different set of raters randomly chosen
Two-way random-effect	Each subject is rated by the same set of raters randomly chosen
Two-way mixed-effect	Each subject is rated by the same set of raters not randomly chosen
Type	
Single rater	Only the ratings from a single rater or instrument are the basis of measurement
Mean of multiple raters	The mean of rating from all raters or of a single instrument is the basis of measurement
Definition	
Absolute agreement	Based on absolute agreement between raters
Consistency	Based on the correlation between scores assigned to subjects by the two raters

Table 2.4: Equivalent ICC Forms Between Shrout and Fleiss and McGraw and Wong (adapted from [40]).

McGraw and Wong convention	**Shrout and Fleiss convention**	**Formulas for Calculating ICC[1]**
One-way random effects, absolute agreement, single rater/measurement	ICC (1,1)	$\frac{MS_R - MS_W}{MS_R + (k+1)MS_W}$
Two-way random effects, consistency, single rater/measurement	-	$\frac{MS_R - MS_E}{MS_R + (k-1)MS_E}$
Two-way random effects, absolute agreement, single rater/measurement	ICC (2,1)	$\frac{MS_R - MS_E}{MS_R + (k-1)MS_E + \frac{k}{n}(MS_C - MS_E)}$
Two-way mixed effects, consistency, single rater/measurement	ICC (3,1)	$\frac{MS_R - MS_E}{MS_R + (k-1)MS_E}$
Two-way mixed effects, absolute agreement, single rater/measurement	-	$\frac{MS_R - MS_E}{MS_R + (k-1)MS_E + \frac{k}{n}(MS_C - MS_E)}$
One-way random effects, absolute agreement, multiple raters/ measurements	ICC (1,k)	$\frac{MS_R - MS_W}{MS_R}$
Two-way random effects, consistency, multiple raters/measurements	-	$\frac{MS_R - MS_E}{MS_R}$
Two-way random effects, absolute agreement, multiple raters/ measurements	ICC (2,k)	$\frac{MS_R - MS_E}{MS_R + \frac{MS_C - MS_E}{n}}$
Two-way mixed effects, consistency, multiple raters/measurements	ICC (3,k)	$\frac{MS_R - MS_E}{MS_R}$
Two-way mixed effects, absolute agreement, multiple raters/measurements	-	$\frac{MS_R - MS_E}{MS_R + \frac{MS_C - MS_E}{n}}$

[1]where MSR = mean square for rows, MSW = mean square for residual sources of variance, MSE = mean square for error; MSC = mean square for columns, n = number of subjects, k = number of raters/measurements.

Table 2.5: Common guidelines for interpretation (adapted from [41]).

Interpretation	**Intervals**	
	Ko and Li	Cicchetti and Sparrow
Poor	<0,50	<0,40
Fair	0,50-0,75	0,40-0,60
Good	0,75-0,90	0,60-0,75
Excellent	0,90-1	0,75-1

2.3.6 Validation studies

In the literature, there are some studies on ECG validation; however, their methodologies vary, and there's no clear framework or guidelines on how to proceed with an ECG validation test. Tables 2.6 and 2.7 present a comparison of some of the ECG validation studies in the literature and regard important parameters such as the gold standard used, what features were extracted, how the exams were made, the population, and the measures of comparison used.

Exams should be one of the first things to consider while validating ECG equipment. There are two options: the exams on both devices can take place concurrently or not. When comparing two exams, taking them both at the same time should be the best option; however, this is not always feasible. Only three of the studies in question had exams that weren't performed concurrently [7, 42, 43]; in the ones where the exams did occur concurrently, this was possible because the devices to be validated used different placements than the gold standard or because the electrodes were positioned in parallel in the same location. The drawback with this strategy is that because the electrode location is different, the signal may not be exactly the same, especially for the precordial leads. However, two intriguing validation studies employ morphological metrics of comparison to determine which 12-lead standard lead their device placement relates to [44, 45].

Regarding the features to be validated, most studies focus on features obtained through R peaks: RR intervals, HR, and HRV. Although there are studies that validate other ECG intervals, it is not as common. Feature extraction from specialists has different methodologies than automatic feature extraction; they usually study every lead as one exam, while in automatic feature extraction, it is possible to study intervals for each lead independently. That being said, there is little or no information on what lead the intervals were extracted from, and there is no assumed correct way to do it. Finally, there are studies that validate assessments by evaluating whether trained specialists can differentiate the same heart problems using both devices.

The population sample is typically too small; only in one study did the researchers compute the number of subjects needed based on 95% confidence intervals [4]. In addition, two more studies employed a sufficient number of people for 95% confidence intervals (and a 5% margin error) [7, 44]. In terms of subject age range, almost every study that indicates the age range utilizes participants who are at least 18 years old, meaning that most studies do not include pediatric subjects. In terms of population type (healthy or pathological), some studies show little interest in distinguishing, while others do. The research has the most diverse population (4-80 years old) and a sufficient number of individuals for 95% confidence intervals[44].

Finally, most studies adopt LoA, paired-t test, ICC, PCC, or another correlation metric as validation metrics. Cohen's kappa is also used for category items, for instance, determining if it is possible to diagnose cardiac problems with both devices. Other studies use the

morphological comparison metric to compare the whole signal. There are several issues with the approaches used in various studies. For starters, many studies do not specify the confidence intervals they are using. Furthermore, many studies employ correlation as a metric of comparison, which is seen as incorrect. Paired t-test are also criticized because they can't distinguish between agreement when the mean differences between the measured values are close to zero, which means this test only compares the mean differences and not the individual differences between subjects [46]. However, all studies that employ the paired t-test as a measure of comparison also use LoA, which can discern agreement when the mean difference is zero.

Table 2.6: ECG validation study comparison.

Year	Study	Gold Standard	Device	Features	Extraction methods	Exam	Population	Measures of Comparison
2021	[7]	12-lead standard	Kadia 6L	PR and QT interval; QTc; QRS duration, axis and amplitude; T wave inversion; ST segment	3 specialists	30s, NS	n=1015; Age=62±17; Male=62.4%	Kappa analysis; Linear regression; LoA; Receiver operator curve
2021	[34]	12-lead standard	AliveCor KardiaMobile 1L	Mean QT/QTc and QRS; HR	2 specialists	30s, S	n=125; Age=61±14; Male=51.4%	LoA; Paired t-test; Se; Specificity
2021	[5]	BrainAmp-ExG	Plugged BT Kit	HR; HRV	Matlab ECG tool developed by the authors	S	n=24; Age=22-57, 28.3±8.8; Male=45.83%	ICC; LoA
2021	[6]	3-lead Holter	MC-100	RR intervals; no. QRS complex	2 cardiologists	24h, S	n=29; Age=55.1±12.8; Male=48.3%	ICC; LoA
2020	[47]	Holter 10-leads	Omegawave device	RR intervals	Adaptive threshold	10 min, S	n=11	LoA; PCC
2020	[48]	12-lead standard	Polar V800	RR intervals; HRV parameters	Kubios Premium software	10 min, S	n=25; Age=18-55, 44.7±10.1; Male=68%	ICC; LoA; Paired t-test
2019	[24]	Biopac MP35 2-lead	BITalino (r)evolution 3-lead	Beat	R-peak Lorenço et al. 2012	20s, S	n=7	RMSE; Correlation coefficient
2019	[4]	Polysomnography system (1-lead)	ECG-belt 1-lead	R peaks, RR intervals; HRV	Kubios HRV Premium Software	6h, S	n=242; Age=43-61, Males=76.85%	LoA; PCC; Paired t-test; RMS; SE

S = ECG simultaneously recorded; NS = ECG not simultaneausly recorded.

Table 2.7: ECG validation study comparison (continuation).

Year	Study	Gold Standard	Device	Features	Extraction methods	Exam	Population	Measures of Comparison
2017	[49]	biosignalsplux research-grade system	BITalino 3-lead; BITalino (r)evolution 3-lead	Beat	R-peak Lorenço et al. 2012	ND	n = 208 segments	Correlation coefficient; RMSE
2017	[44]	12-lead standard	3-lead	HR; QRS complex; RR intervals	Wavelet transform	20s, S	n=391; Age=4-80; 26.90±19.32; Male=60.86%	Correlation coefficient
2016	[50]	3-lead Holter	EQ02 (2-leads belt)	HR; HRV	Vivosense software	24h, S	n=18; Age=27,6±9,4; 19-57; Male=55%	LoA, Paired t-tests; PCC
2016	[51]	3-lead Holter	1-Lead Patch	PR; QRS; QTc	2 specialists	24h, S	n=50; Age=54,8±17,8; Male=66%	Correlation coefficient; Mean; SD; x^2 test
2014	[42]	12-lead standard	BITalino 1-lead (fingertips)	Signal correlation	R-peak Lorenço et al. 2012	30s, NS	n=38; Males=50%	Correlation coefficient; RMSE
2013	[45]	12-lead standard	BITalino 1-lead (fingertips)	Beat	R-peak Lorenço et al. 2012	30s, S	n=11; Male=45.46%	Interquartile range; Median; RMSE
2012	[43]	12-lead standard	3-lead tele-ECG	HRV, QRS, PQ, PR and QT intervals; ST elevation	Manually	NS	n=107; Age=60-72	Cohen's Kappa; LoA

S = ECG simultaneously recorded; NS = ECG not simultaneously recorded.

Chapter 3

Methods

In this chapter, we describe and discuss the design process and choices for our implementation strategy of the proposed approach.

3.1 Introduction

This work had the goal of doing an early validation of the LoggerOne system's ECG 5-lead and was thus separated into two parts: feature extraction and validation. The feature extraction process involves the study of several filters as well as different algorithms for ECG fiducial point extraction. To achieve a valid comparison, ECG signals along with respective fiducial point annotations from the Lobachevsky University Electrocardiography Database (LUDB) [52, 53, 54] were used. For this, Python's toolboxes Neurokit2 (NK) (version 2.3) [55] for neurophysiological data analysis and preprocessing and Scipy for preprocessing were also used. The second section of this work continues after selecting the optimal algorithms and filters for feature extraction. Each lead was independently assessed using statistical techniques such as LoA, ICC, scatter plots, and histograms. LoA plots and ICC were computed using the Statsmodel and Pingouin libraries, respectively. Other data processing and visualization libraries, such as NumPy, Matplotlib, and Pandas, were employed throughout this work.

3.2 Feature Extraction

For the feature extraction algorithm development, only the fiducial points location was considered. The goal was to find the best combination between algorithms and filters for each point individually, optimizing the results without regard to computational time. ECG annotated signals from LUDB were used as a reference, and algorithms from the NK toolbox were used as the base of feature extraction. For comparing performance results, Se, +P, mean, and SD were the base evaluation methods.

3.2.1 Lobachevsky University Electrocardiography Database

The LUDB is an ECG database that can be accessed via the WFDB Python Toolbox, the WFDB Toolbox for Matlab or Octave, and the WFDB Software Package. This database is

one of the most extensive open-access databases, with a total of 200 ECG signals recorded with a Schiller Cardiovit AT-101 cardiograph in the 12-lead configuration. Furthermore, P, T, and QRS complex onsets and offsets were manually annotated by cardiologists for each lead individually, whereas other databases do not have annotations of all fiducial sites for all leads. In terms of exam procedures, specialists recorded the ECG signal for 10 seconds and digitalized it at 500 Hz. The population includes both healthy volunteers and Nizhny Novgorod City Hospital No. 5 patients with various cardiovascular disorders and pacemakers. The patients' ages ranged from 11 to 89 years old, with a mean of 52 years old, and 57.5 % were male [52].

Since the goal of this work is the initial validation of an ECG device, the LUDB was adapted to meet those requirements. Seeing as there is no need to validate the device in this first analysis for some specific cases where the ECG wave deviates significantly from the typical morphology, some signals or waves from LUBD had to be excluded. Additionally, the algorithms didn't even work for some of those cases. As such, the following methodology was applied to exclude the signals:

- Signals with less than 5 beats were excluded since the algorithms don't work on them;
- Signals where the patient has a pacemaker were excluded for their particular morphology, and neither algorithm worked on them;
- Signals with atrial fibrillation and atrial flutter were excluded for their particular morphology;
- Inverted P and T waves were excluded from the signals for performance evaluation since neither algorithm can recognize inverted waves.

The next Tables from 3.1 to 3.8 show the number of available fiducial points for each lead.

Table 3.1: No. of fiducial pints available for Lead I used in this research.

P wave			**QRS complex**			**T wave**		
Onset	Peak	Offset	Onset	Peak	Offset	Onset	Peak	Offset
1364	1364	1364	1528	1528	1528	1231	1231	1231

Table 3.2: No. of fiducial pints available for Lead II used in this research.

P wave			**QRS complex**			**T wave**		
Onset	Peak	Offset	Onset	Peak	Offset	Onset	Peak	Offset
1347	1347	1347	1505	1505	1505	1253	1253	1253

Table 3.3: No. of fiducial pints available for Lead V1 used in this research.

P wave			**QRS complex**			**T wave**		
Onset	Peak	Offset	Onset	Peak	Offset	Onset	Peak	Offset
797	797	797	1515	1521	1521	529	529	529

Table 3.4: No. of fiducial pints available for Lead V2 used in this research.

P wave			QRS complex			T wave		
Onset	Peak	Offset	Onset	Peak	Offset	Onset	Peak	Offset
1208	1209	1209	1492	1499	1499	1185	1185	1185

Table 3.5: No. of fiducial pints available for Lead V3 used in this research.

P wave			QRS complex			T wave		
Onset	Peak	Offset	Onset	Peak	Offset	Onset	Peak	Offset
1353	1353	1353	1521	1526	1526	1265	1265	1265

Table 3.6: No. of fiducial pints available for Lead V4 used in this research.

P wave			QRS complex			T wave		
Onset	Peak	Offset	Onset	Peak	Offset	Onset	Peak	Offset
1326	1326	1326	1496	1496	1496	1232	1232	1232

Table 3.7: No. of fiducial pints available for Lead V5 used in this research.

P wave			QRS complex			T wave		
Onset	Peak	Offset	Onset	Peak	Offset	Onset	Peak	Offset
1368	1368	1368	1536	1536	1536	1250	1250	1250

Table 3.8: No. of fiducial pints available for Lead V6 used in this research.

P wave			QRS complex			T wave		
Onset	Peak	Offset	Onset	Peak	Offset	Onset	Peak	Offset
1368	1368	1368	1534	1534	1534	1230	1230	1230

3.2.2 Neurokit2 Algorithms

The NK toolbox provides both algorithms for R peak detection and for other ECG wave characteristic points. For R peak detection, this toolbox provides some algorithms from the literature as well as an algorithm from the toolbox developers. For the remaining fiducial points, the toolbox includes three algorithms: a CWT and a DWT method that locates all ECG points, and a Peak method that only detects P onset and peak, QRS onset and offset, and T peak and offset. These three methods use the detected R peaks as an argument to find the other fiducial points.

The results of a study conducted by NK's authors that compares all algorithms available in this toolbox led to the adoption of NK's original method for R peak detection for this work [55]. In this study, they used a variety of databases, including LUDB. Regarding the rest of the ECG wave fiducial points, Peak and DWT methods were both chosen to be tested, whereas CWT was out of the question because it didn't deliver good enough results. During the initial tests NK's R peak algorithm performed well, and for the rest of the fiducial points, the Peak algorithm outperformed the DWT algorithm for P and T

waves. The issue is that the Peak algorithm fails to locate the P offset, T onset, and QRS onset and offset. As a result, some changes were made to the original NK's DWT functions to accept external P and T peaks from the Peak function. The Peak method can now be used to obtain the best results for P and T fiducial points, which are then delivered as arguments to the DWT and used to locate the respective wave boundaries. This modified algorithm was known as DWT-Peak and usually produced better results for all points.

3.2.3 Filtering

NK's toolbox includes a function for applying a number filter from the literature. In this work, all of those filters were tested and have the following characteristics:

- **"biosppy":** 3-45 Hz band-pass FIR filter (order = 1.5 x sampling rate);
- **"elgendi2010":** 8-20 Hz band-pass butterworth (order = 2);
- **"engzeemod2012":** High-pass butterworth filter with a low-cut of 4 Hz (order = 2);
- **"hamilton2002":** 8-16 Hz band-pass butterworth (order = 1);
- **"neurokit":** 0.5 Hz high-pass butterworth filter (order = 5), and powerline filtering at 50 Hz using a moving average kernel with the width of one period of 50 Hz;
- **"pantompkins1985":** 5-15 Hz band-pass butterworth (order = 1).

Additionally, Scippy's toolbox was used to test different combinations of orders and frequency bands (based on literature) for butterworth bandpass forward-backward filters using cascaded second-order sections. For P and T waves, filters were tested with orders between 1 and 4 and frequency bands of 0.5–10 Hz and 0.5–20 Hz, whereas for QRS complex bounds, different combinations of filters were tested with orders between 5-100 and frequency passbands with a fixed low-cut of 0.5 and a high-cut varying from 16 to 35 Hz.

3.2.4 Performance methods

Se, +P, mean, and the SD (equation 3.1) were selected as performance metrics to compare the outcomes of various combinations of filters and algorithms. Se was selected as an indicator because it illustrates how well the algorithm locates the existing fiducial points. +P was calculated by considering that a fiducial point is a FP if it has a ±75 ms difference from the annotated point and gives a percentage of the points that don't surpass that limit. Regarding FP limits, they vary from study to study; some considered ±20 ms [56], others ±50 ms [30], or ±120 ms [25]. The limit of ±75 ms as the FP limit was chosen regarding a study that considered the AAMIECAR guideline as a reference [23]. For the mean, a limit

of 15 ms was considered as per Sörnmo and Laguna's suggestion [25, 57]. In addition to the FP performance parameter, FP-R was used to consider R peaks that are found but shouldn't exist. This is only relevant to the R peaks since every other point is calculated considering the R peaks. Lastly, for SD limits (equation 3.1), the CSE work party recommendations were followed [31]. Table 3.9 resumes all performance parameters used.

Table 3.9: Performance parameters resume.

Performance parameter	**Meaning**	**Explanation**
TP	True positives	Every point found less than 75 ms from the annotated point
FN	False negatives	Points not found
FP	False positives	Every point found more than 75 ms from the annotated point
FP-R	False positives (for R peak)	Every point found more than 75 ms from the annotated point plus every R peak found that doesn't actually exist
Se	Sensitivity	Calculated using equation 2.18
+P	Positive predictive value	Calculated using equation 2.19
+P-R	Positive predictive value (for R peaks)	Calculated using equation 2.19, but using FP-R values
Mean	-	Mean of the differences between the algorithm and annotated points
SD	Sample standard deviation	Sample SD of of the differences between the algorithm and annotated points

$$s = \sqrt{\frac{\sum (x_i - \bar{x})^2}{n-1}} \quad (3.1)$$

where s is the sample SD, x_i the individual value, $\bar{x}$ the Sample mean and n the Sample size.

3.2.5 Algorithm and filters applied for feature extraction

The next Tables 3.10 to 3.17 show the final results between algorithms and filters for each lead:

Table 3.10: Algorithm and filters applied to each fiducial point for lead I.

Feature	**Algorithm**	**Filter**
R peak	Neurokit	Neurokit
P peak	DWT-Peak	Butterworth: bandpass of 0.5-10 Hz and 4th order
P onset/offset	DWT-Peak	Butterworth: bandpass of 0.5-20 Hz and 2nd order
T peak, offset	DWT-Peak	Butterworth: bandpass of 0.5-10 Hz and 1st order
T onset	DWT-Peak	Butterworth: bandpass of 0.5-10 Hz and 2nd order
QRS onset	DWT-Peak	Butterworth: bandpass of 0.5-27 Hz and 40th order
QRS offset	DWT-Peak	Butterworth: bandpass of 0.5-27 Hz and 50th order

Table 3.11: Algorithm and filters applied to each fiducial point for lead II.

Feature	Algorithm	Filter
R peak	Neurokit	Biosppy
P wave	DWT-Peak	Butterworth: bandpass of 0.5-20 Hz and 2nd order
T peak, offset	DWT-Peak	Butterworth: bandpass of 0.5-20 Hz and 1st order
T onset	DWT-Peak	Butterworth: bandpass of 0.5-10 Hz and 1st order
QRS onset	DWT-Peak	Butterworth: bandpass of 0.5-26 Hz and 30th order
QRS offset	DWT-Peak	Butterworth: bandpass of 0.5-26 Hz and 50th order

Table 3.12: Algorithm and filters applied to each fiducial point for lead V1.

Feature	Algorithm	Filter
R peak	Neurokit	Biosppy
P wave	DWT-Peak	Butterworth: bandpass of 0.5-20 Hz and 1st order
T peak	DWT-Peak	Butterworth: bandpass of 0.5-10 Hz and 1st order
T onset	DWT-Peak	Butterworth: bandpass of 0.5-20 Hz and 2nd order
T offset	Peak	Neurokit
QRS onset	DWT-Peak	Butterworth: bandpass of 0.5-27 Hz and 60th order
QRS offset	DWT-Peak	Butterworth: bandpass of 0.5-17 Hz and 40th order

Table 3.13: Algorithm and filters applied to each fiducial point for lead V2.

Feature	Algorithm	Filter
R peak	Neurokit	Biosppy
P wave	DWT-Peak	Butterworth: bandpass of 0.5-20 Hz and 1st order
T wave	DWT-Peak	Butterworth: bandpass of 0.5-10 Hz and 2nd order
QRS onset	DWT-Peak	Butterworth: bandpass of 0.5-25 Hz and 40th order
QRS offset	DWT-Peak	Butterworth: bandpass of 0.5-17 Hz and 70th order

Table 3.14: Algorithm and filters applied to each fiducial point for lead V3.

Feature	Algorithm	Filter
R peak	Neurokit	Biosppy
P wave	DWT-Peak	Butterworth: bandpass of 0.5-20 Hz and 2nd order
T peak	DWT-Peak	Butterworth: bandpass of 0.5-20 Hz and 1st order
T onset	DWT-Peak	Butterworth: bandpass of 0.5-10 Hz and 2nd order
T offset	DWT-Peak	Butterworth: bandpass of 0.5-10 Hz and 1st order
QRS onset	DWT-Peak	Butterworth: bandpass of 0.5-23 Hz and 30th order
QRS offset	DWT-Peak	Butterworth: bandpass of 0.5-19 Hz and 10th order

Table 3.15: Algorithm and filters applied to each fiducial point for lead V4.

Feature	Algorithm	Filter
R peak	Neurokit	Biosppy
P wave	DWT-Peak	Butterworth: bandpass of 0.5-20 Hz and 2nd order
T peak and offset	Peak	Butterworth: bandpass of 0.5-20 Hz and 1st order
T onset	DWT-Peak	Butterworth: bandpass of 0.5-10 Hz and 2nd order
QRS onset	DWT-Peak	Butterworth: bandpass of 0.5-26 Hz and 40th order
QRS offset	DWT-Peak	Butterworth: bandpass of 0.5-23 Hz and 60th order

Table 3.16: Algorithm and filters applied to each fiducial point for lead V5.

Feature	Algorithm	Filter
R peak	Neurokit	Neurokit
P wave	DWT-Peak	Butterworth: bandpass of 0.5-20 Hz and 2nd order
T peak and offset	DWT-Peak	Butterworth: bandpass of 0.5-20 Hz and 1st order
T onset	DWT-Peak	Butterworth: bandpass of 0.5-10 Hz and 2nd order
QRS onset	DWT-Peak	Butterworth: bandpass of 0.5-25 Hz and 60th order
QRS offset	DWT-Peak	Butterworth: bandpass of 0.5-27 Hz and 70th order

Table 3.17: Algorithm and filters applied to each fiducial point for lead V6.

Feature	Algorithm	Filter
R peak	Neurokit	Neurokit
P wave	DWT-Peak	Butterworth: bandpass of 0.5-20 Hz and 2nd order
T wave	DWT-Peak	Butterworth: bandpass of 0.5-10 Hz and 2nd order
QRS onset	DWT-Peak	Butterworth: bandpass of 0.5-26 Hz and 50th order
QRS offset	DWT-Peak	Butterworth: bandpass of 0.5-27 Hz and 70th order

3.3 Validation

The validation of the LoggerOne 5-lead ECG system (Fig. 3.1) was made against the COMEN gold standard (Fig. 3.2). The COMEN system is a medical device that can record ECG in both 12-lead and 5-lead configurations, though the 5-lead configuration was chosen for this work. Additionally, while the LoggerOne system has a 16-bit resolution and records signals at 500 Hz, the COMEN system has a 10-bit resolution but also records signals at 500 Hz. To obtain the ECGs, a CE-marked ECG simulator (Fig. 3.3) was used to simulate 51 different signals. The certificate of this simulator and the COMEN certificate are presented in Appendixes A.3 and A.4, respectively.

Figure 3.1: LoggerOne 5-lead system.

Figure 3.2: COMEN system, SRN: CN-MF-000002236.

Figure 3.3: ECG signal simulator SECULIFE PS300.

3.3.1 Signal acquisition

Signal acquisition had a duration of approximately 30 seconds for each record and was done using DIY electrodes (Fig. 3.4) that permitted recording the simulator signals simultaneously by both devices. LoggerOne 5-lead system records leads I, II, and two precordial leads, whereas the COMEN system for 5-leads records leads I, II, and one precordial lead.

To validate all leads (except leads III, aVF, aVL, and aVR, i.e., leads that are computed using the others), all signals had to be recorded six times, one for each precordial lead. Since limb lead signals are available for each of these six configurations, we can choose any records to validate them; in this case, the records made with lead V6 were chosen because all of the records have at least 30 seconds of signal for each simulator variation.

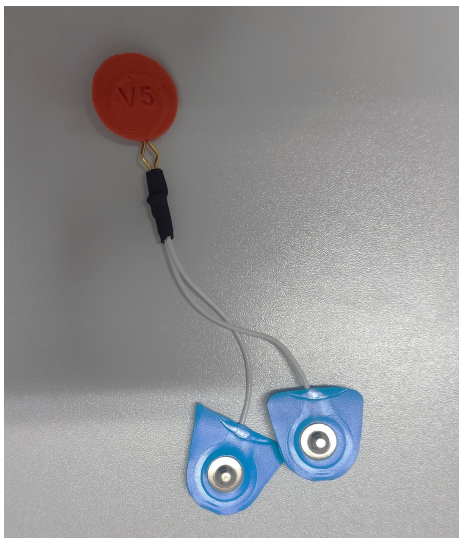

Figure 3.4: ECG electrode that allows recording from two devices.

Using the simulator, it was possible to simulate 51 different signals, varying five different parameters: HR, R peak amplitude, ST elevation, age (adult or pediatric), and specific arrhythmias. Table 2 shows the different parameters for each simulated signal. The following Table 3.18 shows the parameters chosen for each signal.

Table 3.18: Different parameters of each simulated signal.

No.	HR	Amplitude (mV)	ST elevation (mV)	Arrhythmia	Age
1	30	1	0	NA	Adult
2	40	1	0	NA	Adult
3	45	1	0	NA	Adult
4	60	1	0	NA	Adult
5	80	1	0	NA	Adult
6	90	1	0	NA	Adult
7	100	1	0	NA	Adult
8	120	1	0	NA	Adult
9	140	1	0	NA	Adult
10	160	1	0	NA	Adult
11	180	1	0	NA	Adult
12	200	1	0	NA	Adult
13	220	1	0	NA	Adult
14	30	1	0	NA	Pediatric
15	40	1	0	NA	Pediatric
16	60	1	0	NA	Pediatric
17	80	1	0	NA	Pediatric
18	100	1	0	NA	Pediatric
19	120	1	0	NA	Pediatric
20	140	1	0	NA	Pediatric
21	NA	1	0	Atrial Tach	Adult
22	NA	1	0	Paroxysmal Atrial Tach	Adult
23	NA	1	0	Supravent Tach	Adult
24	NA	1	0	Sinus Arrythmia	Adult
25	NA	1	0	Nodal Rhythm	Adult
26	NA	1	0	Atrial PAC	Adult
27	NA	1	0	Nodal PNC	Adult
28	NA	1	0	1st degree HB	Adult
29	NA	1	0	2nd degree HB	Adult
30	NA	1	0	3rd degree HB	Adult
31	NA	1	0	Rt Bundle Branch Block	Adult
32	NA	1	0	Lf Bundle Branch Block	Adult
33	80	0.5	-0.1	ND	Adult
34	80	1.5	-0.1	ND	Adult
35	80	1	-0.1	ND	Adult
36	80	2	-0.1	ND	Adult
37	80	0.5	-0.05	ND	Adult
38	80	1.5	-0.05	ND	Adult
39	80	1	-0.05	ND	Adult
40	80	2	-0.05	ND	Adult
41	80	0.5	0	ND	Adult
42	80	1.5	0	ND	Adult
43	80	2	0	ND	Adult
44	80	0.5	0.05	ND	Adult
45	80	1.5	0.05	ND	Adult
46	80	1	0.05	ND	Adult
47	80	2	0.05	ND	Adult
48	80	0.5	0.01	ND	Adult
49	80	1.5	0.01	ND	Adult
50	80	1	0.01	ND	Adult
51	80	2	0.01	ND	Adult

3.3.2 Normalization

All signals were normalized using equation 2.17 before proceeding to the validation stage. Figs. 3.5 and 3.6 show signals of both devices before and after the normalization step.

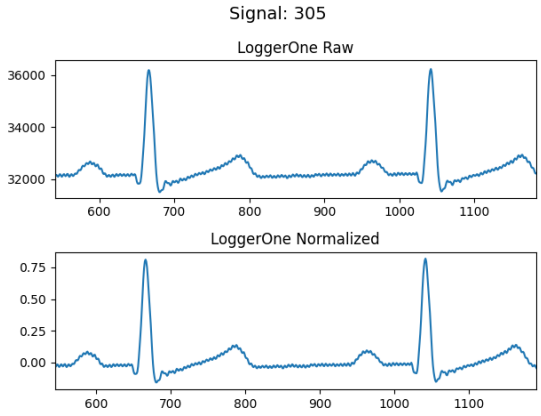

Figure 3.5: LoggerOne signal before and after normalization.

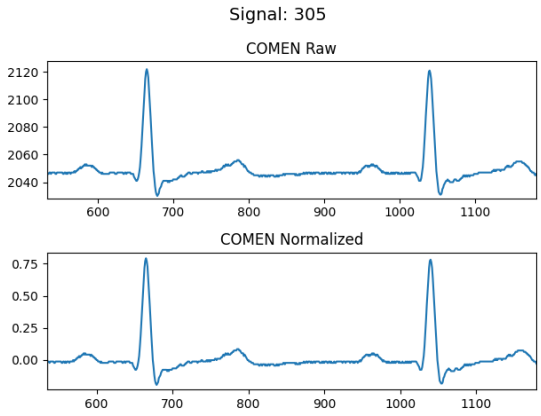

Figure 3.6: COMEN signal before and after normalization.

3.3.3 Validation metrics

To validate the device, the algorithms previously chosen were used for each lead signals for both devices. Before proceeding, all results were verified, and fiducial points that differed considerably from their supposed location were disregarded. An example of this is a P wave that was detected in the T wave of the previous beat. After all beats were verified, EGC typical intervals and segments duration were computed in samples to be validated. The advantage of using these intervals instead of the wave points is that it disregards synchronism problems. Additionally, the intervals from P to P peak and T to T peak between 2 beats and the interval between the T offset and the P onset of the next beat were also computed and validated.

The validation metrics chosen to validate both ECG segments and intervals were LoA, ICC, and scatter plots. For the LoA method, the differences between devices were tested using the Shapiro-Wilk test to verify if they were normally distributed; since they were not, the differences were logarithmically transformed. A second test revealed that the transformed differences were also not normally distributed, so the non-transformed differences were used to calculate LoA, considering 95% confidence intervals. Regarding the ICC, this method was also applied, considering 95% confidence intervals, and Ko and Li's guidelines were chosen to interpret the results. Scatter plots were also used to detect and eliminate outliers derived from the algorithm's errors. Additionally, histograms of the differences between devices were used as support for the other metrics.

As a way to evaluate the signal as a whole, a morphological comparison was made. Signals were normalized and a Savitzky-Golay filter was applied to smooth the ECG signal to reduce the effects of difference in bit resolution. The Savitzky-Golay filter applied had a window length of 17 and was of 4^{th} order, this filter was chosen regarding study [58] that compared different Savitzky-Golay for ECG smoothing and denoising. The smooth signals were then segmented in beats using P onsets and T offsets to calculate the segmenting window, if an algorithm failed to find these fiducial points, a window was selected manually for the respective signal. Finally, the sample SD between LoggerOne and COMEN systems was calculated for all leads using equation 3.1.

Chapter 4

Results and discussion

The chapter presents and discusses the evaluation results of the filters and algorithms tested for each lead, as well as the results of the validation against the gold standard. The results are presented in sections subsections:

- Feature extraction results: Presents the performance of the algorithms used as well as the filters used for each lead. Additionally, specific tests for P and T wave points and later for the QRS complex are presented and addressed;
- Validation results: Presents the validation results in the form of scatter plots, LoA plots, ICC, and a morphological comparison. A discussion on limitations and the results is also made.

4.1 Feature extraction results

4.1.1 Preliminary tests

The Peak, CWT, and DWT algorithms were first put to a preliminary test. For these tests, signals from Lead I were chosen. These tests led to two conclusions: first, the CWT algorithm is not viable since it caused errors and did not work for the majority of signals; second, the Peak method usually performed better for P and T waves than DWT, especially for P and T peaks. The DWT algorithm was modified to accept P and T peaks from the Peak method as a result of the latter conclusion. Both P and T waves delivered improved results as a result of these modifications. Results for all three algorithms are shown in the next Tables 4.1, 4.2, and 4.3.

Table 4.1: Results for NK's R peak and Peak algorithms using the filter "neurokit".

	P onset	**P peak**	**R peak**	**T peak**	**T offset**
Total points	1364	1364	1528	1231	1231
TP	1253	1344	1528	1217	1201
FN	4	4	0	5	5
FP	107	16	0	9	25
FP-R	-	-	2	-	-
Se	99.68	99.70	100	99.59	99.59
+P	92.13	98.82	100	99.27	97.96
+P-R	-	-	99.87	-	-
Mean	2.00	-1.30	-0.78	-0.52	4.27
SD	18.96	6.99	1.01	7.52	12.60

Table 4.2: Results for NK's R peak and DWT algorithms using the filter "neurokit".

	P wave			QRS complex			T wave		
	Onset	**Peak**	**Offset**	**Onset**	**Peak**	**Offset**	**Onset**	**Peak**	**Offset**
Total points	1364	1364	1364	1528	1528	1528	1231	1231	1231
TP	1285	1251	1226	1330	1528	1375	1100	1123	1117
FN	3	1	1	14	0	73	11	4	4
FP	76	112	137	184	0	80	120	104	110
FP-R	-	-	-	-	3	-	-	-	-
Se	99.77	99.92	99.92	98.96	100	94.96	99.01	99.65	99.64
+P	94.42	91.78	89.95	87.85	100	94.50	90.16	91.52	91.04
+P-R	-	-	-	-	99.80	-	-	-	-
Mean	1.42	5.56	5.53	14.08	-0.78	-12.11	-10.82	7.15	13.10
SD	18.78	18.41	20.91	16.15	1.01	19.97	22.79	24.18	30.42

Table 4.3: Results for NK's R peak and DWT-Peak algorithms using the filter "neurokit".

	P wave			QRS complex			T wave		
	Onset	**Peak**	**Offset**	**Onset**	**Peak**	**Offset**	**Onset**	**Peak**	**Offset**
Total points	1364	1364	1364	1528	1528	1528	1231	1231	1231
TP	1334	1344	1348	1329	1528	1383	1141	1199	1187
FN	7	4	4	46	0	37	8	5	5
FP	23	16	12	153	0	108	64	9	21
FP-R	-	-	-	-	2	-	-	-	-
Se	99.48	99.70	99.70	96.65	100	97.39	99.31	99.59	99.59
+P	98.31	98.82	99.12	89.68	100	92.76	94.77	99.27	98.27
+P-R	-	-	-	-	99.85	-	-	-	-
Mean	-3.94	-1.31	-1.65	13.25	-0.78	-13.97	-16.32	-0.52	5.43
SD	11.27	6.99	9.27	15.33	1.01	23.99	13.29	7.52	11.62

As it is possible to see, the DWT-Peak method achieves greater results for P and T waves than either the DWT or Peak methods. When it comes to the QRS complex, DWT-Peak and DWT algorithms produce similar results; in some cases, both algorithms give the same results for QRS complex bounds. However, since these algorithms use P and T peaks to calculate the search window for the QRS complex, DWT-Peak was preferred over the DWT algorithm. Overall, the DWT-Peak method is still the most viable because it finds all ECG fiducial points and shows promising results; nevertheless, since the improvements for T wave are just slightly better when compared to the Peak method, this method will still be employed in further tests.

With the latter results in mind, the next step was to test NK's R peak method with all NK's toolbox filters and evaluate the best R peak results. The best-performing filter was then chosen; usually filters "Neurokit", "Biosppy", and "Engzeemod2012" delivered the best results. Then the optimal R peaks were passed as arguments to Peak and DWT-Peak for further testing to determine the best filter for each fiducial point. The optimal SD results for each fiducial point, however, were usually above the corresponding limits for the P wave and, in particular, for the QRS complex. This prompted the testing of additional filters in an attempt to achieve better results.

4.1.2 P and T wave improvements

With P and T waves needing improvements, P wave regarding the SD and T wave regarding T onset's mean, some other tests were conducted considering Elgendi *et al.* [22] findings and the power spectra of an ECG. Considering these factors, Butterworth bidirectional band-pass filters with passbands of 0.5-10 Hz and 0.5-20 Hz and orders between 1st to 4th order were tested for the DWT-Peak algorithm.

Regarding P wave results, filters with a passband of 0.5-20 Hz and 1st or 2nd order achieve greater results, except for Lead I, where the best results for P peak were achieved with a 0.5-10 Hz bandpass filter of 4th order and Leads V4 and V6 bounds were achieved with 0.5-10 Hz bandpass filters of 3rd and 4th order. Nevertheless, as for leads V4 and V6, when the filters were applied to the simulated signals they didn't perform well, therefore being replaced with a 0.5-20 Hz bandpass filter of 2nd order. When comparing performance between filters (Table 4.4 and 4.5), SD results are worse; however, for both leads, SD values do not exceed the reference values for the respective lead, even if they exceed the average reference. Moreover, the Se and +P difference between each filter is less than 1% for either lead; given these two factors, the change of filter seems appropriate. The mean is the most significant difference. The absolute mean for each fiducial point was less than 15 ms in the first approach, but this number reduced significantly with the new filters, and this difference is likely what influenced the outcome on the simulated signals. When we compare the old filters for either lead (Fig. 4.1 and 4.3) to the new filters (Fig. 4.2 and 4.4), we can clearly see a change in P bounds; the new filters perform better. This disparity in outcomes is consistent across all simulated signals recorded.

Table 4.4: Comparison between filters for P wave on Lead V4.

	P onset		**P offset**	
Filter	0.5-10 Hz 3rd order	0.5-20 Hz 2nd order	0.5-10 Hz 4Th order	0.5-20 Hz 2nd order
Mean	5.33	-0.30	-8.94	-5.35
SD	9.73	12.21	10.36	12.40
SD V4-V6[1]	**12.6**		**13.6**	

[1] Reference values from CSE working party [31]

Table 4.5: Comparison between filters for P wave on Lead V6.

	P onset		**P offset**	
Filter	0.5-10 Hz 3rd order	0.5-20 Hz 2nd order	0.5-10 Hz 4Th order	0.5-20 Hz 2nd order
Mean	4.50	-0.89	-9.83	-6.45
SD	9.91	11.46	9.98	11.64
SD V4-V6[1]	**12.6**		**13.6**	

[1] Reference values from CSE working party [31]

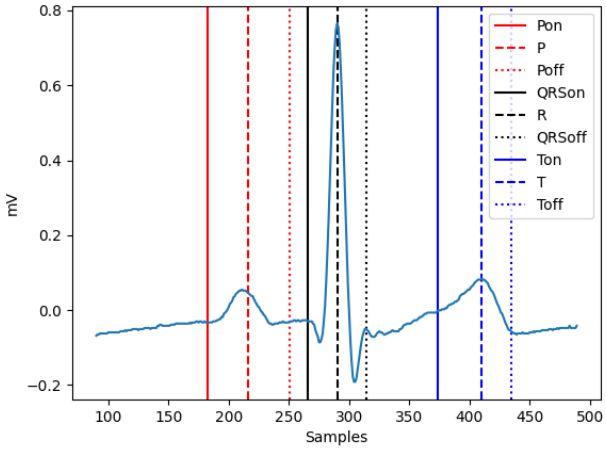

Figure 4.1: P bounds results with 0.5-10 Hz passband for Lead V4.

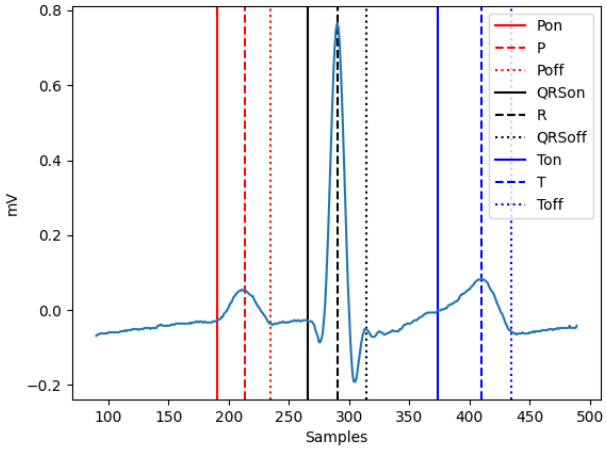

Figure 4.2: P bounds results with 0.5-20 Hz passband for Lead V4.

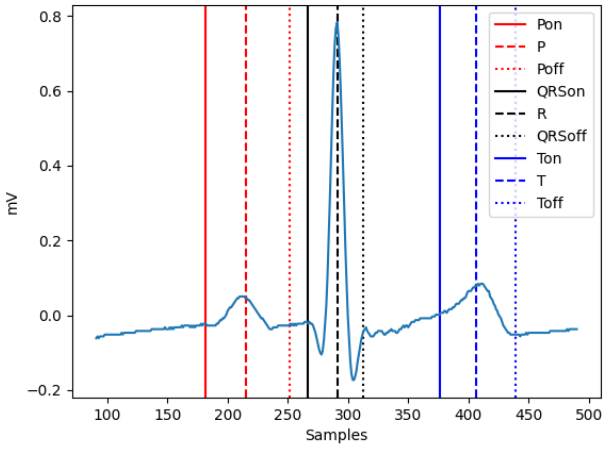

Figure 4.3: P bounds results with 0.5-10 Hz passband for Lead V6.

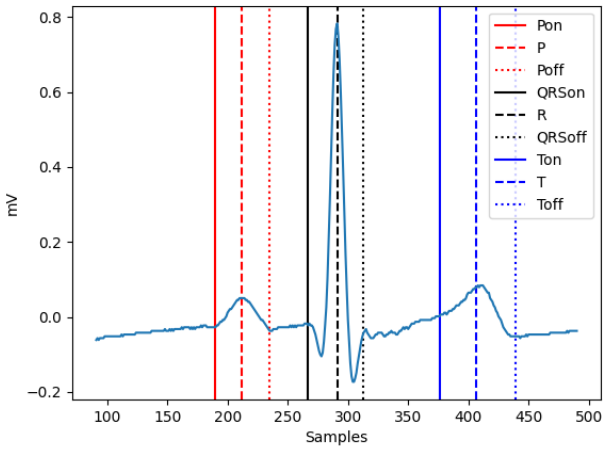

Figure 4.4: P bounds results with 0.5-20 Hz passband for Lead V6.

As for the T wave, both passbands tested delivered good results, with filters of 1st and 2nd orders outperforming those of 3rd and 4th orders. Furthermore, and as expected, T onsets for all leads reveal inferior results, with an absolute mean usually greater than 10 ms, and +P less than 95% for the majority of leads. This is to be expected given that the boundary between the ST segment and the T wave is hardly discernible [15].

4.1.3 QRS boundaries improvements

With the available filters in NK's toolbox, it was not possible to obtain satisfactory results for QRS onsets and offsets since the SD was a lot higher than the reference SD for every filter. So once again, considering Elgendi *et al.* findings [22] and the power spectra of an ECG, new Butterworth bandpass filters were tested.

Higher-order filters appeared to produce better results throughout an initial evaluation, therefore an order of 50 was chosen for the initial tests. Setting this same order for every filter, various Butterworth bidirectional bandpass filters with a fixed low-cut of 0.5 Hz were tested. As for the high-cut, it varied between 20 Hz and 35 Hz for both QRS onset and offset, except for leads V1-V3 QRS offset that showed better results with lower frequencies, so the high-cut varied from 16 Hz to 25 Hz (Tables 4.6 to 4.21). To choose the appropriate frequency for each lead, the mean and SD were the most important factors. Since Se and +P change a lot with the order of the filter and the order is to be tested in the next step, a minimum of 95% was selected as a limit when choosing the frequency. With these considerations in mind, the adequate frequencies chosen are presented in Table 4.22. Overall frequencies range from 17 to 27 Hz, with higher frequencies of 25 to 27 Hz being the most prominent in all leads, with the exception of leads V1-V4 QRS offset, where lower high-cut frequencies of 17 to 23 Hz presented better results.

Table 4.6: Results for Lead I QRS onset when varying frequency.

	20 Hz	**23 Hz**	**25 Hz**	**26 Hz**	**27 Hz**	**30 Hz**	**35 Hz**
Total points	1528	1528	1528	1528	1528	1528	1528
TP	1522	1512	1501	1495	1491	1480	1466
FN	0	9	22	28	32	34	30
FP	6	7	5	5	5	14	32
Se	100	99.41	98.56	98.16	97.90	97.75	97.99
+P	99.61	99.54	99.67	99.67	99.67	99.06	97.86
Mean	7.56	4.28	2.56	1.85	1.30	0.47	1.44
SD	5.90	6.03	5.78	5.74	5.80	6.89	9.94

Table 4.7: Results for Lead I QRS offset when varying frequency.

	20 Hz	**23 Hz**	**25 Hz**	**26 Hz**	**27 Hz**	**30 Hz**	**35 Hz**
Total points	1528	1528	1528	1528	1528	1528	1528
TP	1527	1523	1522	1520	1520	1516	1512
FN	1	4	6	7	8	12	15
FP	0	1	0	1	0	0	1
Se	99.93	99.74	99.61	99.54	99.48	99.21	99.02
+P	100	99.93	100	99.93	100	100	99.93
Mean	-6.03	-2.92	-1.28	-0.66	-0.14	0.43	0.56
SD	5.63	5.70	5.62	5.77	5.94	6.80	7.94

Table 4.8: Results for Lead II QRS onset when varying frequency.

	20 Hz	**23 Hz**	**25 Hz**	**26 Hz**	**27 Hz**	**30 Hz**	**35 Hz**
Total points	1505	1505	1505	1505	1505	1505	1505
TP	1500	1496	1501	1497	1493	1467	1464
FN	1	6	3	3	4	14	19
FP	4	3	1	5	8	24	22
Se	99.93	99.60	99.80	99.80	99.73	99.05	98.72
+P	99.73	99.80	99.93	99.67	99.47	98.39	98.52
Mean	7.22	3.75	2.05	1.57	1.18	0.79	0.96
SD	4.40	4.42	4.27	4.84	5.61	7.78	9.04

Table 4.9: Results for Lead II QRS offset when varying frequency.

	20 Hz	**23 Hz**	**25 Hz**	**26 Hz**	**27 Hz**	**30 Hz**	**35 Hz**
Total points	1505	1505	1505	1505	1505	1505	1505
TP	1500	1500	1497	1499	1497	1500	1486
FN	1	1	3	2	3	2	7
FP	4	4	5	4	5	3	12
Se	99.93	99.93	99.80	99.87	99.80	99.87	99.53
+P	99.73	99.73	99.67	99.73	99.67	99.80	99.20
Mean	-5.70	-2.40	-0.76	-0.20	0.11	0.84	0.99
SD	6.34	6.29	7.33	6.99	7.91	7.93	11.05

Table 4.10: Results for Lead V1 QRS onset when varying frequency.

	20 Hz	**23 Hz**	**25 Hz**	**26 Hz**	**27 Hz**	**30 Hz**	**35 Hz**
Total points	1515	1515	1515	1515	1515	1515	1515
TP	1512	1502	1482	1476	1476	1459	1458
FN	3	13	33	39	39	56	57
FP	0	0	0	0	0	0	0
Se	99.80	99.14	97.82	97.43	97.43	96.30	96.24
+P	100	100	100	100	100	100	100
Mean	13.41	9.30	7.15	6.20	5.40	4.00	3.73
SD	6.51	6.10	6.06	5.95	5.84	6.34	7.62

Table 4.11: Results for Lead V1 QRS offset when varying frequency.

	16 Hz	**17 Hz**	**18 Hz**	**19 Hz**	**20 Hz**	**23 Hz**	**25 Hz**
Total points	1521	1521	1521	1521	1521	1521	1521
TP	1507	1508	1510	1495	1506	1508	1498
FN	12	11	10	13	14	13	15
FP	2	2	1	0	1	0	8
Se	99.21	99.28	99.34	99.14	99.08	99.15	99.01
+P	99.87	99.87	99.93	100	99.93	100	99.47
Mean	-0.98	0.12	1.17	2.10	2.89	4.63	5.68
SD	7.63	7.64	7.19	6.82	6.65	6.39	6.76

Table 4.12: Results for Lead V2 QRS onset when varying frequency.

	20 Hz	**23 Hz**	**25 Hz**	**26 Hz**	**27 Hz**	**30 Hz**	**35 Hz**
Total points	1492	1492	1492	1492	1492	1492	1492
TP	1484	1459	1439	1424	1401	1367	1352
FN	8	32	50	64	84	116	115
FP	0	1	3	4	7	9	25
Se	99.46	97.85	96.64	95.70	94.34	92.18	92.16
+P	100	99.93	99.79	99.72	99.50	99.35	98.18
Mean	11.29	7.17	5.32	4.64	4.14	3.26	3.94
SD	5.42	5.26	5.57	5.69	6.50	7.51	9.87

Table 4.13: Results for Lead V2 QRS offset when varying frequency.

	16 Hz	**17 Hz**	**18 Hz**	**19 Hz**	**20 Hz**	**23 Hz**	**25 Hz**
Total points	1499	1499	1499	1499	1499	1499	1499
TP	1496	1496	1496	1496	1495	1489	1488
FN	3	3	3	3	4	9	9
FP	0	0	0	0	0	1	2
Se	99.80	99.80	99.80	99.80	99.73	99.40	99.40
+P	100	100	100	100	100	99.93	99.87
Mean	-1.37	-0.10	1.01	2.01	2.79	4.68	5.56
SD	6.20	6.02	5.83	5.71	5.42	5.56	5.56

Table 4.14: Results for Lead V3 QRS onset when varying frequency.

	20 Hz	**23 Hz**	**25 Hz**	**26 Hz**	**27 Hz**	**30 Hz**	**35 Hz**
Total points	1521	1521	1521	1521	1521	1521	1521
TP	1510	1493	1477	1466	1454	1396	1379
FN	8	27	39	49	56	92	93
FP	3	1	5	6	11	33	49
Se	99.47	98.22	97.43	96.77	96.29	93.82	93.68
+P	99.80	99.93	99.66	99.59	99.25	97.69	96.57
Mean	9.85	5.83	4.04	3.38	2.97	3.12	3.92
SD	4.75	4.91	5.84	6.30	7.19	10.04	11.93

Table 4.15: Results for Lead V3 QRS offset when varying frequency.

	16 Hz	**17 Hz**	**18 Hz**	**19 Hz**	**20 Hz**	**23 Hz**	**25 Hz**
Total points	1526	1526	1526	1526	1526	1526	1526
TP	1525	1525	1525	1525	1524	1524	1520
FN	1	1	1	1	1	2	6
FP	0	0	0	0	1	0	0
Se	99.93	99.93	99.93	99.93	99.93	99.87	99.61
+P	100	100	100	100	99.93	100	100
Mean	-3.31	-1.92	-0.75	0.29	1.16	3.24	4.17
SD	6.45	6.29	6.16	6.00	5.95	5.66	5.62

Table 4.16: Results for Lead V4 QRS onset when varying frequency.

	20 Hz	**23 Hz**	**25 Hz**	**26 Hz**	**27 Hz**	**30 Hz**	**35 Hz**
Total points	1496	1496	1496	1496	1496	1496	1496
TP	1494	1474	1450	1417	1397	1327	1292
FN	1	22	44	74	91	160	177
FP	1	0	2	5	8	9	27
Se	99.93	98.53	97.05	95.04	93.88	89.24	87.95
+P	99.93	100	99.86	99.65	99.43	99.33	97.95
Mean	8.46	4.60	2.75	2.00	1.55	0.46	2.21
SD	3.86	3.79	4.28	4.88	5.59	7.02	10.39

Table 4.17: Results for Lead V4 QRS offset when varying frequency.

	17 Hz	**18 Hz**	**19 Hz**	**20 Hz**	**23 Hz**	**25 Hz**	**26 Hz**
Total points	1496	1496	1496	1496	1496	1496	1496
TP	1496	1496	1496	1496	1494	1482	1481
FN	0	0	0	0	2	14	15
FP	0	0	0	0	0	0	0
Se	100	100	100	100	99.87	99.06	99.00
+P	100	100	100	100	100	100	100
Mean	-6.47	-5.05	-3.80	-2.57	0.18	1.55	2.07
SD	6.94	6.74	6.59	6.50	6.26	6.09	6.00

Table 4.18: Results for Lead V5 QRS onset when varying frequency.

	20 Hz	**23 Hz**	**25 Hz**	**26 Hz**	**27 Hz**	**30 Hz**	**35 Hz**
Total points	1536	1536	1536	1536	1536	1536	1536
TP	1524	1505	1478	1452	1424	1331	1366
FN	7	28	56	81	110	200	146
FP	5	3	2	3	2	5	24
Se	99.54	98.17	96.35	94.72	92.83	86.94	90.34
+P	99.67	99.80	99.86	99.79	99.86	99.63	98.27
Mean	7.72	4.12	2.39	1.68	1.10	-0.42	0.34
SD	4.79	4.38	4.27	4.46	4.22	5.61	8.22

Table 4.19: Results for Lead V5 QRS offset when varying frequency.

	20 Hz	**23 Hz**	**25 Hz**	**26 Hz**	**27 Hz**	**30 Hz**	**35 Hz**
Total points	1536	1536	1536	1536	1536	1536	1536
TP	1533	1530	1517	1503	1504	1504	1502
FN	2	5	18	32	31	31	27
FP	1	1	1	1	1	1	7
Se	99.87	99.67	98.83	97.92	97.98	97.98	98.23
+P	99.93	99.93	99.93	99.93	99.93	99.93	99.54
Mean	-5.47	-2.36	-0.90	-0.27	0.20	1.37	1.92
SD	5.88	5.91	5.68	5.66	5.73	5.93	8.41

Table 4.20: Results for Lead V6 QRS onset when varying frequency.

	20 Hz	**23 Hz**	**25 Hz**	**26 Hz**	**27 Hz**	**30 Hz**	**35 Hz**
Total points	1534	1534	1534	1534	1534	1534	1534
TP	1520	1512	1496	1473	1441	1399	1456
FN	7	19	37	60	92	132	70
FP	7	3	1	1	1	3	8
Se	99.54	98.76	97.59	96.09	94.00	91.38	95.41
+P	99.54	99.80	99.93	99.93	99.93	99.79	99.45
Mean	7.33	4.14	2.55	1.93	1.49	0.28	0.64
SD	4.81	4.09	3.73	3.62	4.18	5.13	7.10

Table 4.21: Results for Lead V6 QRS offset when varying frequency.

	20 Hz	**23 Hz**	**25 Hz**	**26 Hz**	**27 Hz**	**30 Hz**	**35 Hz**
Total points	1534	1534	1534	1534	1534	1534	1534
TP	1532	1521	1511	1508	1502	1500	1500
FN	1	12	22	24	31	31	30
FP	1	1	1	2	1	3	4
Se	99.93	99.22	98.56	98.43	97.98	97.98	98.04
+P	99.93	99.93	99.93	99.87	99.93	99.80	99.73
Mean	-6.53	-3.31	-1.68	-1.15	-0.51	-0.13	0.07
SD	5.35	5.26	5.29	6.14	5.36	7.29	8.24

Table 4.22: Frequencies chosen for each lead.

Lead	I	II	V1	V2	V3	V4	V5	V6
QRS onset	27 Hz	26 Hz	27 Hz	25 Hz	23 Hz	26 Hz	25 Hz	26 Hz
QRS offset	27 Hz	26 Hz	17 Hz	17 Hz	19 Hz	23 Hz	27 Hz	27 Hz

After deciding on the frequencies for each lead and fiducial point, the next step was to try out various orders. For each lead, orders ranging from 5 to 80 were tested (Tables 4.23 to 4.38). This time, when determining the appropriate order mean, SD, Se, and +P were all considered, with the goal of achieving the lowest possible value for all of these variables. We obtain better results with higher-order filters (Table 4.39), and the SD for each fiducial point for each lead does not exceed the reference SD.

Table 4.23: Results for Lead I QRS onset when varying order.

	5th	**10th**	**20th**	**30th**	**40th**	**50th**	**60th**	**70th**	**80th**
Total points	1528	1528	1528	1528	1528	1528	1528	1528	1528
TP	1509	1492	1487	1490	1493	1491	1491	1485	1490
FN	8	28	35	33	30	32	32	38	33
FP	11	8	6	5	5	5	5	5	5
Se	99.47	98.16	97.70	97.83	98.03	97.90	97.90	97.50	97.83
+P	99.28	99.47	99.60	99.67	99.67	99.67	99.67	99.66	99.67
Mean	2.74	1.68	1.37	1.29	1.28	1.30	1.31	1.29	1.32
SD	6.65	6.33	5.94	5.77	5.75	5.80	5.80	5.77	5.80

Table 4.24: Results for Lead I QRS offset when varying order.

	5th	**10th**	**20th**	**30th**	**40th**	**50th**	**60th**	**70th**	**80th**
Total points	1528	1528	1528	1528	1528	1528	1528	1528	1528
TP	1506	1510	1515	1517	1519	1520	1518	1519	1516
FN	20	18	13	11	9	8	9	8	11
FP	2	0	0	0	0	0	1	1	1
Se	98.69	98.82	99.15	99.28	99.41	99.48	99.41	99.48	99.28
+P	99.87	100.00	100.00	100.00	100.00	100.00	99.93	99.93	99.93
Mean	-1.49	-0.42	-0.24	-0.16	-0.15	-0.14	-0.20	-0.22	-0.17
SD	5.63	5.86	5.93	5.85	5.85	5.94	6.02	6.01	6.01

Table 4.25: Results for Lead II QRS onset when varying order.

	5th	**10th**	**20th**	**30th**	**40th**	**50th**	**60th**	**70th**
Total points	1505	1505	1505	1505	1505	1505	1505	1505
TP	1481	1488	1496	1499	1498	1497	1498	1497
FN	4	5	3	1	2	3	3	4
FP	20	12	6	5	5	5	4	4
Se	99.73	99.67	99.80	99.93	99.87	99.80	99.80	99.73
+P	98.67	99.20	99.60	99.67	99.67	99.67	99.73	99.73
Mean	3.56	2.23	1.70	1.63	1.58	1.57	1.54	1.54
SD	7.18	6.06	5.04	4.97	4.84	4.84	4.73	4.74

Table 4.26: Results for Lead II QRS offset when varying order.

	5th	10th	20th	30th	40th	50th	60th	70th
Total points	1505	1505	1505	1505	1505	1505	1505	1505
TP	1478	1492	1497	1498	1498	1499	1499	1497
FN	2	2	3	3	3	2	2	3
FP	25	11	5	4	4	4	4	5
Se	99.86	99.87	99.80	99.80	99.80	99.87	99.87	99.80
+P	98.34	99.27	99.67	99.73	99.73	99.73	99.73	99.67
Mean	-2.79	-0.96	-0.36	-0.25	-0.18	-0.20	-0.20	-0.18
SD	14.41	10.07	7.21	7.07	7.01	6.99	7.01	7.03

Table 4.27: Results for Lead V1 QRS onset when varying order.

	5th	10th	20th	30th	40th	50th	60th	70th
Total points	1515	1515	1515	1515	1515	1515	1515	1515
TP	1439	1455	1461	1466	1472	1476	1478	1477
FN	76	60	54	49	43	39	37	38
FP	0	0	0	0	0	0	0	0
Se	94.98	96.04	96.44	96.77	97.16	97.43	97.56	97.49
+P	100	100	100	100	100	100	100	100
Mean	6.87	5.82	5.50	5.44	5.40	5.40	5.36	5.37
SD	6.23	5.90	5.85	5.84	5.84	5.84	5.83	5.84

Table 4.28: Results for Lead V1 QRS offset when varying order.

	5th	10th	20th	30th	40th	50th	60th	70th
Total points	1521	1521	1521	1521	1521	1521	1521	1521
TP	1498	1501	1508	1509	1510	1508	1506	1509
FN	21	17	12	11	10	11	13	10
FP	2	3	1	1	1	2	2	2
Se	98.62	98.88	99.21	99.28	99.34	99.28	99.14	99.34
+P	99.87	99.80	99.93	99.93	99.93	99.87	99.87	99.87
Mean	0.39	0.22	0.15	0.14	0.15	0.12	0.14	0.10
SD	7.42	7.46	7.42	7.43	7.42	7.64	7.61	7.69

Table 4.29: Results for Lead V2 QRS onset when varying order.

	5th	10th	20th	30th	40th	50th	60th	70th	80th
Total points	1492	1492	1492	1492	1492	1492	1492	1492	1492
TP	1386	1400	1423	1431	1444	1439	1436	1441	1441
FN	97	83	63	57	46	50	53	47	47
FP	9	9	6	4	2	3	3	4	4
Se	93.46	94.40	95.76	96.17	96.91	96.64	96.44	96.84	96.84
+P	99.35	99.36	99.58	99.72	99.86	99.79	99.79	99.72	99.72
Mean	7.18	5.93	5.43	5.36	5.32	5.32	5.33	5.36	5.30
SD	6.39	6.20	5.84	5.74	5.53	5.57	5.60	5.79	5.88

Table 4.30: Results for Lead V2 QRS offset when varying order.

	5th	10th	20th	30th	40th	50th	60th	70th	80th
Total points	1499	1499	1499	1499	1499	1499	1499	1499	1499
TP	1496	1497	1496	1497	1496	1496	1498	1498	1496
FN	2	2	3	2	3	3	1	1	3
FP	1	0	0	0	0	0	0	0	0
Se	99.87	99.87	99.80	99.87	99.80	99.80	99.93	99.93	99.80
+P	99.93	100	100	100	100	100	100	100	100
Mean	0.04	-0.07	-0.09	-0.10	-0.10	-0.10	-0.10	-0.10	-0.09
SD	6.14	6.10	5.99	6.01	6.01	6.02	6.02	6.02	6.04

Table 4.31: Results for Lead V3 QRS onset when varying order.

	5th	10th	20th	30th	40th	50th	60th	70th
Total points	1521	1521	1521	1521	1521	1521	1521	1521
TP	1477	1488	1493	1498	1496	1493	1497	1495
FN	31	29	24	22	24	27	23	25
FP	13	4	4	1	1	1	1	1
Se	97.94	98.09	98.42	98.55	98.42	98.22	98.49	98.36
+P	99.13	99.73	99.73	99.93	99.93	99.93	99.93	99.93
Mean	7.43	6.17	5.91	5.85	5.83	5.83	5.80	5.80
SD	5.84	5.01	5.04	4.92	4.91	4.91	4.90	4.86

Table 4.32: Results for Lead V3 QRS offset when varying order.

	5th	10th	20th	30th	40th	50th	60th	70th
Total points	1526	1526	1526	1526	1526	1526	1526	1526
TP	1521	1525	1525	1525	1525	1525	1526	1526
FN	4	1	1	1	1	1	0	0
FP	1	0	0	0	0	0	0	0
Se	99.74	99.93	99.93	99.93	99.93	99.93	100	100
+P	99.93	100	100	100	100	100	100	100
Mean	0.32	0.30	0.28	0.28	0.28	0.29	0.29	0.30
SD	6.03	5.94	5.96	5.98	5.99	6.00	6.02	6.02

Table 4.33: Results for Lead V4 QRS onset when varying order.

	5th	10th	20th	30th	40th	50th	60th	70th
Total points	1496	1496	1496	1496	1496	1496	1496	1496
TP	1350	1355	1390	1411	1423	1417	1419	1412
FN	134	133	98	82	70	74	75	79
FP	12	8	8	3	3	5	2	5
Se	90.97	91.06	93.41	94.51	95.31	95.04	94.98	94.70
+P	99.12	99.41	99.43	99.79	99.79	99.65	99.86	99.65
Mean	3.78	2.51	2.23	2.02	1.98	2.00	1.98	2.02
SD	6.71	5.38	5.25	4.67	4.63	4.88	4.58	4.96

Table 4.34: Results for Lead V4 QRS offset when varying order.

	5th	10th	20th	30th	40th	50th	60th	70th
Total points	1496	1496	1496	1496	1496	1496	1496	1496
TP	1493	1490	1494	1493	1493	1494	1495	1494
FN	3	6	2	3	3	2	1	2
FP	0	0	0	0	0	0	0	0
Se	99.80	99.60	99.87	99.80	99.80	99.87	99.93	99.87
+P	100	100	100	100	100	100	100	100
Mean	-0.08	0.14	0.20	0.21	0.21	0.18	0.18	0.19
SD	6.13	6.21	6.25	6.26	6.27	6.26	6.26	6.26

Table 4.35: Results for Lead V5 QRS onset when varying order.

	5th	10th	20th	30th	40th	50th	60th	70th	80th
Total points	1536	1536	1536	1536	1536	1536	1536	1536	1536
TP	1432	1452	1475	1481	1482	1478	1483	1482	1481
FN	100	82	60	53	52	56	52	54	55
FP	4	2	1	2	2	2	1	0	0
Se	93.47	94.65	96.09	96.54	96.61	96.35	96.61	96.48	96.42
+P	99.72	99.86	99.93	99.87	99.87	99.86	99.93	100	100
Mean	3.39	2.61	2.46	2.46	2.43	2.39	2.37	2.43	2.42
SD	4.08	4.14	4.11	4.24	4.37	4.27	4.15	3.95	3.89

Table 4.36: Results for Lead V5 QRS offset when varying order.

	5th	10th	20th	30th	40th	50th	60th	70th	80th
Total points	1536	1536	1536	1536	1536	1536	1536	1536	1536
TP	1510	1497	1499	1499	1499	1504	1504	1512	1503
FN	24	38	36	36	36	31	31	22	32
FP	2	1	1	1	1	1	1	2	1
Se	98.44	97.52	97.65	97.65	97.65	97.98	97.98	98.57	97.92
+P	99.87	99.93	99.93	99.93	99.93	99.93	99.93	99.87	99.93
Mean	-0.54	0.01	0.19	0.21	0.23	0.20	0.17	0.14	0.18
SD	5.66	5.67	5.66	5.68	5.68	5.73	5.83	5.81	5.79

Table 4.37: Results for Lead V6 QRS onset when varying order.

	5th	10th	20th	30th	40th	50th	60th	70th	80th
Total points	1534	1534	1534	1534	1534	1534	1534	1534	1534
TP	1462	1445	1450	1471	1473	1473	1468	1463	1472
FN	71	86	81	62	60	60	65	70	62
FP	1	3	3	1	1	1	1	1	0
Se	95.37	94.38	94.71	95.96	96.09	96.09	95.76	95.43	95.96
+P	99.93	99.79	99.79	99.93	99.93	99.93	99.93	99.93	100
Mean	2.94	2.27	2.00	1.95	1.90	1.93	1.90	1.86	1.89
SD	3.85	4.06	3.94	3.64	3.77	3.62	3.61	3.48	3.38

Table 4.38: Results for Lead V6 QRS offset when varying order.

	5th	10th	20th	30th	40th	50th	60th	70th	80th
Total points	1534	1534	1534	1534	1534	1534	1534	1534	1534
TP	1503	1503	1502	1504	1503	1502	1506	1509	1504
FN	30	31	31	29	30	31	26	23	27
FP	1	0	1	1	1	1	2	2	3
Se	98.04	97.98	97.98	98.11	98.04	97.98	98.30	98.50	98.24
+P	99.93	100.00	99.93	99.93	99.93	99.93	99.87	99.87	99.80
Mean	-1.74	-0.85	-0.60	-0.58	-0.58	-0.51	-0.61	-0.58	-0.67
SD	5.34	5.17	5.38	5.44	6.15	5.36	6.22	5.58	7.20

Table 4.39: Orders chosen for each lead.

Lead	I	II	V1	V2	V3	V4	V5	V6
QRS onset	40	30	60	40	30	40	60	50
QRS offset	50	50	40	70	60	60	70	70

4.1.4 Final results

After all testing has been completed, the final results for each lead may be found in Tables 4.40 to 4.47. Except for some P and T wave points in precordial leads, the majority of results for Se and +P were over 95%. In the case of V1, this is due to a smaller total number of fiducial points. Given that lead V1 has more inverted P and T waves, many waves have been excluded since the algorithms are unable to identify inverted waves. Furthermore, the T onset is a fiducial point of challenging detection, which explains why +P results for leads V1-V3 are less than 95%. In terms of mean values, all outcomes fell below the absolute limit of 15 ms, with T onset exhibiting the highest overall values. Finally, regarding the SD values, P onset exceeds the reference values in most leads (I, II, V1, V2, V3), and the P offset of leads V1 and V2 also surpasses the limits. However, P offset results may be derived from the lower number of total fiducial points. Only the QRS onset of leads V1 and V2 exceeds the reference value in the QRS complex. The SD of T offset for all leads not only remains below the reference value but also differs significantly.

Overall, the results are promising, especially given that the algorithm and toolbox used were not validated. The authors of NK's toolbox only presented one study for their R peak detection algorithm, and the results obtained here are consistent with that study. One of the most serious shortcomings of this algorithm is its inability to detect inverted waves. As a result, those waves were excluded, affecting lead V1. Because the sample size for this lead is so small, the results should not be considered optimal.

As for the limits considered for FP, ±75 seemed to be a higher-than-necessary limit. If we consider the length of a P wave (60 ms to 110 ms), for example, a P onset that the algorithm locates after the actual P peak is considered a TP. This may lead to an ambiguous number of FP and TP and, as a consequence, ambiguous Se and +P values.

The absolute mean has been found to be an important performance parameter. Even if

the SD values are within the reference values, fiducial points deviate significantly more if the absolute mean values are high (>5 ms) compared to when the absolute mean is 5 ms. In subsequent studies, the mean limits should be shorter and probably different for each fiducial point, as the SD reference values are. Choosing a new reference value for the mean, on the other hand, is rather subjective, so shortening it to 10 ms should be a good start.

Although the majority of the SD results are within reference values, the P bounds and QRS onsets still need to be optimized. Furthermore, two recommendations from the CSE working party were compromised: using the CSE database and calculating each fiducial point using three leads. Given that the CSE database is not online, the LUDB was used instead. As for the second recommendation, the use of three leads is merely a suggestion, and given that this work revolves around validating each lead individually, it was preferred to validate the algorithms individually as well. SD results may be improved in future studies if these recommendations are followed.

Table 4.40: Final results for Lead I.

	P wave			**QRS complex**			**T wave**		
	Onset	**Peak**	**Offset**	**Onset**	**Peak**	**Offset**	**Onset**	**Peak**	**Offset**
Total points	1364	1364	1364	1528	1528	1528	1231	1231	1231
TP	1336	1358	1349	1493	1528	1520	1211	1221	1218
FN	3	1	1	30	0	8	5	5	5
FP	25	5	14	5	0	0	15	5	8
FP-R	-	-	-	-	2	-	-	-	-
Se	99.78	99.93	99.93	98.03	100	99.48	99.59	99.59	99.59
+P	98.16	99.63	98.97	99.66	100	100	98.78	99.59	99.35
+P-R	-	-	-	-	99.87	-	-	-	-
Mean	-3.29	-0.69	-3.99	1.28	-0.78	-0.14	-10.18	-0.69	-1.68
SD	10.64	7.43	9.26	5.75	1.01	5.94	11.82	5.01	7.40
SD I-III[1]	8.0	-	12.8	7.8	-	12.4	-	-	32.8

[1]Reference values from CSE working party [31]

Table 4.41: Final results for Lead II.

	P wave			**QRS complex**			**T wave**		
	Onset	**Peak**	**Offset**	**Onset**	**Peak**	**Offset**	**Onset**	**Peak**	**Offset**
Total points	1347	1347	1347	1505	1505	1505	1253	1253	1253
TP	1314	1320	1319	1499	1505	1499	1216	1235	1230
FN	3	0	0	1	0	2	10	1	1
FP	10	7	8	5	0	4	27	17	22
FP-R	-	-	-	-	8	-	-	-	-
Se	99.77	100	100	99.93	100	99.87	99.18	99.92	99.92
+P	99.24	99.47	99.40	99.67	100	99.73	97.83	98.64	98.24
+P-R	-	-	-	-	99.47	-	-	-	-
Mean	-1.43	-0.99	-3.39	1.63	-0.96	-0.20	-9.80	-0.80	4.51
SD	8.08	5.48	9.85	4.97	1.14	6.99	14.27	10.70	13.27
SD I-III[1]	8.0	-	12.8	7.8	-	12.4	-	-	32.8

[1]Reference values from CSE working party [31]

Table 4.42: Final results for Lead V1.

	P wave			QRS complex			T wave		
	Onset	**Peak**	**Offset**	**Onset**	**Peak**	**Offset**	**Onset**	**Peak**	**Offset**
Total points	797	797	797	1515	1521	1521	537	529	529
TP	728	727	725	1478	1502	1510	453	483	495
FN	12	11	11	37	0	10	16	12	16
FP	57	59	61	0	19	1	60	34	18
FP-R	-	-	-	-	27	-	-	-	-
Se	98.38	98.51	98.51	97.56	100	99.34	96.59	97.58	96.87
+P	92.74	92.49	92.24	100	98.75	99.93	88.30	93.42	96.49
+P-R	-	-	-	-	98.23	-	-	-	-
Mean	-4.00	-4.00	-2.94	5.36	-1.58	0.15	-5.24	6.17	0.85
SD	20.18	20.13	19.06	5.83	5.11	7.42	29.46	19.18	17.79
SD V1-V3[1]	12.4	-	14.4	5.2	-	9.4	-	-	28.6

[1]Reference values from CSE working party [31]

Table 4.43: Final results for Lead V2.

	P wave			QRS complex			T wave		
	Onset	**Peak**	**Offset**	**Onset**	**Peak**	**Offset**	**Onset**	**Peak**	**Offset**
Total points	1208	1209	1209	1492	1499	1499	1185	1185	1185
TP	1095	1098	1107	1444	1492	1498	1144	1173	1166
FN	61	58	58	46	0	1	10	6	6
FP	52	53	44	2	7	0	31	6	13
FP-R	-	-	-	-	14	-	-	-	-
Se	94.72	94.98	95.02	96.91	100	99.93	99.13	99.49	99.49
+P	95.47	95.40	96.18	99.86	99.53	100.00	97.36	99.49	98.90
+P-R	-	-	-	-	99.07	-	-	-	-
Mean	2.52	2.18	3.38	5.32	-1.04	-0.10	-13.03	0.09	1.20
SD	16.44	13.90	14.55	5.53	3.95	6.02	14.69	7.65	10.19
SD V1-V3[1]	12.4	-	14.4	5.2	-	9.4	-	-	28.6

[1]Reference values from CSE working party [31]

Table 4.44: Final results for Lead V3.

	P wave			QRS complex			T wave		
	Onset	**Peak**	**Offset**	**Onset**	**Peak**	**Offset**	**Onset**	**Peak**	**Offset**
Total points	1353	1353	1353	1521	1526	1526	1265	1265	1265
TP	1305	1315	1314	1498	1525	1526	1186	1245	1226
FN	14	11	11	22	0	0	15	10	8
FP	34	27	28	1	1	0	64	10	31
FP-R	-	-	-	-	3	-	-	-	-
Se	98.94	99.17	99.17	98.55	100	100	98.75	99.20	99.35
+P	97.46	97.99	97.91	99.93	99.93	100	94.88	99.20	97.53
+P-R	-	-	-	-	99.80	-	-	-	-
Mean	0.44	0.37	-3.06	5.85	-1.33	0.29	-14.89	-0.01	2.11
SD	12.94	10.50	13.64	4.92	1.74	6.02	17.54	8.40	12.00
SD V1-V3[1]	12.4	-	14.4	5.2	-	9.4	-	-	28.6

[1]Reference values from CSE working party [31]

Table 4.45: Final results for Lead V4.

	P wave			QRS complex			T wave		
	Onset	**Peak**	**Offset**	**Onset**	**Peak**	**Offset**	**Onset**	**Peak**	**Offset**
Total points	1326	1326	1326	1496	1496	1496	1232	1232	1232
TP	1288	1295	1294	1423	1496	1495	1149	1207	1196
FN	17	15	15	70	0	1	19	5	6
FP	21	16	17	3	0	0	64	20	30
FP-R	-	-	-	-	5	-	-	-	-
Se	98.70	98.85	98.85	95.31	100	99.93	98.37	99.59	99.50
+P	98.40	98.78	98.70	99.79	100	100	94.72	98.37	97.55
+P-R	-	-	-	-	99.67	-	-	-	-
Mean	-0.30	-0.99	-5.35	1.98	-0.96	0.18	-11.38	0.63	6.94
SD	12.21	9.04	12.40	4.63	0.96	6.26	17.92	13.93	15.33
SD V4-V6[1]	12.6	-	13.6	5.2	-	12.0	-	-	28.8

[1]Reference values from CSE working party [31]

Table 4.46: Final results for Lead V5.

	P wave			QRS complex			T wave		
	Onset	**Peak**	**Offset**	**Onset**	**Peak**	**Offset**	**Onset**	**Peak**	**Offset**
Total points	1368	1368	1368	1536	1536	1536	1250	1250	1250
TP	1334	1343	1346	1483	1536	1512	1205	1241	1235
FN	14	11	11	52	0	22	9	4	6
FP	20	14	11	1	0	2	36	5	9
FP-R	-	-	-	-	1	-	-	-	-
Se	98.96	99.19	99.19	96.61	100	98.57	99.26	99.68	99.52
+P	98.52	98.97	99.19	99.93	100	99.87	97.10	99.60	99.28
+P-R	-	-	-	-	99.93	-	-	-	-
Mean	-0.54	-1.20	-6.23	2.37	-0.39	0.14	-13.45	-0.98	4.49
SD	10.85	7.86	12.18	4.15	0.98	5.81	14.77	4.36	7.42
SD V4-V6[1]	12.6	-	13.6	5.2	-	12.0	-	-	28.8

[1]Reference values from CSE working party [31]

Table 4.47: Final results for Lead V6.

	P wave			QRS complex			T wave		
	Onset	**Peak**	**Offset**	**Onset**	**Peak**	**Offset**	**Onset**	**Peak**	**Offset**
Total points	1368	1368	1368	1534	1534	1534	1230	1230	1230
TP	1324	1336	1335	1473	1534	1509	1194	1210	1203
FN	11	9	9	60	0	23	17	12	13
FP	25	15	16	1	0	2	19	8	14
FP-R	-	-	-	-	7	-	-	-	-
Se	99.18	99.33	99.33	96.09	100	98.50	98.60	99.02	98.93
+P	98.15	98.89	98.82	99.93	100	99.87	98.43	99.34	98.85
+P-R	-	-	-	-	99.54575	-	-	-	-
Mean	-0.89	-1.73	-6.45	1.93	-0.807	-0.58	-11.47	0.05	-0.47
SD	11.46	7.86	11.64	3.62	0.77	5.58	12.41	6.93	9.16
SD V4-V6[1]	12.6	-	13.6	5.2	-	12.0	-	-	28.8

[1]Reference values from CSE working party [31]

4.2 Validation results

4.2.1 Scatter plots

Scatter plots were evaluated to eliminate potential outliers and to provide a general assessment of the results. All results for each lead appear to correlate with the algorithm results in this first approach. T wave had the worst results; the scatter plots are extremely dispersed, and when compared to algorithm results, this can be explained by examining both T onset and offset, but especially T onset, which is the fiducial point with the worst performance results. Furthermore, every other interval calculated with these fiducial points (ST segment and ST interval) yields poor results. Between these two intervals, the ST segment results are as bad as the T wave results because it is calculated using T onsets, whereas the ST interval is calculated using T offsets, showing better results. As for the P wave, the scatter plot is not as dispersed as the T wave, but the results for this wave are not as good as the QRS complex results, which once again agrees with the algorithm results. In the same way that intervals calculated using T wave boundaries correlate with T wave scatter plot results and algorithm results, the same applies to P wave boundaries and their intervals. All scatter plots can be found in Appendix A.1.

4.2.2 Bland-Altman plots

Overall, considering the final results for each algorithm, LoA results (4.48 and 4.49) are as expected; most results correlate with scatter plots and algorithm results. From all leads, V1 presents the worst results, derived from the algorithm for V1 not being optimized; on the other hand, lead V5 shows the best results. If intervals calculated with T onset are disregarded (T wave and ST segment), the agreement between the COMEN system and the LoggerOne system seems great. One thing to notice, though, is that the mean (or bias) is negative for most results, which means the LoggerOne system intervals and segments are greater than the ones extracted from COMEN signals. The ST segment and TP interval are the only ones where, for all leads, the contrary applies. One final thing to notice is that the lead V4 ST interval shows relatively worse results than the other leads. LoA plots can be found in Appendix A.2 for visual context.

Table 4.48: Bland-Altman plot for leads I, II, V1 and V2.

	Lead I		Lead II		Lead V1		Lead V2	
Interval	**Bias**	**LoA**	**Bias**	**LoA**	**Bias**	**LoA**	**Bias**	**LoA**
Pw	-1.12	[-5.4; 3.1]	-0.93	[-5.2; 3.3]	-3.67	[-8.9; 1.5]	-1.41	[-5.4; 2.6]
Tw	-4.77	[-25; 15]	-4.55	[-26; 17]	-4.43	[-14; 4.6]	-1.82	[-5.2; 1.6]
QRS	-0.32	[-1.6; 0.93]	-0.41	[-1.8; 0.94]	-0.66	[-1.7; 0.41]	-0.52	[1.7; 0.69]
PRs	0.93	[-1.3; 3.1]	0.83	[-1.2; 2.8]	2.2	[-1.2; 5.6]	0.97	[-0.84; 2.8]
PRi	-0.11	[-2.7; 2.5]	-0.12	[-2.3; 2.1]	-1.61	[-4.5; 1.3]	-0.73	[-3; 1.5]
QT	-1.32	[-3.1; 0.47]	-0.77	[-2.6; 1.1]	-2.97	[-5.7; -0.21]	-1.74	[-3.5; -0.01]
STs	4.18	[-17; 25]	4.87	[-19; 28]	2.06	[-6.3; 10]	0.45	[-2.3; 3.2]
STi	-1.03	[-2.7; 0.6]	-0.38	[-2.2; 1.4]	-2.33	[-5; 0.36]	-1.23	[-3; 0.54]
RR	-0.76	[-1.9; 0.42]	-0.76	[-1.9; 0.4]	-0.73	[-2; 0.53]	-0.78	[-1.9; 0.35]
TP	0.84	[-2.4; 4.1]	0.24	[-3.4; 3.9]	3.9	[0.11; 7.7]	1.64	[-1.9; 5.2]
PP	-0.75	[-2.4; 0.86]	-0.74	[-2.3; 0.81]	-0.71	[-3; 1.6]	-0.76	[-2.3; 0.77]
TT	-0.76	[-2.7; 1.1]	-0.76	[-2.7; 1.2]	-0.72	[-2.4; 0.95]	-0.78	[-2.2; 0.6]

Table 4.49: Bland-Altman plot for leads V3, V4, V5 and V6.

	Lead V3		Lead V4		Lead V5		Lead V6	
Interval	**Bias**	**LoA**	**Bias**	**LoA**	**Bias**	**LoA**	**Bias**	**LoA**
Pw	-0.98	[-4.2; 2.2]	-0.63	[-3.7; 2.4]	-1.04	[-4.3; 2.2]	-1.07	[-5.3; 3]
Tw	-2.27	[-7.9; 3.3]	-2.09	[-14; 9.9]	-2.97	[-19; 13]	-4.8	[-23; 14]
QRS	-0.36	[-1.4; 0.71]	1.72	[0.52; 2.9]	-0.24	[-1.3; 0.77]	-0.33	[-1.5; 0.89]
PRs	0.67	[-0.77; 2.1]	0.62	[-2.4; 3.6]	0.8	[-1.1; 2.7]	0.93	[-1.1; 3]
PRi	-0.16	[-2.6; 2.3]	0	[-1.9; 1.9]	-0.27	[-2.5; 2]	-0.06	[-2.4; 2.3]
QT	-1.2	[-2.6; -0.16]	-0.87	[-2.4; 0.68]	-0.77	[-2.5; 0.94]	-1.62	[-3.2; -0.02]
STs	1.25	[-4.2; 6.7]	-0.13	[-13; 13]	2.78	[-14; 19]	3.98	[-16; 24]
STi	-0.86	[-2.3; 0.59]	-2.59	[-4.1; -1.1]	-0.56	[-2.3; 1.2]	-1.31	[-2.8; 0.19]
RR	-0.74	[-1.9; 0.42]	-0.76	[-2.2; 0.67]	-0.71	[-1.9; 0.47]	-0.76	[-1.9; 0.4]
TP	0.79	[-2.1;3.7]	0.14	[-2.5; 2.8]	0.34	[-2.3; 2.9]	1.03	[-1.8; 3.8]
PP	-0.73	[-2.1; 0.62]	-0.76	[-2.3; 0.77]	-0.71	[-2.2; 0.78]	-0.75	[-2.4; 0.86]
TT	-0.75	[-2.3; 0.79]	-0.77	[-2.5; 0.97]	-0.71	[-2.4; 0.99]	-0.77	[-2.3; 0.78]

4.2.3 ICC

ICC results (4.50 and 4.51) do not always agree with the previous results. When comparing P and T wave results, one would expect T wave results to be less reliable, but this is not the case. T waves show excellent reliability in some leads (V1, V2, and V4), whereas P wave results show good or even lower reliability. Furthermore, when we look at the confidence intervals for the P wave, we see that they have larger limits than the T wave. When we analyze these results using histograms of the differences between devices, we can observe that the P wave differences (Fig. 4.5) have a smaller range and better results than the T wave differences (Fig. 4.6), and this holds true for all leads. This is not the only case; for the QRS interval, the same holds true for leads, with lead I exhibiting excellent reliability and the others exhibiting good to poor reliability, and only one (lead V5) exhibiting good reliability. Furthermore, when we compare histograms for QRS interval differences between leads I and II (Fig. 4.7 and 4.8), we can find that both leads have good results, which, when combined with the LoA for these leads, demonstrates excellent agreement.

Every other lead demonstrates the same level of agreement.

The main source of this outcome is the discrepancy in interval ranges (4.52). When comparing P and T waves, T waves have a wider interval range than P waves, and because ICC also reflects interrater reliability, a narrower range leads to inaccurate conclusions. Lead I has a broader range for QRS intervals than any other lead, resulting in inaccurate results for those leads.

All other ICC results appear to be in agreement with LoA results, with the majority of results demonstrating excellent reliability. The ICC for the ST interval is excellent; nevertheless, the confidence interval is large, which is not desirable.

Table 4.50: ICC plot for leads I, II, V1 and V2.

	Lead I		**Lead II**		**Lead V1**		**Lead V2**	
Interval	**IC**	**CI 95%**	**IC**	**CI 95%**	**IC**	**CI 95%**	**IC**	**CI 95%**
Pw	0.61	[0.43; 0.72]	0.61	[0.48; 0.7]	0.43	[-0.09; 0.72]	0.73	[0.44; 0.85]
Tw	0.81	[0.71; 0.87]	0.75	[0.65; 0.81]	0.93	[0.64; 0.97]	0.95	[0.66; 0.98]
QRS	0.99	[0.98; 0.99]	0.59	[0.36; 0.73]	0.51	[-0.05; 0.76]	0.54	[0.13; 0.73]
PRs	0.99	[0.95; 1]	0.99	[0.96; 1]	0.98	[0.67: 0.99]	0.99	[0.92; 1]
PRi	0.99	[0.99; 0.99]	1.00	[1; 1]	0.99	[0.87; 1]	0.99	[0.99; 1]
QT	1.00	[0.93; 1]	1.00	[0.99; 1]	0.99	[0.53; 1]	1.00	[0.82; 1]
STs	0.88	[0.83; 0.91]	0.75	[0.65; 0.81]	0.98	[0.96; 0.99]	0.97	[0.97; 0.98]
STi	1.00	[0.97; 1]	1.00	[1; 1]	1.00	[0.78; 1]	1.00	[0.97; 1]
RR	1.00	[1; 1]	1.00	[1; 1]	1.00	[1; 1]	1.00	[1; 1]
TP	1.00	[1; 1]	1.00	[1; 1]	1.00	[0.93; 1]	1.00	[1; 1]
PP	1.00	[1; 1]	1.00	[1; 1]	1.00	[1; 1]	1.00	[1; 1]
TT	1.00	[1; 1]	1.00	[1; 1]	1.00	[1; 1]	1.00	[1; 1]

Table 4.51: ICC for leads V3, V4, V5 and V6.

	Lead V3		**Lead V4**		**Lead V5**		**Lead V6**	
Interval	**IC**	**CI 95%**	**IC**	**CI 95%**	**IC**	**CI 95%**	**IC**	**CI 95%**
Pw	0.78	[0.57; 0.87]	0.77	[0.68; 0.83]	0.74	[0.51; 0.85]	0.64	[0.47; 0.75]
Tw	0.70	[0.31; 0.84]	0.93	[0.91; 0.95]	0.88	[0.83; 0.91]	0.83	[0.72; 0.89]
QRS	0.67	[0.39; 0.8]	0.30	[-0.05; 0.65]	0.76	[0.64; 0.84]	0.69	[0.51; 0.79]
PRs	0.99	[0.97; 1]	0.99	[0.98; 0.99]	0.99	[0.96; 1]	0.99	[0.94; 1]
PRi	1.00	[0.99; 1]	1.00	[1; 1]	0.99	[0.99; 1]	1.00	[0.99; 1]
QT	1.00	[0.89; 1]	1.00	[0.98; 1]	1.00	[0.99; 1]	1.00	[0.76; 1]
STs	0.92	[0.87; 0.95]	0.96	[0.96; 0.96]	0.93	[0.9; 0.94]	0.89	[0.84; 0.92]
STi	1.00	[0.98; 1]	0.99	[0.23; 1]	1.00	[1; 1]	1.00	[0.88; 1.]
RR	1.00	[1; 1]	1.00	[1; 1]	1.00	[1; 1]	1.00	[1; 1]
TP	1.00	[1; 1]	1.00	[1; 1]	1.00	[1; 1]	1.00	[1; 1]
PP	1.00	[1; 1]	1.00	[1; 1]	1.00	[1; 1]	1.00	[1; 1]
TT	1.00	[1; 1]	1.00	[1; 1]	1.00	[1; 1]	1.00	[1; 1]

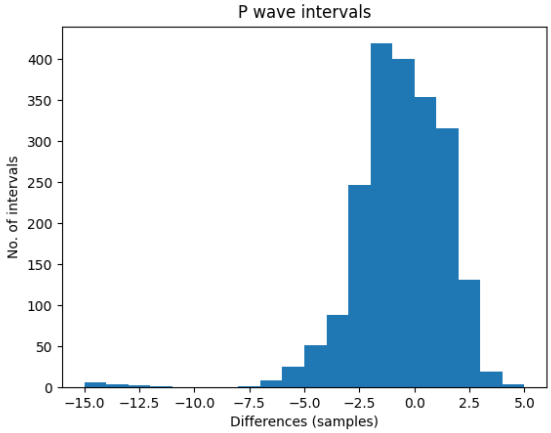

Figure 4.5: Histogram of P wave differences for lead I.

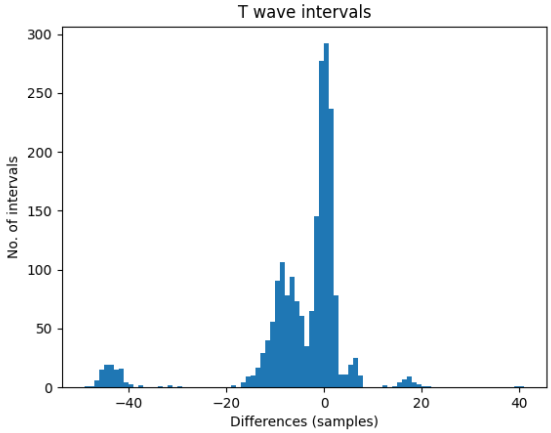

Figure 4.6: Histogram of T wave differences for lead I.

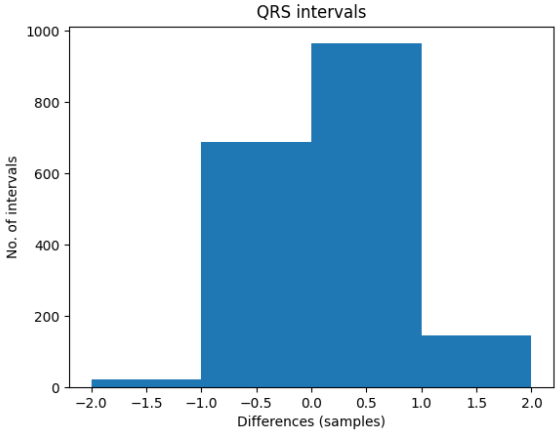

Figure 4.7: Histogram of QRS interval differences for lead I.

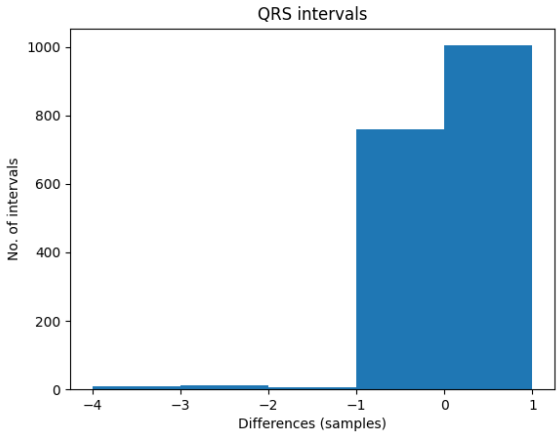

Figure 4.8: Histogram of QRS interval differences for lead II.

Table 4.52: Interval ranges for each device in samples.

	COMEN	**LoggerOne**
Pw - Lead I	[34; 56]	[37; 58]
Tw - Lead I	[55; 115]	[58; 115]
QRS - Lead I	[44; 78]	[44; 79]
QRS - Lead II[1]	[46;51]	[46;51]

[1]The other leads present similar QT intervals ranges as lead II

4.2.4 Morphological comparison

In this comparison, the normalized signals were first smooth using a Savitzky-Golay filter, Figs. 4.9 and 4.10 show the signal before the filter and after. The morphological results show that the signals of the devices don't diverge greatly from one other 4.53. Aside from the fact that the beats are mathematically similar, there are no other conclusions or guidelines for this type of validation. Furthermore, we can see in Fig. 4.10 that there is little variation between both signals save for a slight amplitude difference.

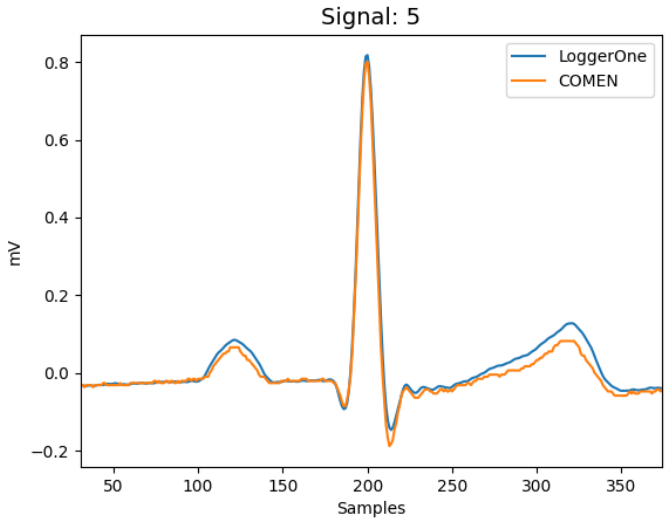

Figure 4.9: LoggerOne and COMEN signal after normalization.

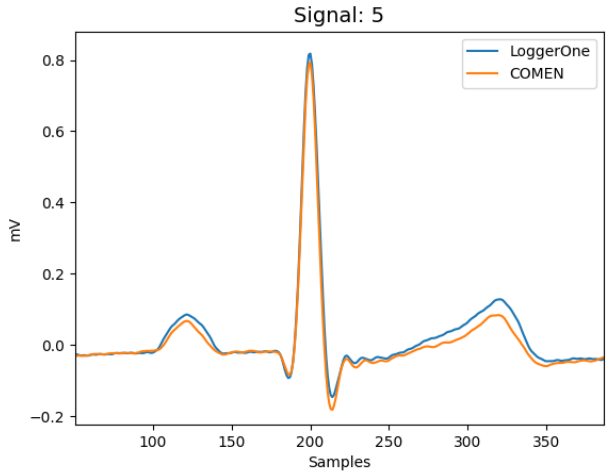

Figure 4.10: LoggerOne and COMEN signal after normalization and smoothing.

Table 4.53: SD between devices for each lead.

	Lead I	**Lead II**	**Lead V1**	**Lead V2**	**Lead V3**	**Lead V4**	**Lead V5**	**Lead V6**
SD (mV)	0.021	0.022	0.020	0.017	0.016	0.019	0.028	0.021

4.2.5 Final considerations

Except for T wave intervals, ST intervals, and ST segments, the validation results indicate great agreement. However, because the algorithm used considerably influences the final results, it is incorrect to infer that the devices do not agree on those parameters. Furthermore, ICC has significant limitations as a validation method if the range of intervals employed is narrow; hence, it may not be a good validation approach for ECG or at least

for specific ECG parameters. Because the use of simulated signals can affect these ranges, testing on real patients in a variety of circumstances may help overcome ICC range limits.

It is important to note that when signals from both devices are synchronized by the first R peak, LoggerOne signals diverge from COMEN signals over time. One possible explanation is that the internal clocks of both devices differ [59]. The drift difference between the first and last beats of a signal is shown in Figs. 4.11 and 4.12. There is also a difference in amplitude between the first and last beats. This is due to devices' varying rates of adjusting to a new signal input from the simulator.

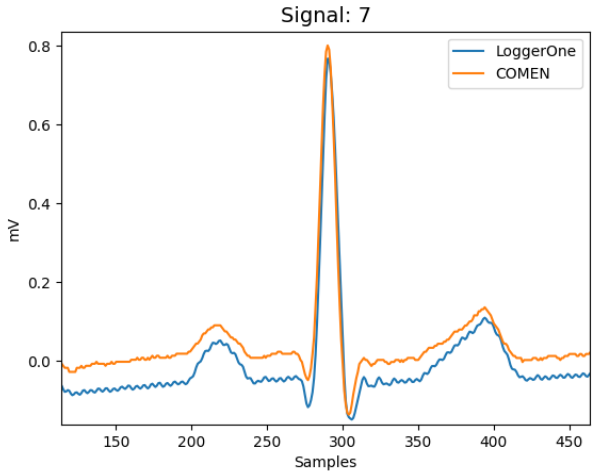

Figure 4.11: First beat of signal 7.

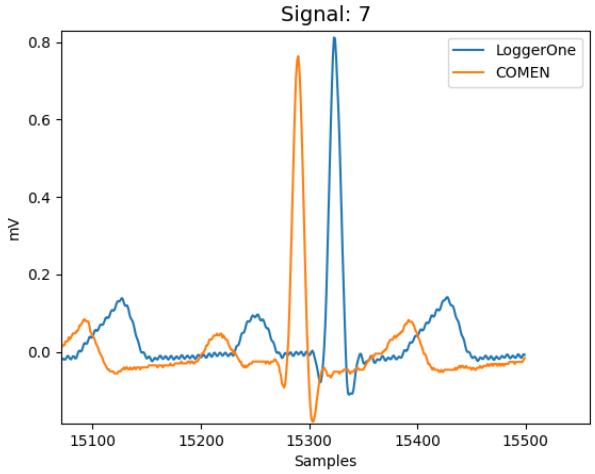

Figure 4.12: Last beat of signal 7.

Chapter 5

Conclusions and Future Work

This chapter presents the main conclusions drawn from the research work described in this dissertation and also discusses some research topics that may be addressed as a continuation or a complement of this work.

5.1 Conclusion

This work not only studies the efficacy of different ECG segmentation algorithms but also employs them to extract fiducial points for ECG device validation. The algorithms used delivered good SD results, with the exception of P onsets in leads I, II, V1, V2, and V3, as well as P offsets and QRS onsets in leads V1, and V2. These results must be optimized for the algorithm to be considered valid. Reference SD values exist only for P and QRS complex onsets and offsets, and for T offsets, for the rest of the fiducial points, there are no reference values. So, for those points without reference values, no clinical conclusion can be drawn; however, based on the SD and mean results, as well as the subsequent performance of the algorithms in the simulated signals, we can conclude that the algorithm used worked well for P, T, and R peaks across all leads, but not so well for T onsets. Finally, the mean as a performance measure proved to be extremely essential, and a reference limit of 15 ms looked excessive.

In terms of validation results, it has been established that the performance of the algorithms used has a significant impact on validation results, even though those results did not limit all validation results. T onsets, as the most difficult and least accurate fiducial point to detect across all leads, resulted in ambiguous validation results for intervals and segments that require that point as a reference, such as the T wave and ST segment. Furthermore, each of the validation methods employed has distinct constraints. To begin with, there are no ECG criteria for LoA, i.e., nothing that determines what bias and intervals indicate an excellent or poor agreement. On the other hand, there are rules that define low and excellent reliability for the ICC approach. However, the range of samples used has a large influence on ICC values, which restricts validation conclusions. Finally, while the morphological method adds little to this work, it does rule out signals from both devices being completely distinct.

Some of the intervals and segments utilized for validation are not clinically relevant and may be removed from additional validation tests. Because RR intervals are already utilized to calculate heart rate, intervals from P to P or T to T peaks, for example, provide no

clinically relevant information. The ST segment is clinically relevant, although not for its duration but for its elevation.

Finally, the work done cannot ensure that the LoggerOne system for 5-lead ECG is valid because it is restricted by the algorithms employed, and since these algorithms are not valid, validation results are limited by that as well. Furthermore, the validation data came from an ECG simulator, and an actual population of patients is required to demonstrate that this device works. However, this study is simply a preliminary approach to validating the device, a means of determining whether the device is ready for future validation tests. Given these parameters plus the outcomes of this study, the LoggerOne system for 5-lead ECG is ready for further testing in a human population.

5.2 Future Work

More work can be done to validate LoggerOne, however, clinical validation takes more time since recording signals on real patients requires far more resources than using a simulator. Having said that, clinical validation of this medical device is critical. To improve future clinical validation studies, a diverse range of patients, including young children and adults with normal and abnormal heart problems, must be addressed. In terms of methodology, approved ECG segmentation software should be employed for further validation. One of the drawbacks of this approach can be addressed by using appropriate software. In terms of the validation methods utilized, LoA appears to be a good approach to use again, however, ICC should be used with caution. Morphology approaches, on the other hand, demonstrate no relevance in subsequent validation tests. Lastly, the work accomplished can be translated to other ECG lead placements, such as the 12-lead ECG.

Bibliography

[1] S. Pal, *ECG Monitoring: Present Status and Future Trend*, 01 2017. [Online]. Available: https://doi.org/10.1016/B978-0-12-801238-3.10892-X 1

[2] [Online]. Available: https://www.who.int/health-topics/cardiovascular-diseases#tab=tab_1 1

[3] B. Cannon, "Cardiovascular disease: Biochemistry to behaviour," *Nature*, vol. 493, pp. S2–3, 01 2013. [Online]. Available: https://doi.org/10.1038/493S2a 1

[4] P. Fontana, N. R. A. Martins, M. Camenzind, R. M. Rossi, F. Baty, M. Boesch, O. D. Schoch, M. H. Brutsche, and S. Annaheim, "Clinical applicability of a textile 1-lead ecg device for overnight monitoring," *Sensors*, vol. 19, no. 11, 2019. [Online]. Available: https://doi.org/10.3390/s19112436 1, 19, 23, 25

[5] R. E. Wagner, H. Plácido da Silva, and K. Gramann, "Validation of a low-cost electrocardiography (ecg) system for psychophysiological research," *Sensors*, vol. 21, no. 13, 2021. [Online]. Available: https://doi.org/10.3390/s21134485 1, 19, 25

[6] S. Kwon, S.-R. Lee, E.-K. Choi, H.-J. Ahn, H.-S. Song, Y.-S. Lee, and S. Oh, "Validation of adhesive single-lead ecg device compared with holter monitoring among non-atrial fibrillation patients," *Sensors*, vol. 21, no. 9, 2021. [Online]. Available: https://doi.org/10.3390/s21093122 1, 25

[7] M. Azram, N. Ahmed, L. Leese, M. Brigham, R. Bowes, S. Wheatcroft, M. Ngantcha, B. Stegemann, G. Crowther, and M. Tayebjee, "Clinical validation and evaluation of the novel six lead handheld ecg recorder compared to the 12 lead ecg in unselected cardiology patients (evalecg cardio)," *European Heart Journal - Digital Health*, vol. 2, 09 2021. [Online]. Available: https://doi.org/10.1093/ehjdh/ztab083 1, 19, 23, 25

[8] S. Soon, H. Svavarsdottir, C. Downey, and D. Jayne, "Wearable devices for remote vital signs monitoring in the outpatient setting: An overview of the field," *BMJ Innovations*, vol. 6, pp. bmjinnov–2019, 01 2020. [Online]. Available: http://dx.doi.org/10.1136/bmjinnov-2019-000354 1

[9] F. Kusumoto, *Cardiac Anatomy and Electrophysiology*. Cham: Springer International Publishing, 2020, pp. 3–11. [Online]. Available: https://doi.org/10.1007/978-3-030-40341-6_1 5, 6

[10] N. AlHinai, "Chapter 1 - introduction to biomedical signal processing and artificial intelligence," in *Biomedical Signal Processing and Artificial Intelligence in Healthcare*, ser. Developments in Biomedical Engineering and Bioelectronics,

W. Zgallai, Ed. Academic Press, 2020, pp. 1–28. [Online]. Available: https://doi.org/10.1016/B978-0-12-818946-7.00001-9 5

[11] S. Pal, "Ecg monitoring: Present status and future trend," in *Encyclopedia of Biomedical Engineering*, R. Narayan, Ed. Oxford: Elsevier, 2019, pp. 363–379. [Online]. Available: https://doi.org/10.1016/B978-0-12-801238-3.10892-X 5

[12] X. Wei, S. Yohannan, and J. R. Richards, "Physiology, cardiac repolarization dispersion and reserve," 2020. 5, 6, 7

[13] R. E. Klabunde, *Cardiac Anatomy and Electrophysiology*. Wolters Kluwer. 7, 8

[14] S. Chandra, A. Sharma, and G. K. Singh, "Feature extraction of ecg signal," *Journal of Medical Engineering & Technology*, vol. 42, no. 4, pp. 306–316, 2018, pMID: 30251572. [Online]. Available: https://doi.org/10.1080/03091902.2018.1492039 8

[15] J. C. R. Machado, *Eletrocardiografia clínica*. LIDEL, 2023. 8, 9, 10, 11, 43

[16] T. Nguyen gia, M. Jiang, A. M. Rahmani, T. Westerlund, K. Mankodiya, P. Liljeberg, and H. Tenhunen, "Fog computing in body sensor networks: An energy efficient approach," 01 2015. 8

[17] P. W. Macfarlane, "The influence of age and sex on the electrocardiogram," *Advances in experimental medicine and biology*, vol. 1065, p. 93—106, 2018. [Online]. Available: https://doi.org/10.1007/978-3-319-77932-4_6 9, 10

[18] F. Kusumoto, *Physics of Electrocardiography*. Cham: Springer International Publishing, 2020, pp. 13–22. [Online]. Available: https://doi.org/10.1007/978-3-030-40341-6_2 10, 11, 12, 13

[19] B. Vandenberk, E. Vandael, T. Robyns, J. Vandenberghe, C. Garweg, V. Foulon, J. Ector, and R. Willems, "Which qt correction formulae to use for qt monitoring?" *Journal of the American Heart Association*, vol. 5, no. 6, p. e003264, 2016. [Online]. Available: https://doi.org/10.1161/jaha.116.003264 10

[20] J. L. Salinet and O. Luppi Silva, "Chapter 2 - ecg signal acquisition systems," in *Developments and Applications for ECG Signal Processing*, J. P. do Vale Madeiro, P. C. Cortez, J. M. da Silva Monteiro Filho, and A. R. A. Brayner, Eds. Academic Press, 2019, pp. 29–51. [Online]. Available: https://doi.org/10.1016/B978-0-12-814035-2.00008- 11, 12, 13

[21] S. Kaplan Berkaya, A. K. Uysal, E. Sora Gunal, S. Ergin, S. Gunal, and M. B. Gulmezoglu, "A survey on ecg analysis," *Biomedical Signal Processing and Control*, vol. 43, pp. 216–235, 2018. [Online]. Available: https://doi.org/10.1016/j.bspc.2018.03.003 14, 15, 16, 17

[22] M. Elgendi, M. Meo, and D. Abbott, "A proof-of-concept study: Simple and effective detection of p and t waves in arrhythmic ecg signals," *Bioengineering*, vol. 3, no. 4, 2016. [Online]. Available: https://doi.org/10.3390/bioengineering3040026 15, 17, 41, 43

[23] G. Li, D. Huang, L. Wang, J. Zhou, J. Chen, K. Wu, and W. Xu, "A new method of detecting the characteristic waves and their onset and end in electrocardiogram signals," *Biomedical Signal Processing and Control*, vol. 75, p. 103607, 2022. [Online]. Available: https://doi.org/10.1016/j.bspc.2022.103607 15, 17, 30

[24] D. Batista, H. Plácido da Silva, A. Fred, C. Moreira, M. Reis, and H. Ferreira, "Benchmarking of the bitalino biomedical toolkit against an established gold standard," vol. 6, pp. 32–36, 05 2019. [Online]. Available: https://doi.org/10.1049/htl.2018.5037 16, 19, 25

[25] I. Beraza and I. Romero, "Comparative study of algorithms for ecg segmentation," *Biomedical Signal Processing and Control*, vol. 34, pp. 166–173, 2017. [Online]. Available: https://doi.org/10.1016/j.bspc.2017.01.013 16, 17, 30, 31

[26] S. Chandra, A. Sharma, and G. K. Singh, "Feature extraction of ecg signal," *Journal of Medical Engineering & Technology*, vol. 42, no. 4, pp. 306–316, 2018, pMID: 30251572. [Online]. Available: https://doi.org/10.1080/03091902.2018.1492039 17

[27] P. Sherathia and V. Patel, "Sensitivity and positive prediction accuracy analysis for r peak detection in ecg feature extraction," 04 2017, pp. 680–685. [Online]. Available: https://doi.org/10.1109/I2CT.2017.8226216 17

[28] H. Yanık, E. Değirmenci, B. Buyukakilli, D. Karpuz, O. Kılınç, and S. Gurgul, "Electrocardiography (ecg) analysis and a new feature extraction method using wavelet transform with scalogram analysis," *Biomedizinische Technik. Biomedical engineering*, vol. -1, 05 2020. [Online]. Available: https://doi.org/10.1515/bmt-2019-0147 17

[29] R. Jané, A. Blasi, J. I. García, and P. Laguna, "Evaluation of an automatic threshold based detector of waveform limits in holter ecg with the qt database," *Computers in Cardiology 1997*, pp. 295–298, 1997. [Online]. Available: https://doi.org/10.1109/CIC.1997.647889 17

[30] Q. Qin, J. Li, Y. Yue, and C. Liu, "An adaptive and time-efficient ecg r-peak detection algorithm," *Journal of Healthcare Engineering*, vol. 2017, pp. 1–14, 09 2017. [Online]. Available: https://doi.org/10.1155/2017/5980541 17, 30

[31] M. J. L. Willems, "Recommendations for measurement standards in quantitative electrocardiography. the cse working party." *European heart journal*, vol. 6 10,

pp. 815–25, 1985. [Online]. Available: https://doi.org/10.1093/oxfordjournals.eurheartj.a061766 18, 31, 41, 53, 54, 55

[32] S. Haghayegh, H.-A. Kang, S. Khoshnevis, M. H. Smolensky, and K. R. Diller, "A comprehensive guideline for bland–altman and intra class correlation calculations to properly compare two methods of measurement and interpret findings," *Physiological Measurement*, vol. 41, no. 5, p. 055012, jun 2020. [Online]. Available: https://dx.doi.org/10.1088/1361-6579/ab86d6 18, 19

[33] R. Lucia, G. Zucchelli, V. Barletta, A. Cori, M. Giannotti Santoro, M. Parollo, L. Segreti, S. Viani, V. Tommasina, L. Paperini, E. Soldati, and M. Bongiorni, "The in-ear region as a novel anatomical site for ecg signal detection: validation study on healthy volunteers," *Journal of Interventional Cardiac Electrophysiology*, vol. 60, 01 2021. [Online]. Available: https://doi.org/10.1007/s10840-020-00709-x 19

[34] L. Beers, L. P. van Adrichem, J. C. L. Himmelreich, E. P. M. Karregat, J. S. S. G. de Jong, P. G. Postema, J. R. de Groot, W. A. M. Lucassen, and R. E. Harskamp, "Manual qt interval measurement with a smartphone-operated single-lead ecg versus 12-lead ecg: a within-patient diagnostic validation study in primary care," *BMJ Open*, vol. 11, no. 11, 2021. [Online]. Available: https://doi.org/10.1136/bmjopen-2021-055072 19, 25

[35] P. Ranganathan, C. Pramesh, and R. Aggarwal, "Common pitfalls in statistical analysis: Measures of agreement," *Perspectives in Clinical Research*, vol. 8, p. 187, 10 2017. [Online]. Available: https://doi.org/10.4103/picr.PICR_123_17 19

[36] G. M. Foody, "Explaining the unsuitability of the kappa coefficient in the assessment and comparison of the accuracy of thematic maps obtained by image classification," *Remote Sensing of Environment*, vol. 239, p. 111630, 2020. [Online]. Available: https://doi.org/10.1016/j.rse.2019.111630 19, 20

[37] P. Schober, C. Boer, and L. Schwarte, "Correlation coefficients: Appropriate use and interpretation," *Anesthesia Analgesia*, vol. 126, p. 1, 02 2018. [Online]. Available: https://doi.org/10.1213/ane.0000000000002864 20

[38] N. Özgür Doğan, "Bland-altman analysis: A paradigm to understand correlation and agreement," *Turkish Journal of Emergency Medicine*, vol. 18, no. 4, pp. 139–141, 2018. [Online]. Available: https://doi.org/10.1016/j.tjem.2018.09.001 20, 21

[39] J. M. Bland and D. G. Altman, "Agreement between methods of measurement with multiple observations per individual," *Journal of Biopharmaceutical Statistics*, vol. 17, no. 4, pp. 571–582, 2007, pMID: 17613642. [Online]. Available: https://doi.org/10.1080/10543400701329422 21

[40] T. K. Koo and M. Y. Li, "A guideline of selecting and reporting intraclass correlation coefficients for reliability research," *Journal of Chiropractic Medicine*, vol. 15, no. 2, pp. 155–163, 2016. [Online]. Available: https://doi.org/10.1016/j.jcm.2016.02.012 21, 22

[41] G. Perinetti, "Statips part iv: Selection, interpretation and reporting of the intraclass correlation coefficient," *South European Journal of Orthodontics and Dentofacial Research*, vol. 5, 05 2018. [Online]. Available: https://doi.org/10.5937/sejodr5-17434 21, 22

[42] H. Plácido da Silva, C. Carreiras, A. Lourenco, A. Fred, R. Neves, and R. Ferreira, "Off-the-person electrocardiography: performance assessment and clinical correlation," *Health and Technology*, vol. 4, 04 2015. [Online]. Available: https://doi.org/10.1016/j.ahj.2016.11.006 23, 26

[43] R. Antonicelli, C. Ripa, A. Abbatecola, C. Capparuccia, L. Ferrara, and L. Spazzafumo, "Validation of the 3-lead tele-ecg versus the 12-lead tele-ecg and the conventional 12-lead ecg method in older people," *Journal of telemedicine and telecare*, vol. 18, pp. 104–8, 03 2012. [Online]. Available: https://doi.org/10.1258/jtt.2011.110613 23, 26

[44] M. Marouf, G. Vukomanovic, L. Saranovac, and M. Bozic, "Multi-purpose ecg telemetry system," *BioMedical Engineering OnLine*, vol. 16, 06 2017. [Online]. Available: https://doi.org/10.1186/s12938-017-0371-6 23, 26

[45] C. Carreiras., A. LourenÇo., H. Plácido da Silva., and A. Fred., "Comparative study of medical-grade and off-the-person ecg systems," in *Proceedings of the International Congress on Cardiovascular Technologies (CARDIOTECHNIX 2013) - IWoPE*, INSTICC. SciTePress, 2013, pp. 115–120. [Online]. Available: https://doi.org/10.5220/0004675501150120 23, 26

[46] N. Pandis, "Validation of the 3-lead tele-ecg versus the 12-lead tele-ecg and the conventional 12-lead ecg method in older people," *American Journal of Orthodontics and Dentofacial Orthopedics*, vol. 160, pp. 767–768, 11 2021. [Online]. Available: https://doi.org/10.1016/j.ajodo.2021.07.001 24

[47] J. Naranjo-Orellana, J. F. Ruso Álvarez, and J. L. Rojo-Álvarez, "Comparison of omegawave device and an ambulatory ecg for rr interval measurement at rest," *International Journal of Sports Medicine*, vol. 42, 08 2020. [Online]. Available: https://doi.org/10.1055/a-1157-9220 25

[48] B. T. Cilhoroz, D. Giles, A. Zaleski, B. Taylor, B. Fernhall, and L. Pescatello, "Validation of the polar v800 heart rate monitor and comparison of artifact correction methods among adults with hypertension," *PLoS ONE*, vol. 15, 10 2020. [Online]. Available: https://doi.org/10.1371/journal.pone.0240220 25

[49] D. Batista, H. Silva, and A. Fred, "Experimental characterization and analysis of the bitalino platforms against a reference device," in *2017 39th Annual International Conference of the IEEE Engineering in Medicine and Biology Society (EMBC)*, 2017, pp. 2418–2421. [Online]. Available: https://doi.org/10.1109/EMBC.2017.8037344 26

[50] A. Akintola, V. van de Pol, D. Bimmel, A. Maan, and D. van Heemst, "Comparative analysis of the equivital eq02 lifemonitor with holter ambulatory ecg device for continuous measurement of ecg, heart rate, and heart rate variability: A validation study for precision and accuracy," *Frontiers in Physiology*, vol. 7, 09 2016. [Online]. Available: https://doi.org/10.3389/fphys.2016.00391 26

[51] W. Smith, F. Riddell, M. Madon, and M. Gleva, "Comparison of diagnostic value using a small, single channel, p-wave centric sternal ecg monitoring patch with a standard 3-lead holter system over 24hours," *American Heart Journal*, vol. 185, 11 2016. [Online]. Available: https://doi.org/10.1016/j.ahj.2016.11.006 26

[52] A. Kalyakulina, I. Yusipov, V. Moskalenko, A. Nikolskiy, K. Kosonogov, N. Zolotykh, and M. Ivanchenko, "Lobachevsky university electrocardiography database (version 1.0.1)," Jan 2021. [Online]. Available: https://doi.org/10.13026/eegm-h675 27, 28

[53] A. Kalyakulina, I. Yusipov, V. Moskalenko, A. Nikolskiy, K. Kosonogov, G. Osipov, N. Zolotykh, and M. Ivanchenko, "Ludb: A new open-access validation tool for electrocardiogram delineation algorithms," *IEEE Access*, vol. 8, pp. 186 181–186 190, 01 2020. [Online]. Available: https://doi.org/10.1109/ACCESS.2020.3029211 27

[54] A. L. Goldberger, L. A. N. Amaral, L. Glass, J. M. Hausdorff, P. C. Ivanov, R. G. Mark, J. E. Mietus, G. B. Moody, C.-K. Peng, and H. E. Stanley, "Physiobank, physiotoolkit, and physionet," *Circulation*, vol. 101, no. 23, pp. e215–e220, 2000. [Online]. Available: https://doi.org/10.1161/01.cir.101.23.e215 27

[55] D. Makowski, T. Pham, Z. J. Lau, J. C. Brammer, F. Lespinasse, H. Pham, C. Schölzel, and S. H. A. Chen, "Neurokit2: A python toolbox for neurophysiological signal processing," *Behavior Research Methods*, vol. 53, no. 4, pp. 1689–1696, 2 2021. [Online]. Available: https://doi.org/10.3758/s13428-020-01516-y 27, 29

[56] R. Huo, L. Zhang, F. Liu, Y. Wang, Y. Liang, and S. Wei, "Ecg segmentation algorithm based on bidirectional hidden semi-markov model," *Computers in Biology and Medicine*, vol. 150, p. 106081, 2022. [Online]. Available: https://doi.org/10.1016/j.compbiomed.2022.106081 30

[57] P. Laguna, N. Thakor, P. Caminal, R. Jané, H. Yoon, A. Bayés de Luna, V. Marti, and J. Guindo, "New algorithm for qt interval analysis in 24-hour holter ecg: performance and applications," *Medical and Biological Engineering*

and Computing, vol. 28, no. 1, pp. 67–73, Jan. 1990. [Online]. Available: https://doi.org/10.1007/bf02441680 31

[58] S. Hargittai, "Savitzky-golay least-squares polynomial filters in ecg signal processing," vol. 32, 10 2005, pp. 763 – 766. [Online]. Available: http://dx.doi.org/10.1109/CIC.2005.1588216 38

[59] D. Batista, H. Plácido da Silva, A. Fred, C. Moreira, M. Reis, and H. A. Ferreira, "Benchmarking of the bitalino biomedical toolkit against an established gold standard," *Healthcare technology letters*, vol. 6, no. 2, p. 32—36, April 2019. [Online]. Available: https://doi.org/10.1049/htl.2018.5037 62

Appendix A

Appendix

A.1 Scatter plot results

A.1.1 Lead I

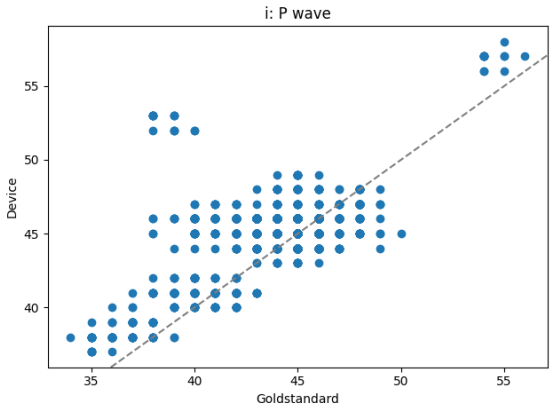

Figure A.1: P wave scatter plot for Lead I.

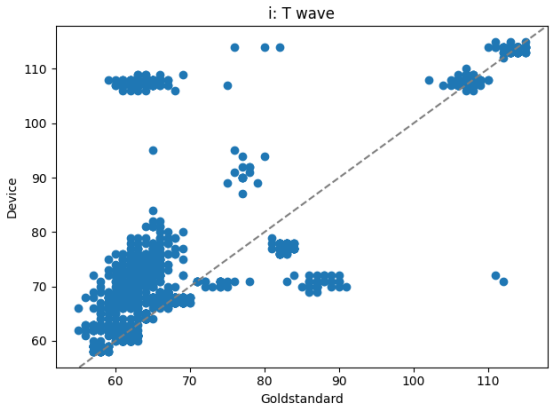

Figure A.2: T wave scatter plot for Lead I.

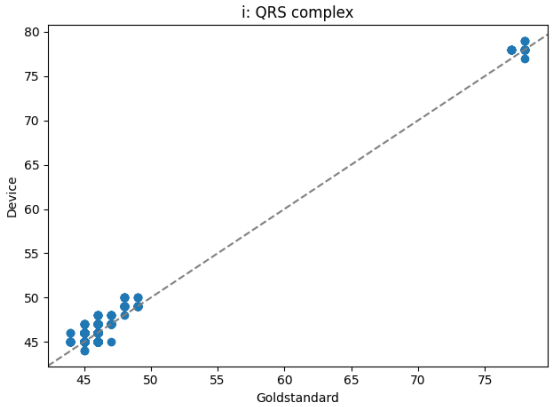

Figure A.3: QRS interval scatter plot for Lead I.

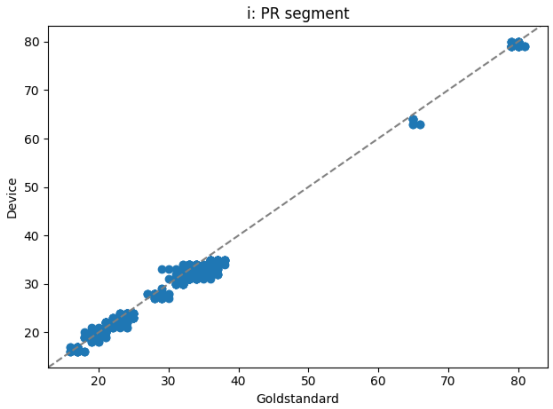

Figure A.4: PR segment scatter plot for Lead I.

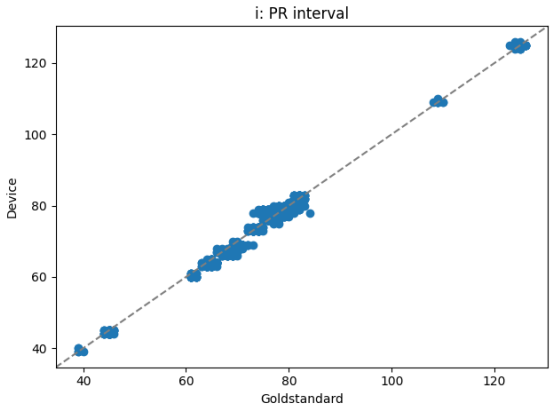

Figure A.5: PR interval scatter plot for Lead I.

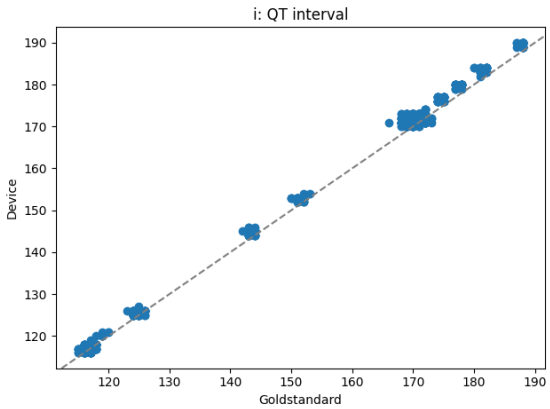

Figure A.6: QT interval scatter plot for Lead I.

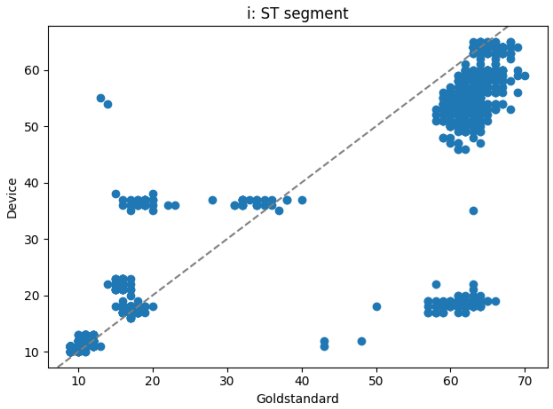

Figure A.7: ST segment scatter plot for Lead I.

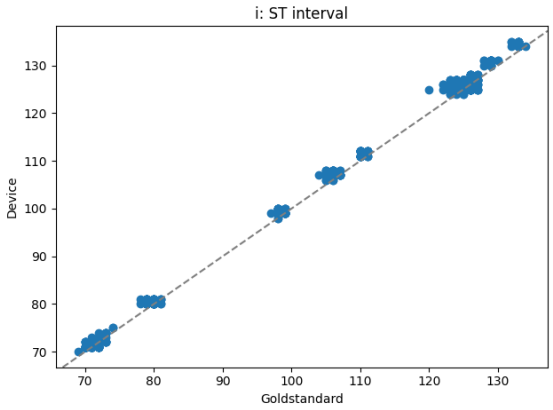

Figure A.8: ST interval scatter plot for Lead I.

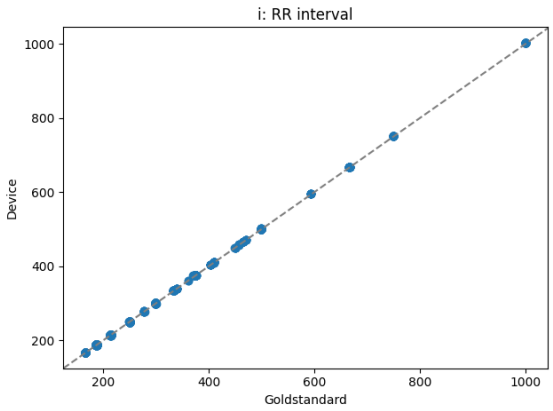

Figure A.9: RR interval scatter plot for Lead I.

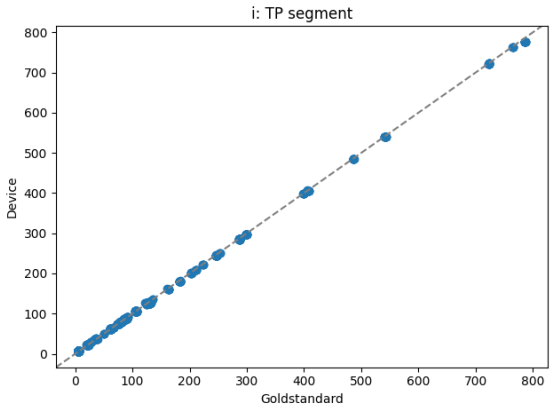

Figure A.10: TP segment scatter plot for Lead I.

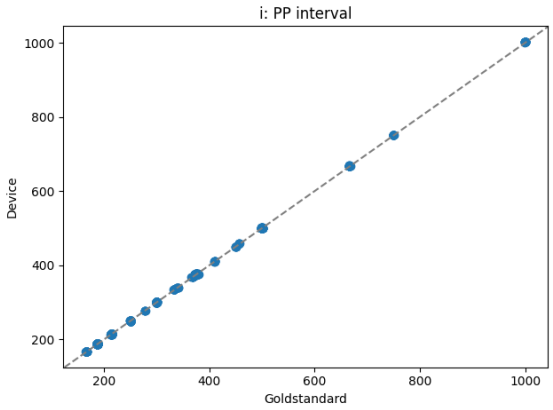

Figure A.11: PP interval scatter plot for Lead I.

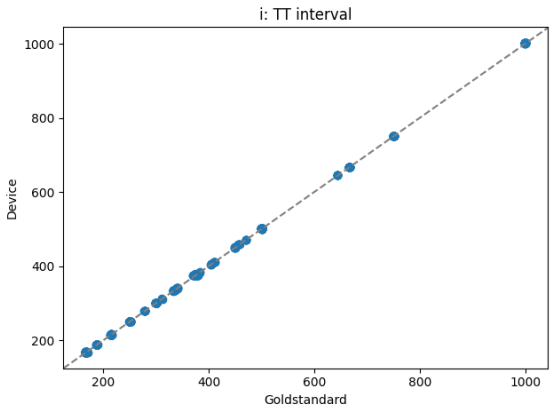

Figure A.12: TT interval scatter plot for Lead I.

A.1.2 Lead II

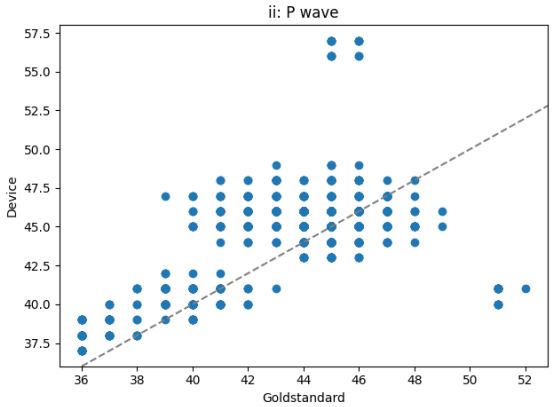

Figure A.13: P wave scatter plot for Lead II.

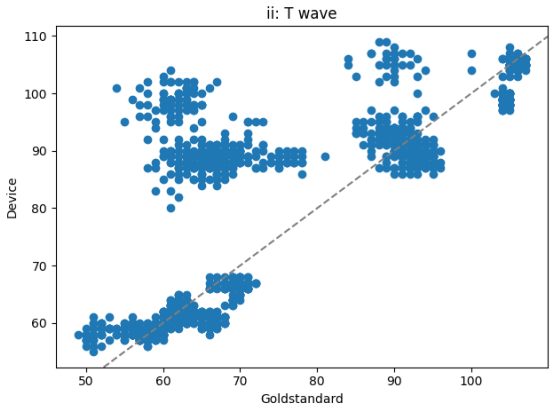

Figure A.14: T wave scatter plot for Lead II.

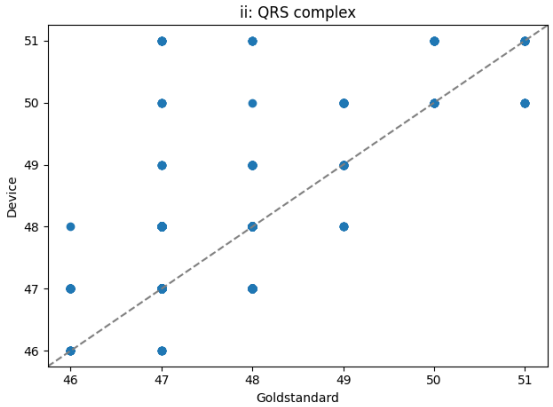

Figure A.15: QRS interval scatter plot for Lead II.

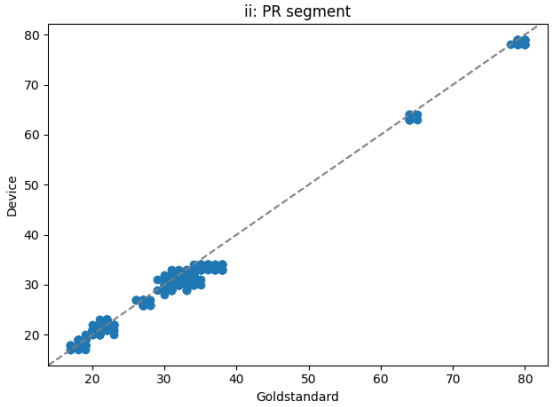

Figure A.16: PR segment scatter plot for Lead II.

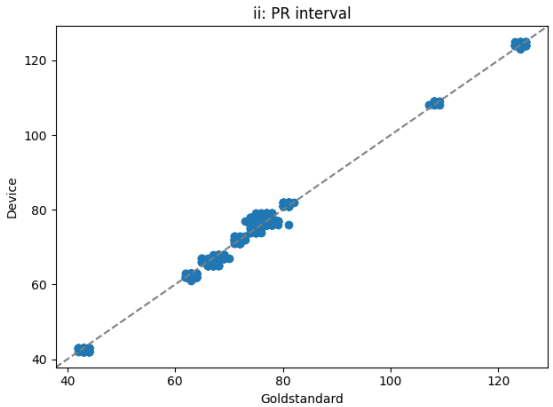

Figure A.17: PR interval scatter plot for Lead II.

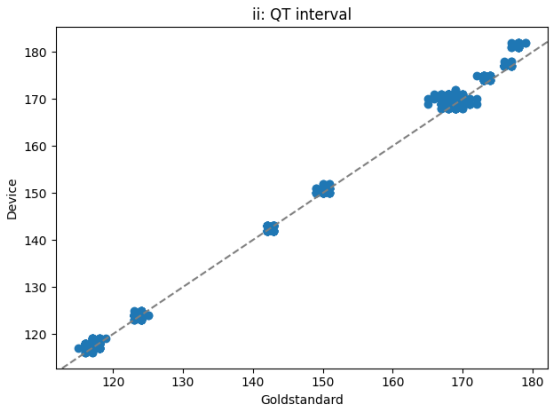

Figure A.18: QT interval scatter plot for Lead II.

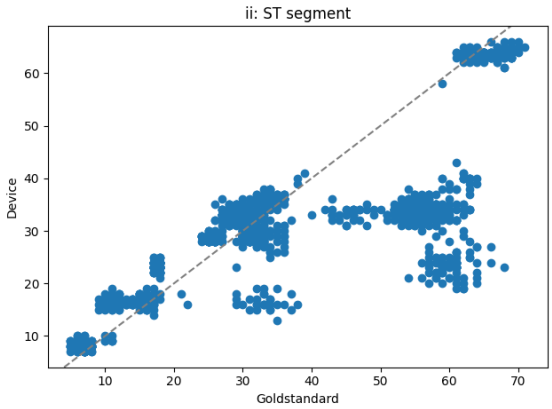

Figure A.19: ST segment scatter plot for Lead II.

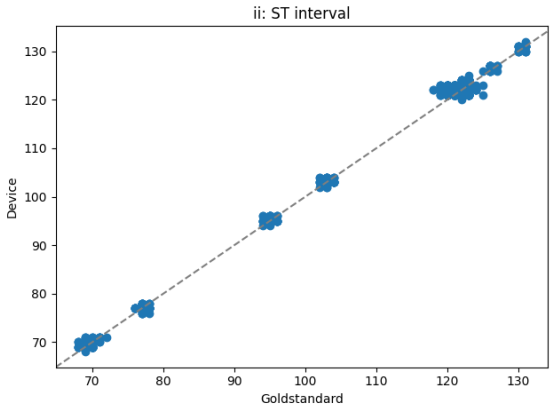

Figure A.20: ST interval scatter plot for Lead II.

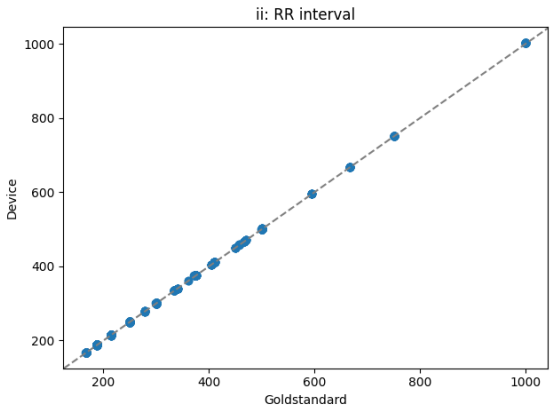

Figure A.21: RR interval scatter plot for Lead II.

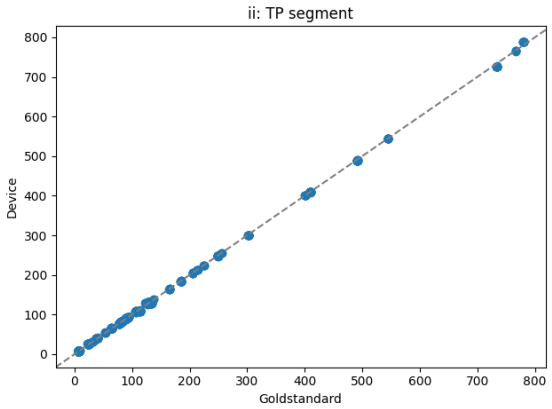

Figure A.22: TP segment scatter plot for Lead II.

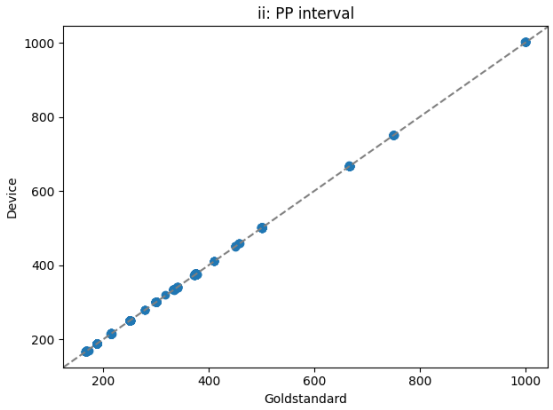

Figure A.23: PP interval scatter plot for Lead II.

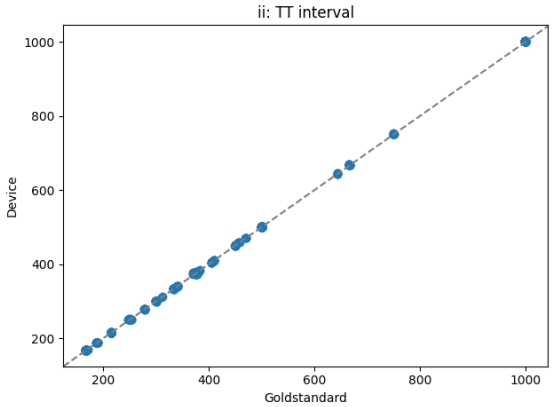

Figure A.24: TT interval scatter plot for Lead II.

A.1.3 Lead V1

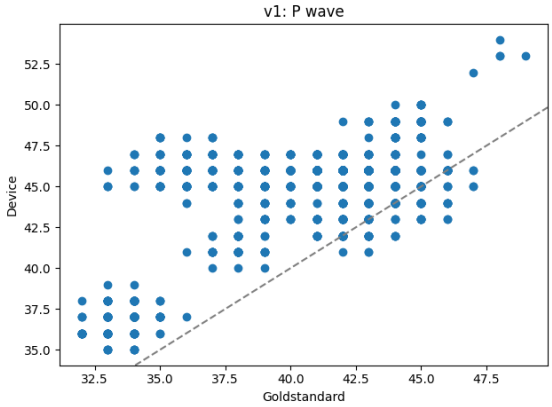

Figure A.25: P wave scatter plot for Lead V1.

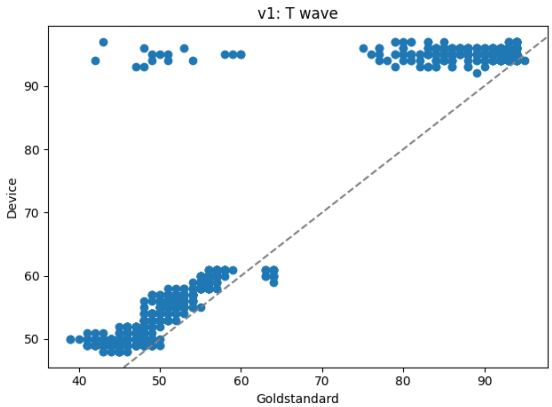

Figure A.26: T wave scatter plot for Lead V1.

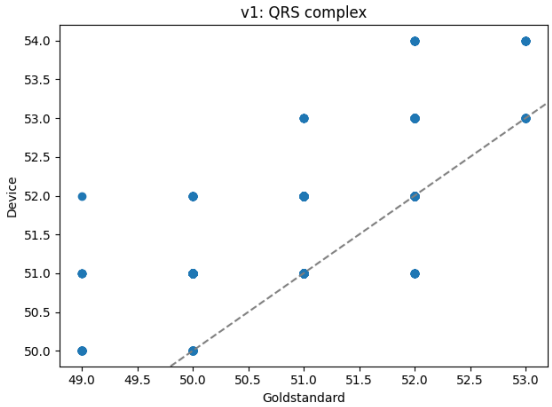

Figure A.27: QRS interval scatter plot for Lead V1.

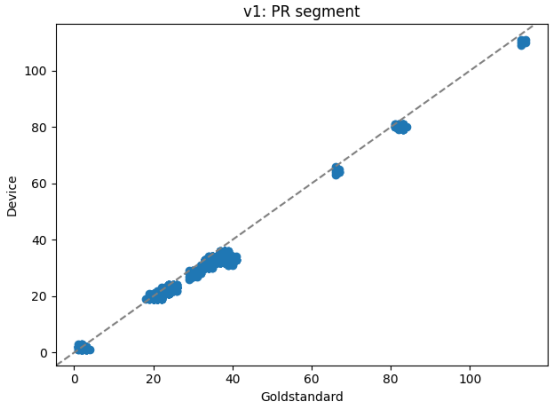

Figure A.28: PR segment scatter plot for Lead V1.

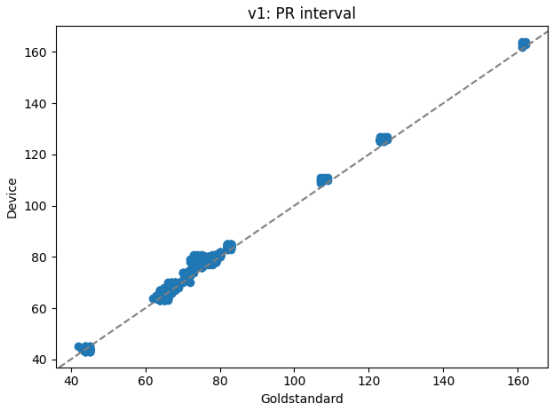

Figure A.29: PR interval scatter plot for Lead V1.

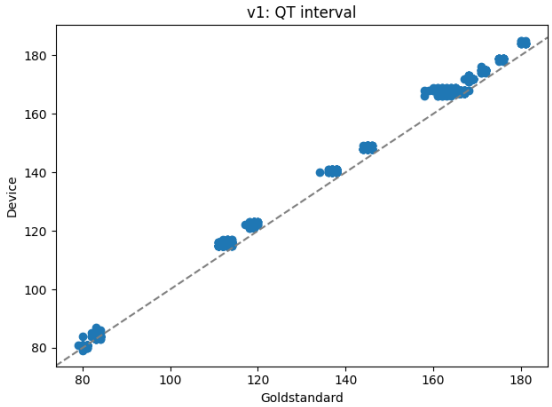

Figure A.30: QT interval scatter plot for Lead V1.

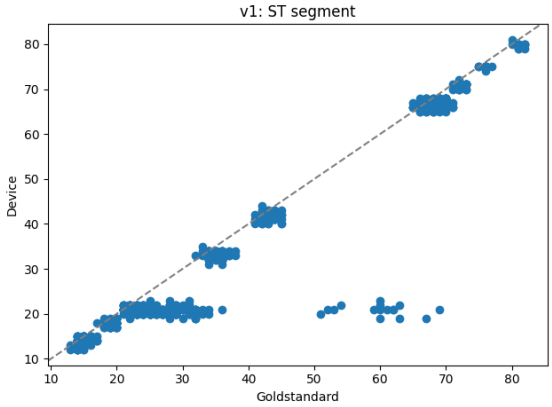

Figure A.31: ST segment scatter plot for Lead V1.

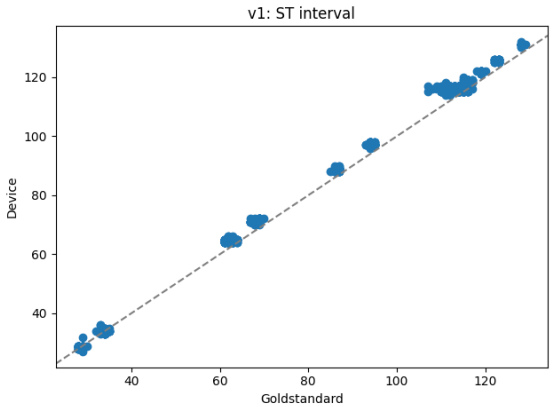

Figure A.32: ST interval scatter plot for Lead V1.

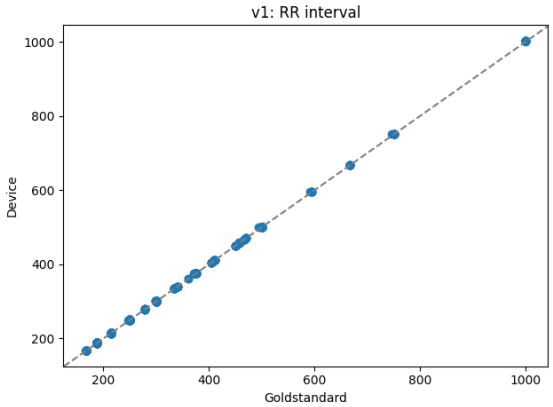

Figure A.33: RR interval scatter plot for Lead V1.

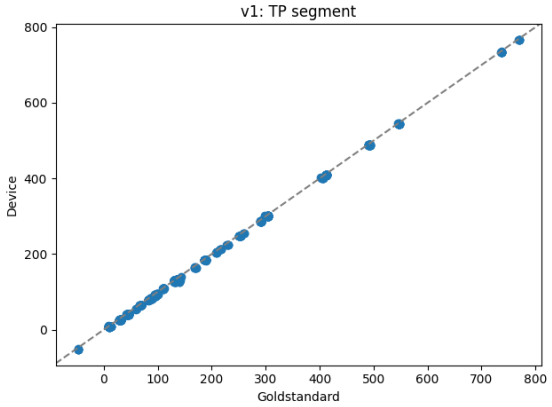

Figure A.34: TP segment scatter plot for Lead V1.

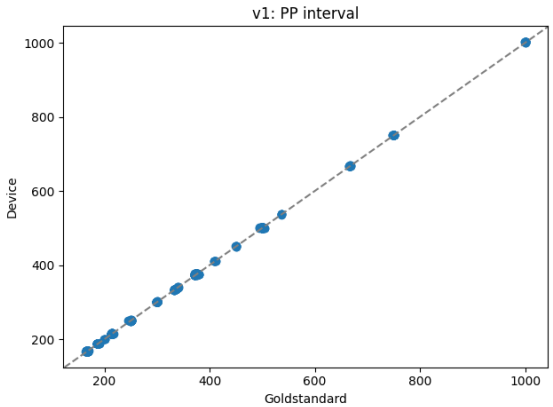

Figure A.35: PP interval scatter plot for Lead V1.

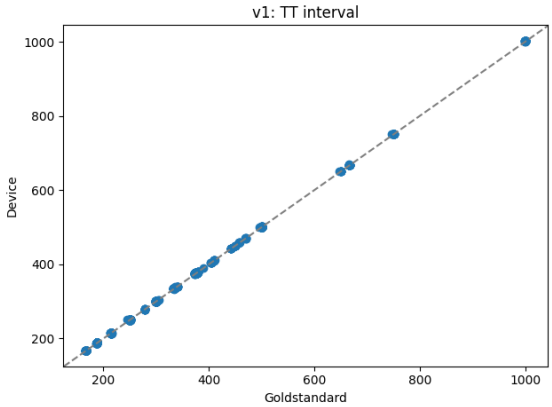

Figure A.36: TT interval scatter plot for Lead V1.

A.1.4 Lead V2

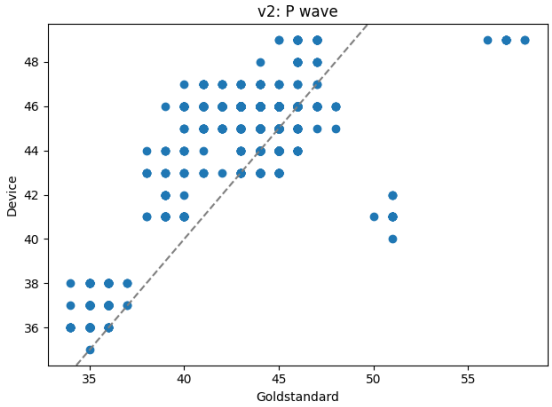

Figure A.37: P wave scatter plot for Lead V2.

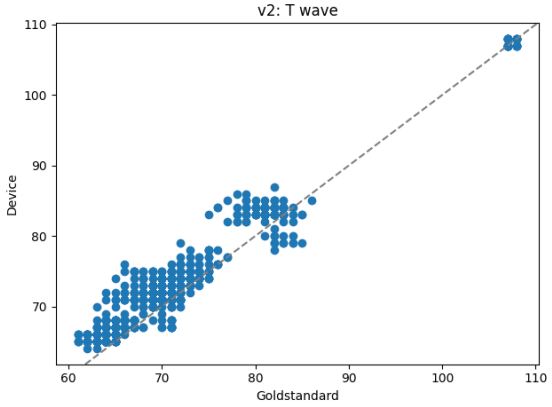

Figure A.38: T wave scatter plot for Lead V2.

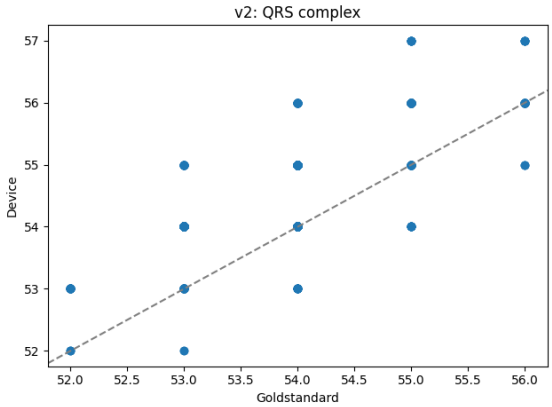

Figure A.39: QRS interval scatter plot for Lead V2.

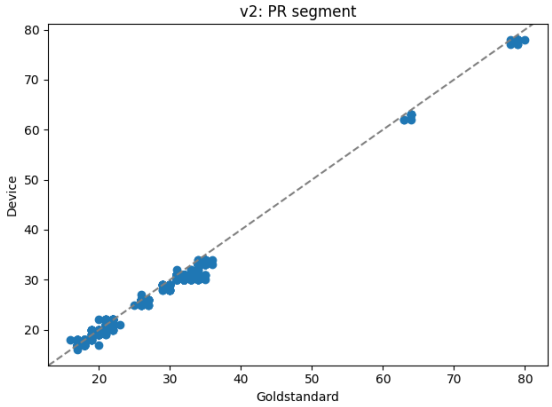

Figure A.40: PR segment scatter plot for Lead V2.

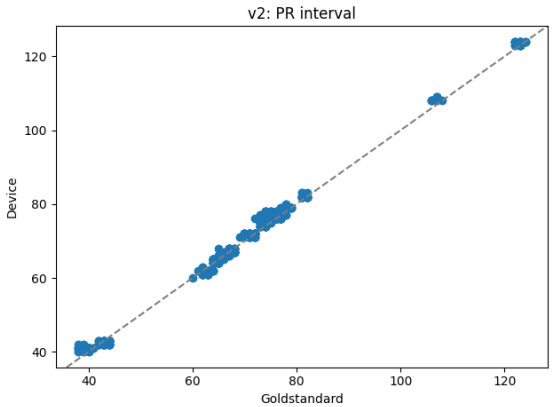

Figure A.41: PR interval scatter plot for Lead V2.

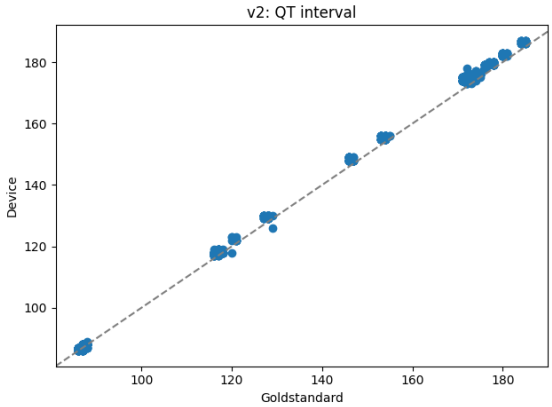

Figure A.42: QT interval scatter plot for Lead V2.

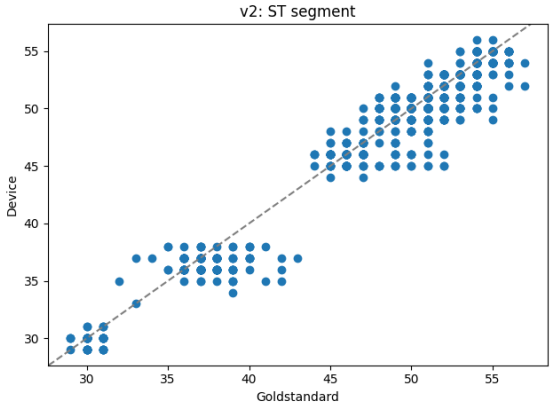

Figure A.43: ST segment scatter plot for Lead V2.

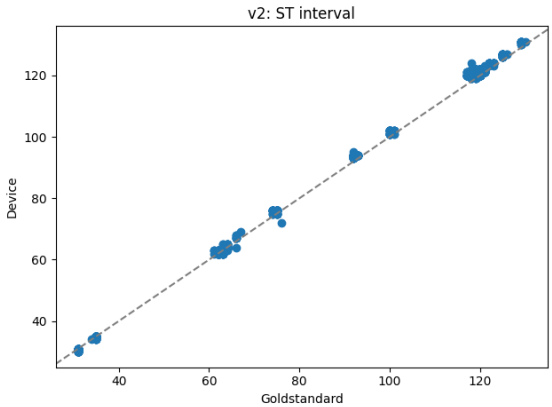

Figure A.44: ST interval scatter plot for Lead V2.

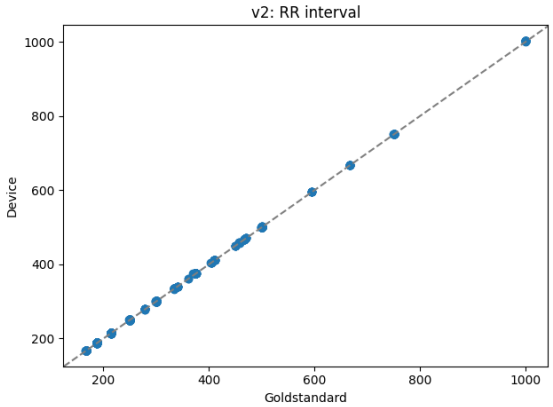

Figure A.45: RR interval scatter plot for Lead V2.

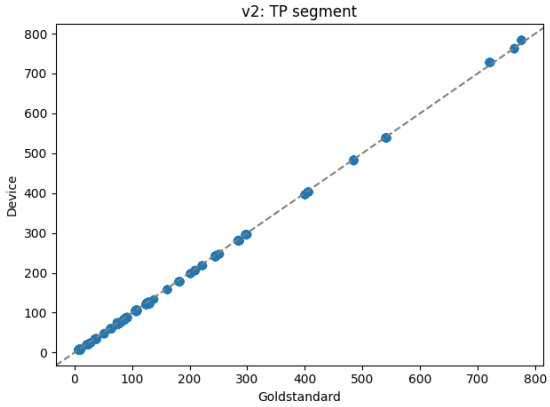

Figure A.46: TP segment scatter plot for Lead V2.

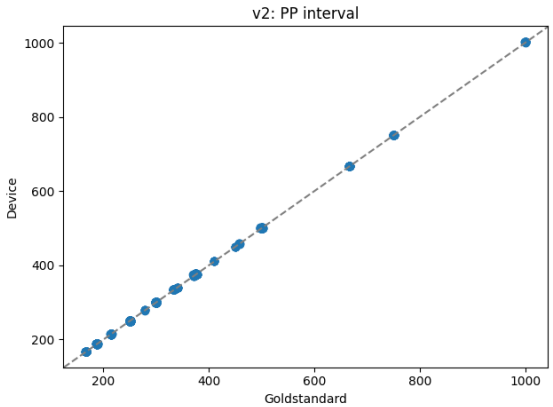

Figure A.47: PP interval scatter plot for Lead V2.

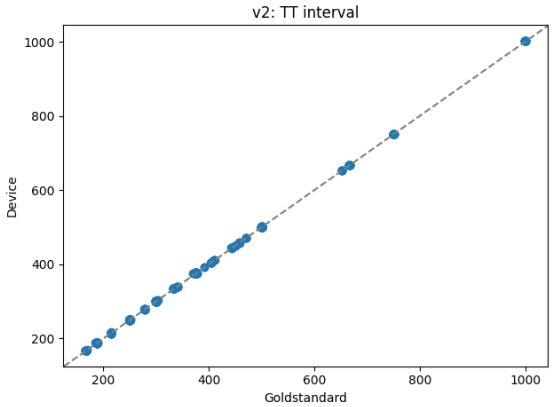

Figure A.48: TT interval scatter plot for Lead V2.

A.1.5 Lead V3

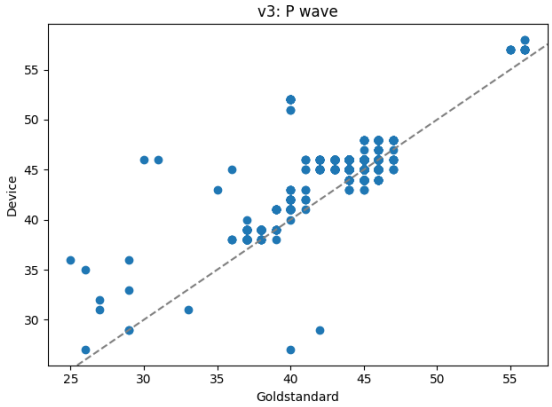

Figure A.49: P wave scatter plot for Lead V3.

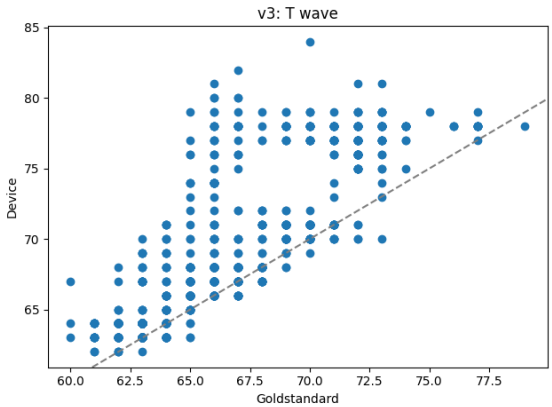

Figure A.50: T wave scatter plot for Lead V3.

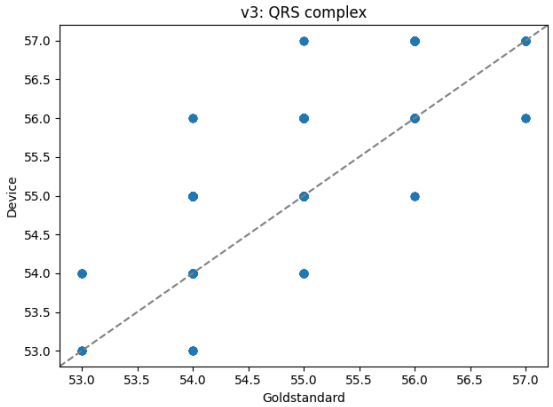

Figure A.51: QRS interval scatter plot for Lead V3.

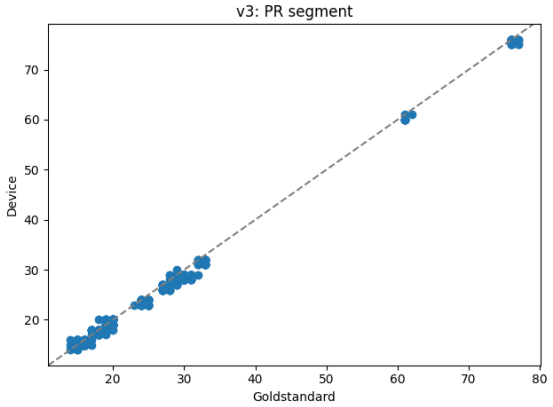

Figure A.52: PR segment scatter plot for Lead V3.

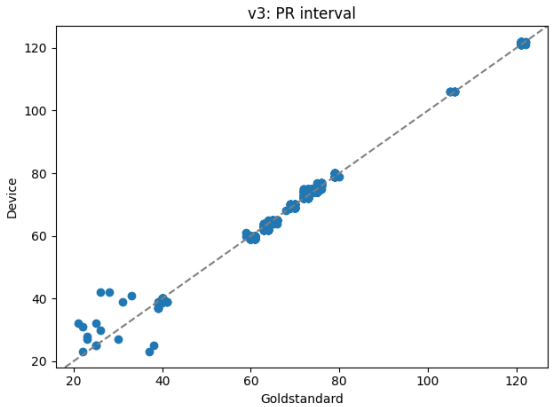

Figure A.53: PR interval scatter plot for Lead V3.

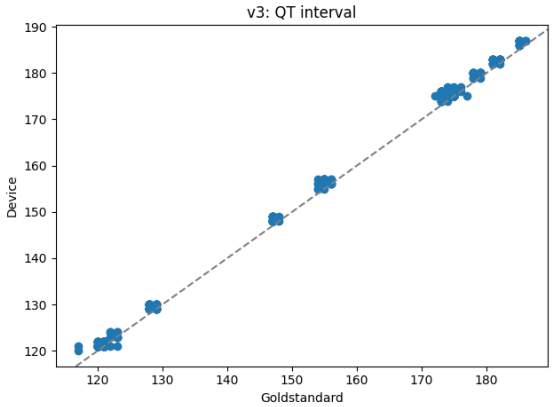

Figure A.54: QT interval scatter plot for Lead V3.

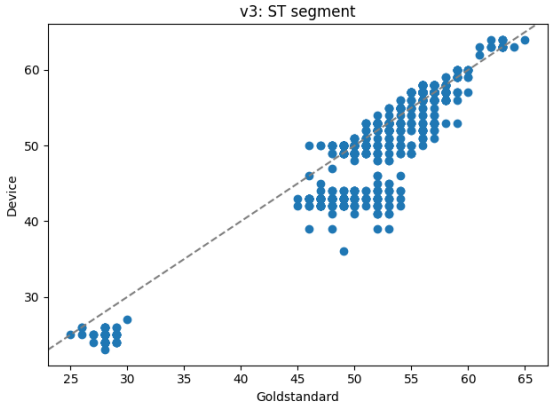

Figure A.55: ST segment scatter plot for Lead V3.

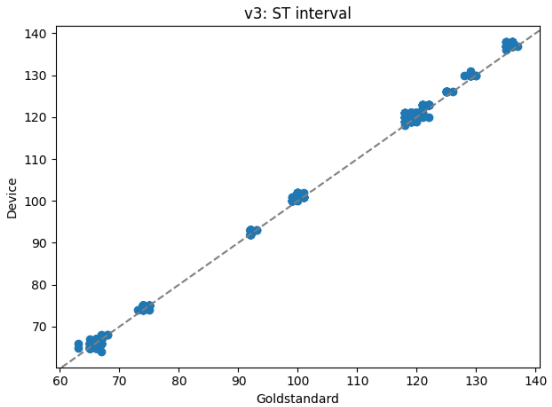

Figure A.56: ST interval scatter plot for Lead V3.

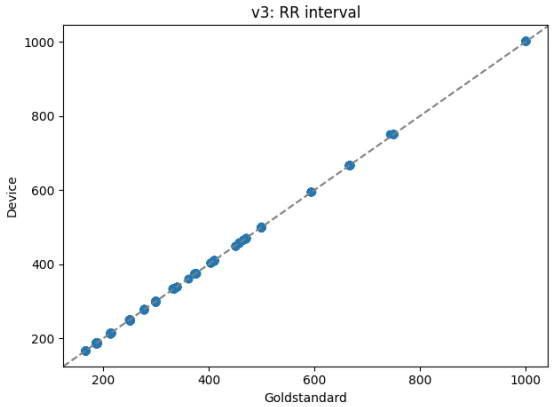

Figure A.57: RR interval scatter plot for Lead V3.

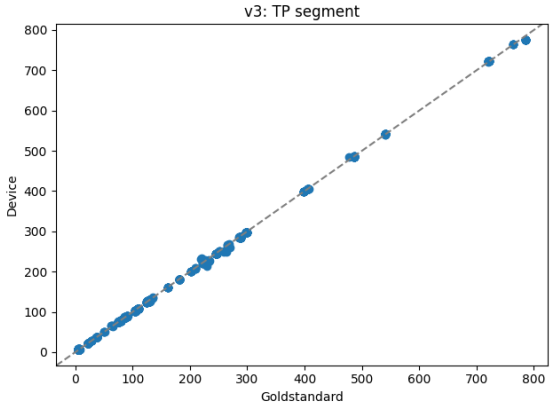

Figure A.58: TP segment scatter plot for Lead V3.

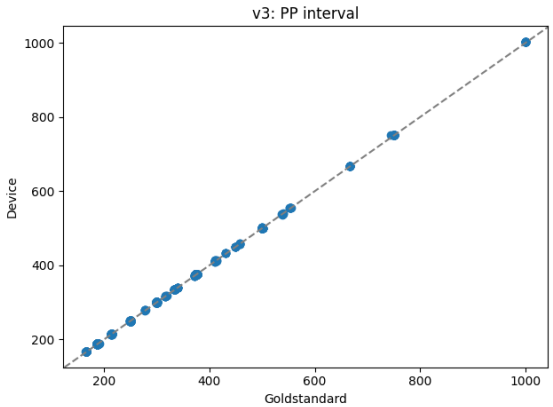

Figure A.59: PP interval scatter plot for Lead V3.

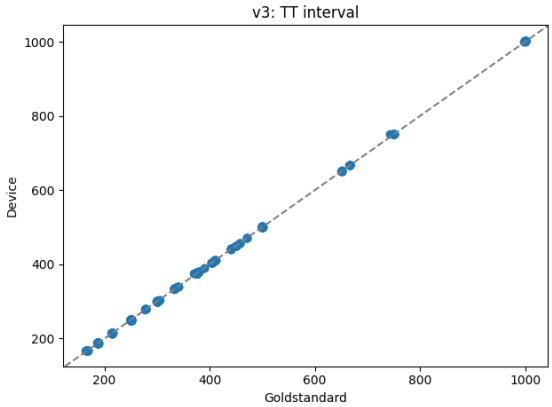

Figure A.60: TT interval scatter plot for Lead V3.

A.1.6 Lead V4

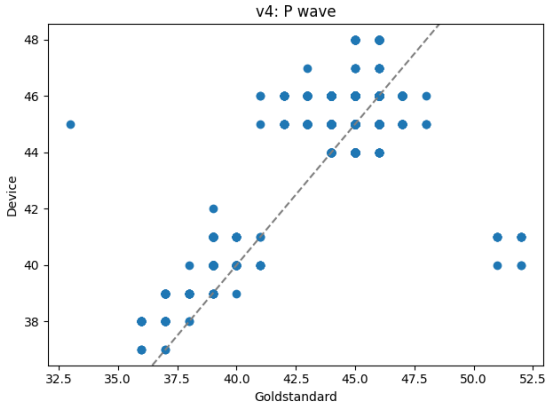

Figure A.61: P wave scatter plot for Lead V4.

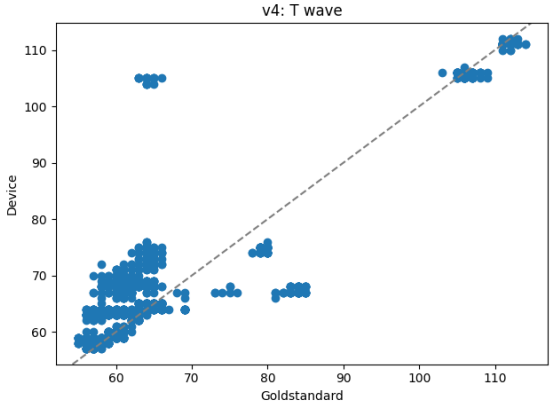

Figure A.62: T wave scatter plot for Lead V4.

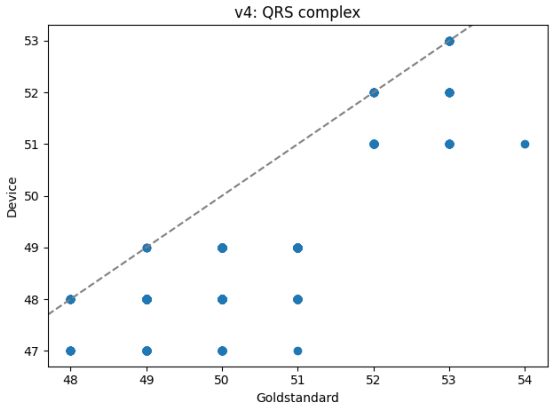

Figure A.63: QRS interval scatter plot for Lead V4.

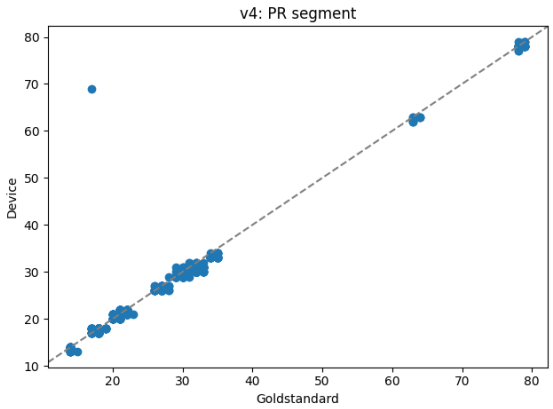

Figure A.64: PR segment scatter plot for Lead V4.

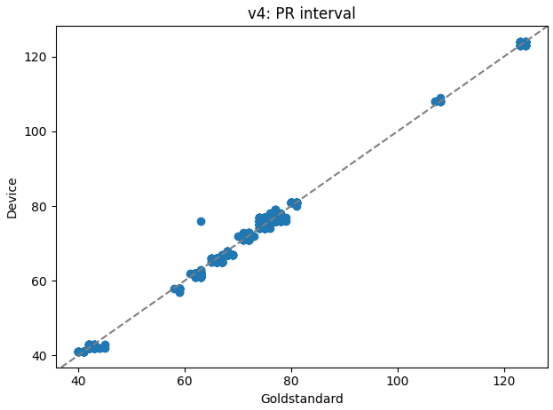

Figure A.65: PR interval scatter plot for Lead V4.

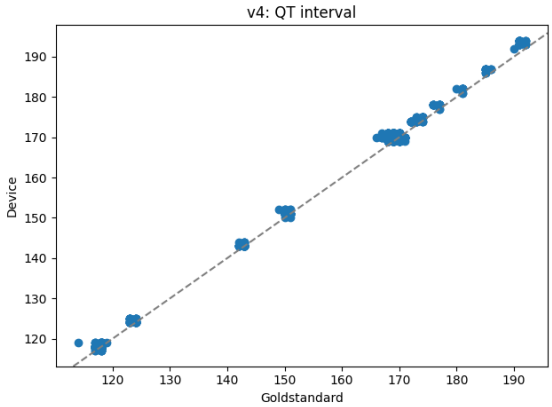

Figure A.66: QT interval scatter plot for Lead V4.

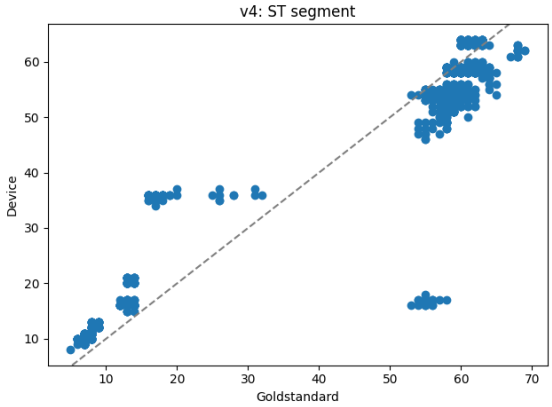

Figure A.67: ST segment scatter plot for Lead V4.

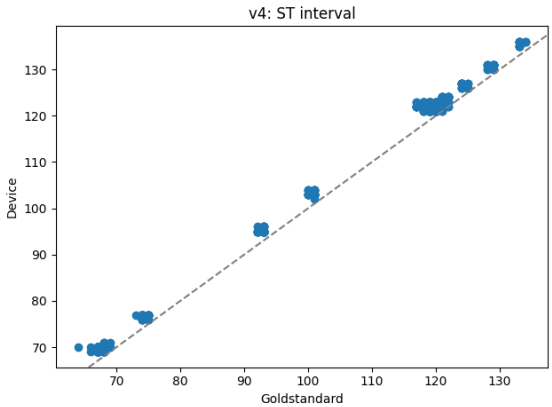

Figure A.68: ST interval scatter plot for Lead V4.

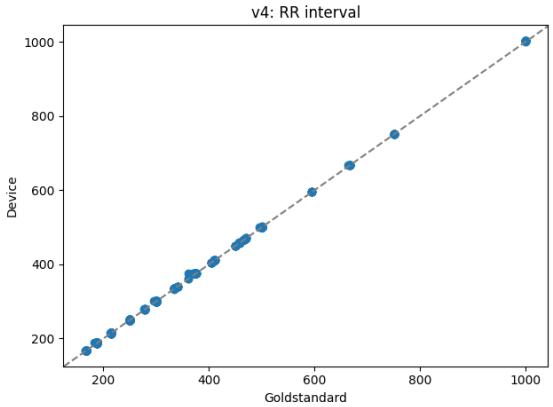

Figure A.69: RR interval scatter plot for Lead V4.

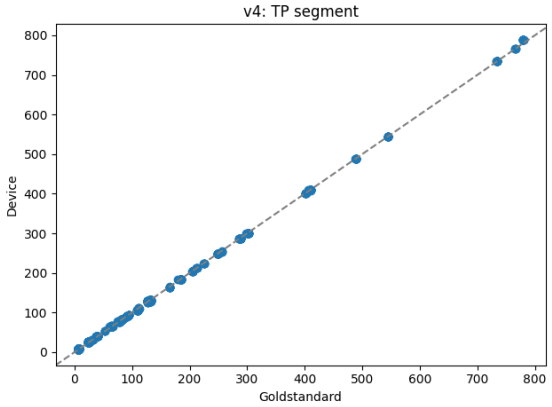

Figure A.70: TP segment scatter plot for Lead V4.

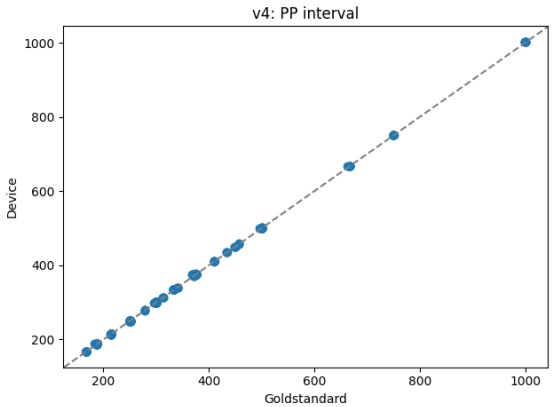

Figure A.71: PP interval scatter plot for Lead V4.

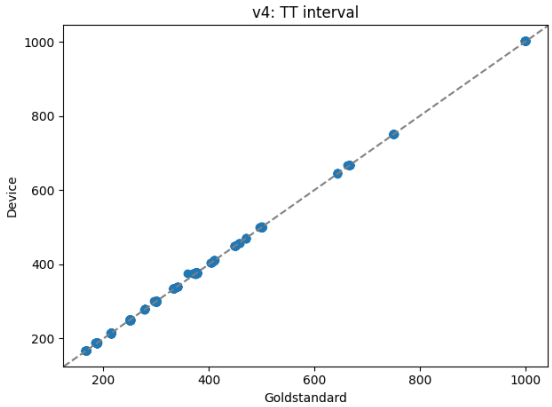

Figure A.72: TT interval scatter plot for Lead V4.

A.1.7 Lead V5

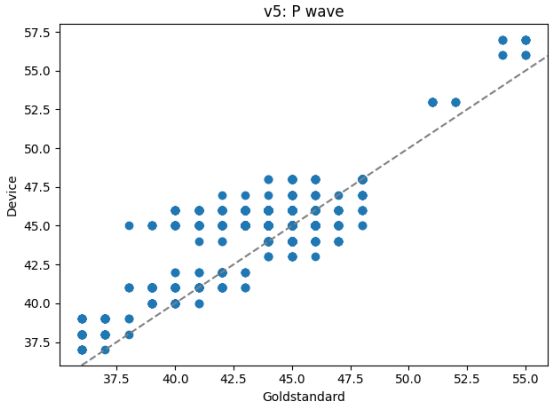

Figure A.73: P wave scatter plot for Lead V5.

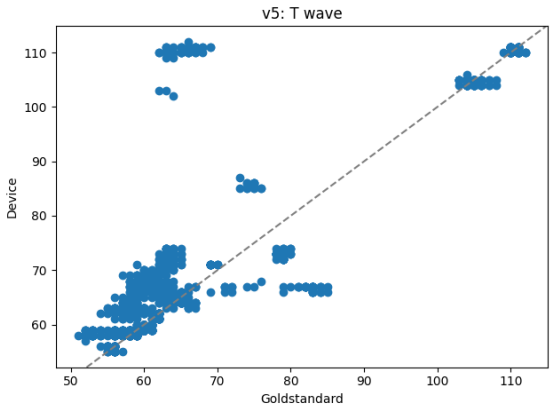

Figure A.74: T wave scatter plot for Lead V5.

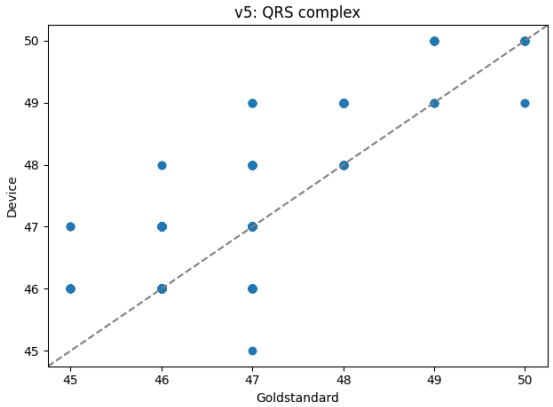

Figure A.75: QRS interval scatter plot for Lead V5.

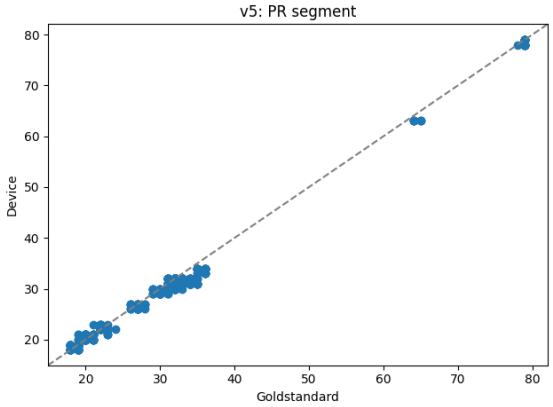

Figure A.76: PR segment scatter plot for Lead V5.

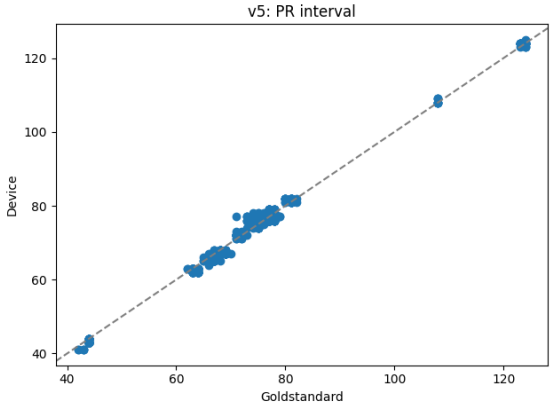

Figure A.77: PR interval scatter plot for Lead V5.

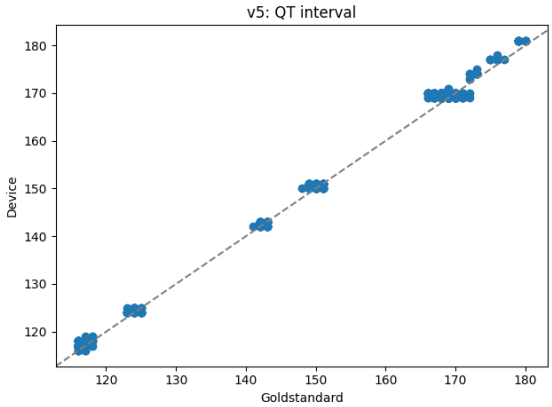

Figure A.78: QT interval scatter plot for Lead V5.

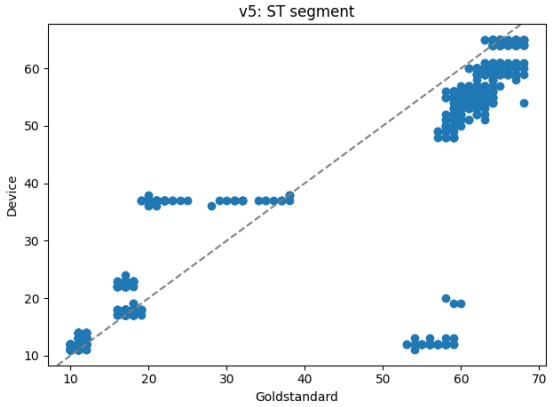

Figure A.79: ST segment scatter plot for Lead V5.

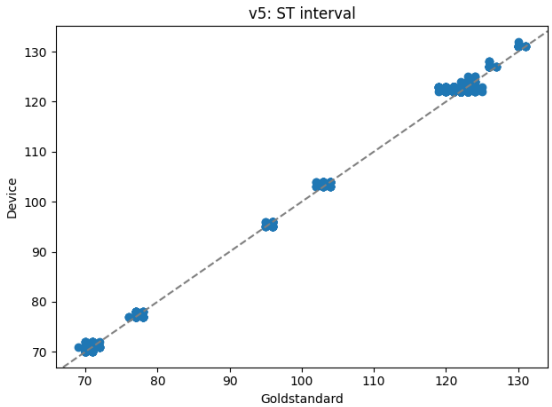

Figure A.80: ST interval scatter plot for Lead V5.

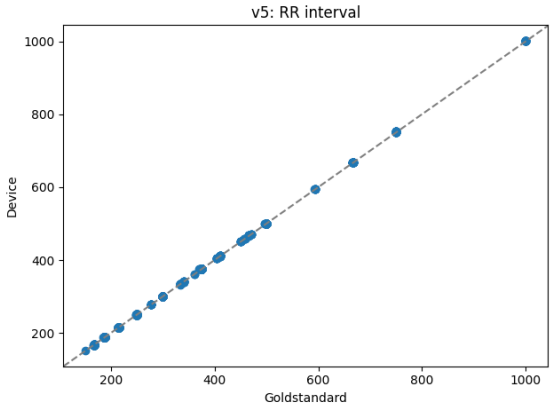

Figure A.81: RR interval scatter plot for Lead V5.

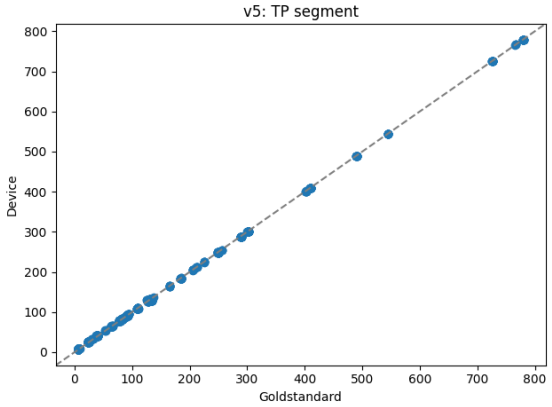

Figure A.82: TP segment scatter plot for Lead V5.

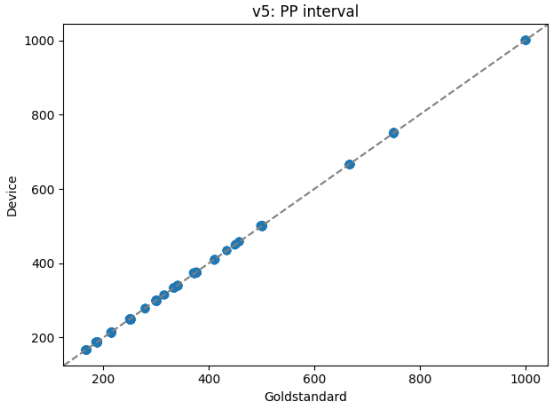

Figure A.83: PP interval scatter plot for Lead V5.

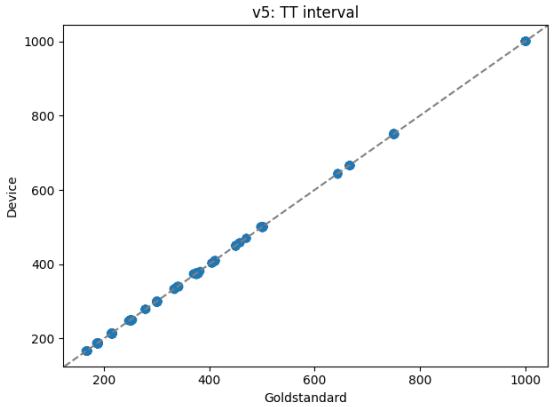

Figure A.84: TT interval scatter plot for Lead V5.

A.1.8 Lead V6

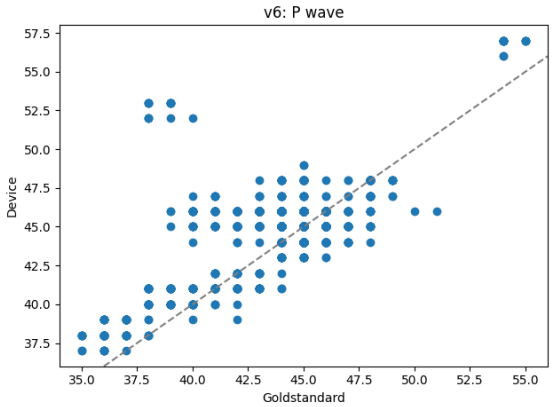

Figure A.85: P wave scatter plot for Lead V6.

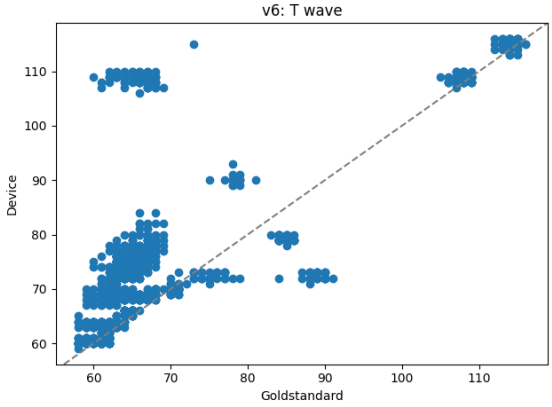

Figure A.86: T wave scatter plot for Lead V6.

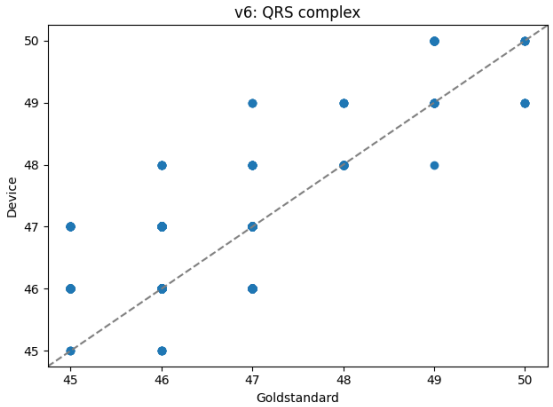

Figure A.87: QRS interval scatter plot for Lead V6.

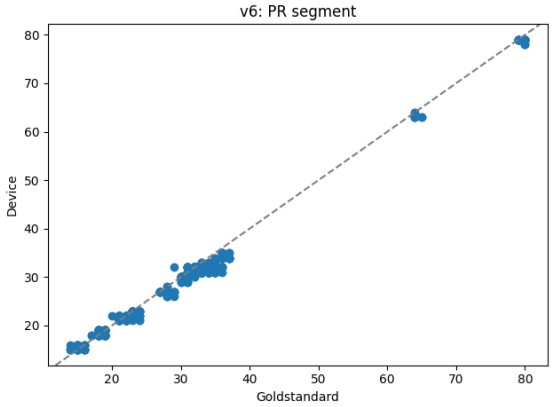

Figure A.88: PR segment scatter plot for Lead V6.

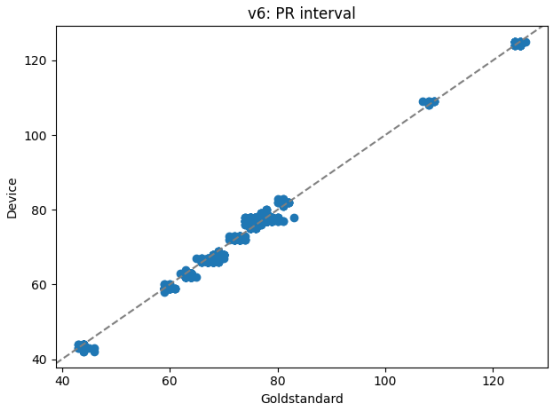

Figure A.89: PR interval scatter plot for Lead V6.

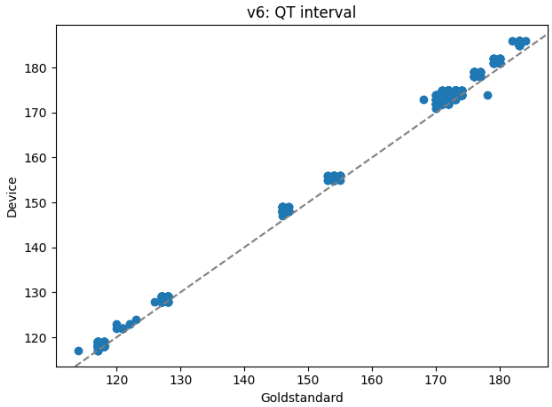

Figure A.90: QT interval scatter plot for Lead V6.

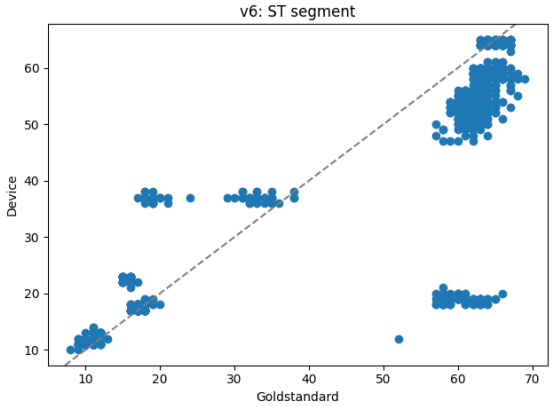

Figure A.91: ST segment scatter plot for Lead V6.

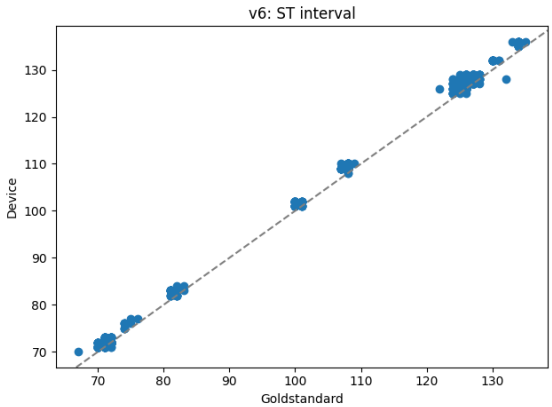

Figure A.92: ST interval scatter plot for Lead V6.

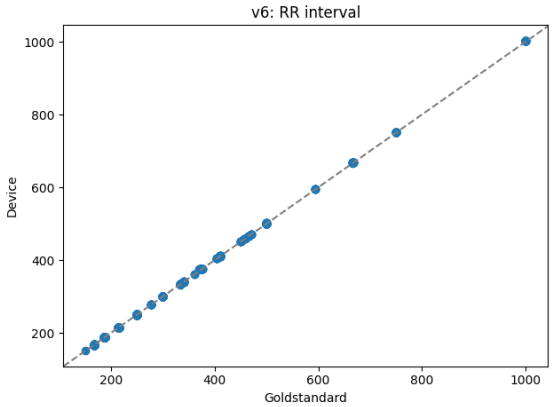

Figure A.93: RR interval scatter plot for Lead V6.

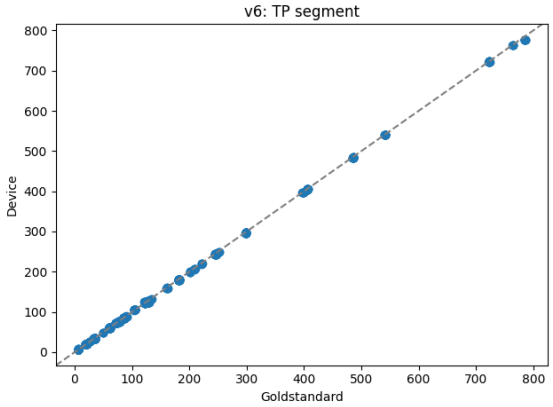

Figure A.94: TP segment scatter plot for Lead V6.

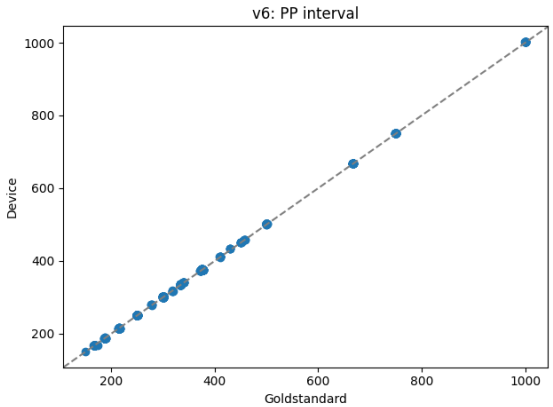

Figure A.95: PP interval scatter plot for Lead V6.

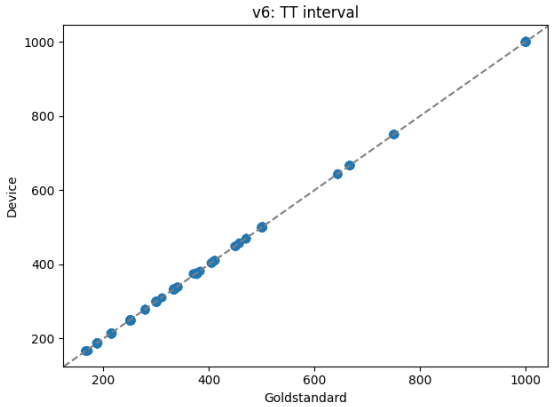

Figure A.96: TT interval scatter plot for Lead V6.

A.2 Bland-Altman results

A.2.1 Lead I

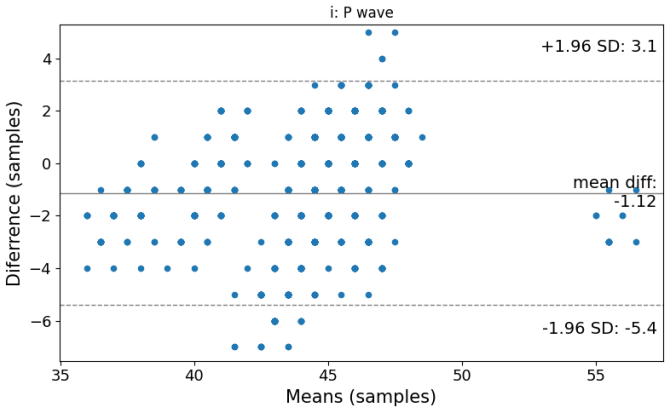

Figure A.97: P wave Bland-Altman plot for Lead I.

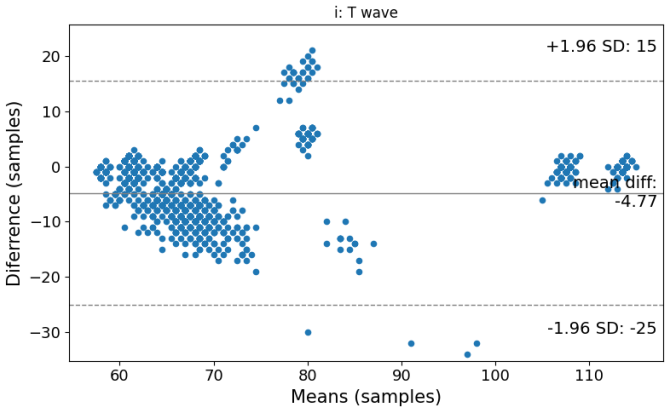

Figure A.98: T wave Bland-Altman plot for Lead I.

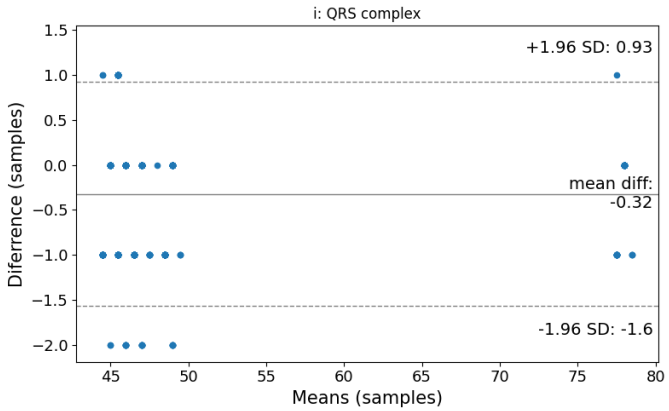

Figure A.99: QRS interval Bland-Altman plot for Lead I.

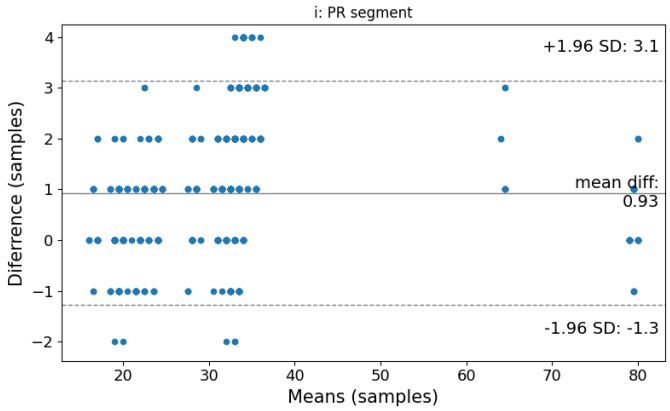

Figure A.100: PR segment Bland-Altman plot for Lead I.

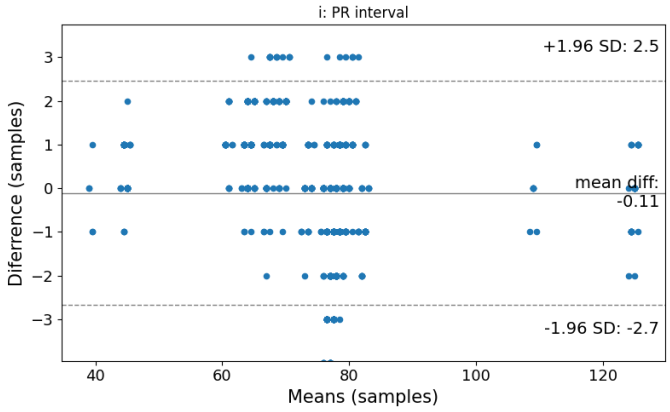

Figure A.101: PR interval Bland-Altman plot for Lead I.

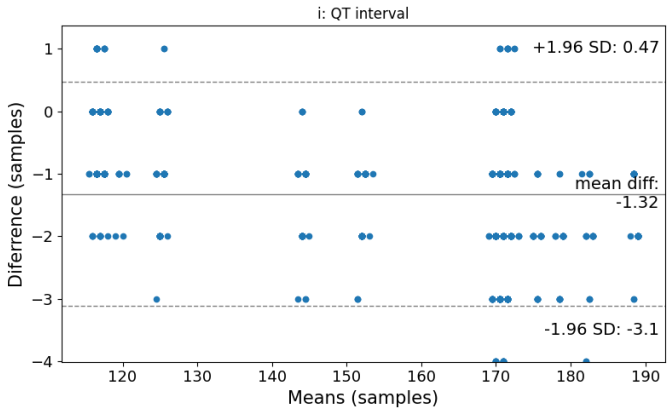

Figure A.102: QT interval Bland-Altman plot for Lead I.

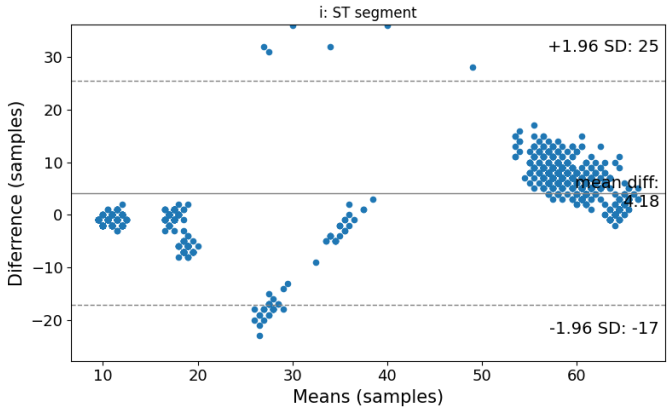

Figure A.103: ST segment Bland-Altman plot for Lead I.

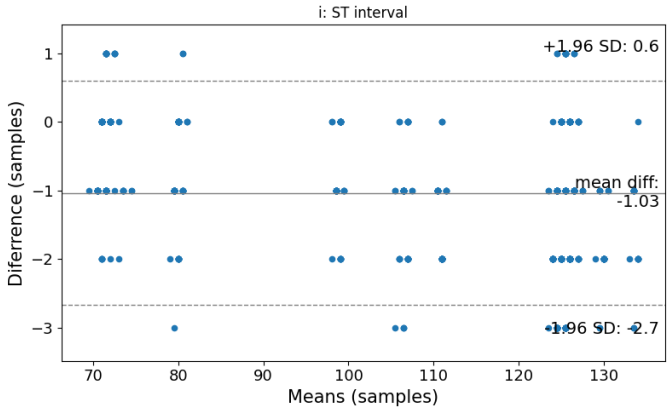

Figure A.104: ST interval Bland-Altman plot for Lead I.

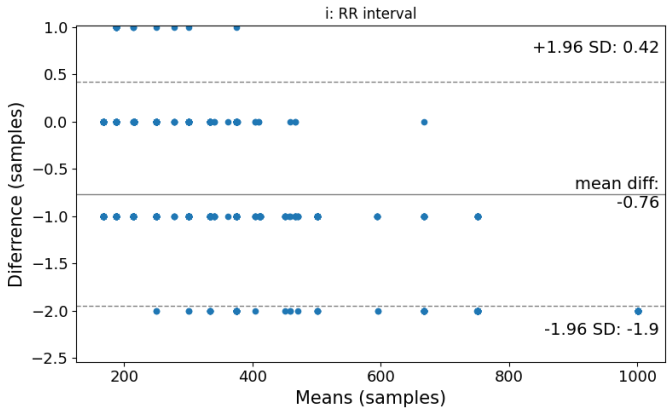

Figure A.105: RR interval Bland-Altman plot for Lead I.

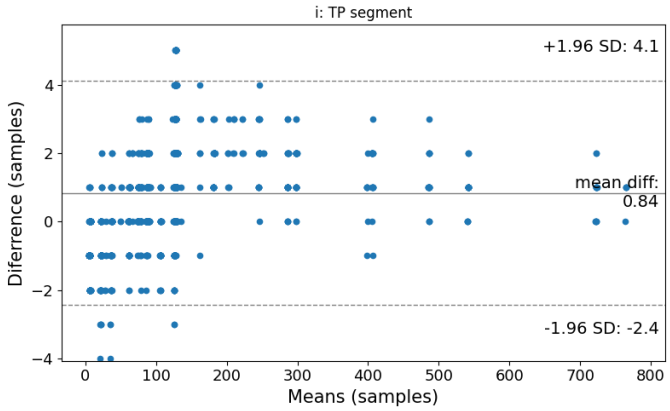

Figure A.106: TP segment Bland-Altman plot for Lead I.

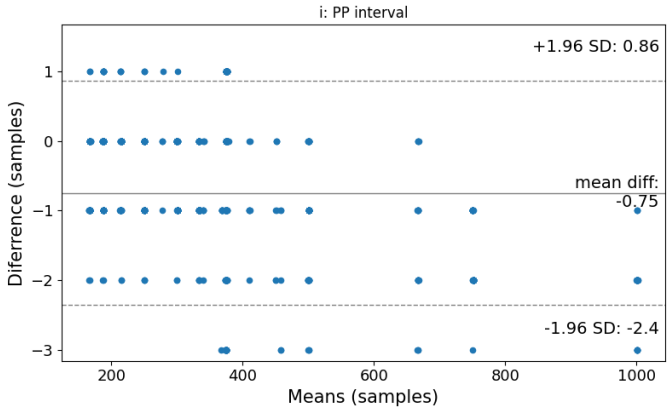

Figure A.107: PP interval Bland-Altman plot for Lead I.

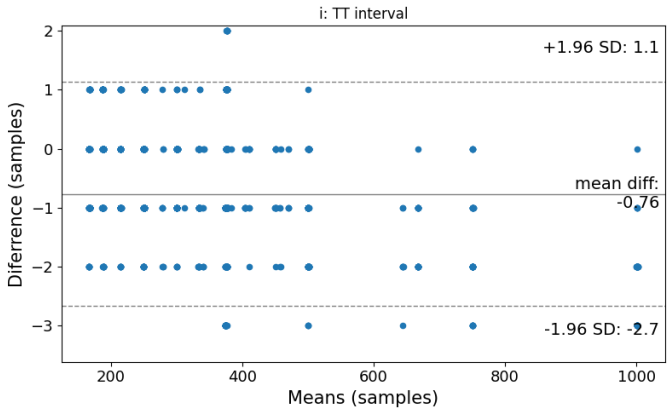

Figure A.108: TT interval Bland-Altman plot for Lead I.

A.2.2 Lead II

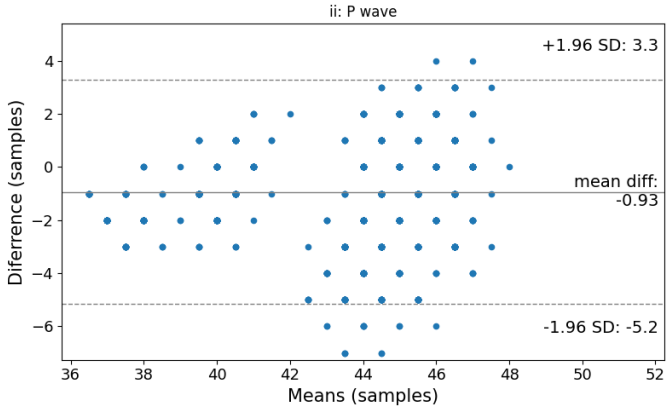

Figure A.109: P wave Bland-Altman plot for Lead II.

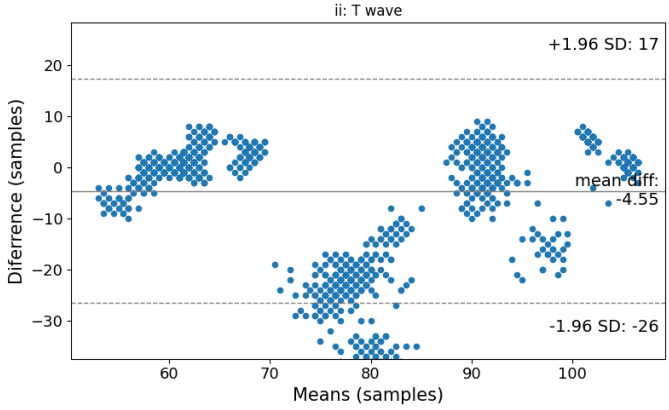

Figure A.110: T wave Bland-Altman plot for Lead II.

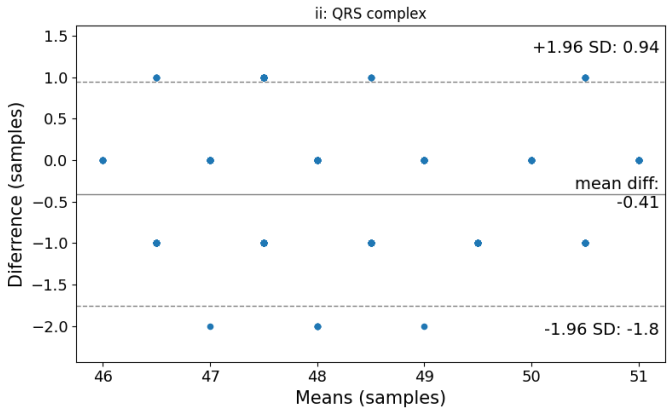

Figure A.111: QRS interval Bland-Altman plot for Lead II.

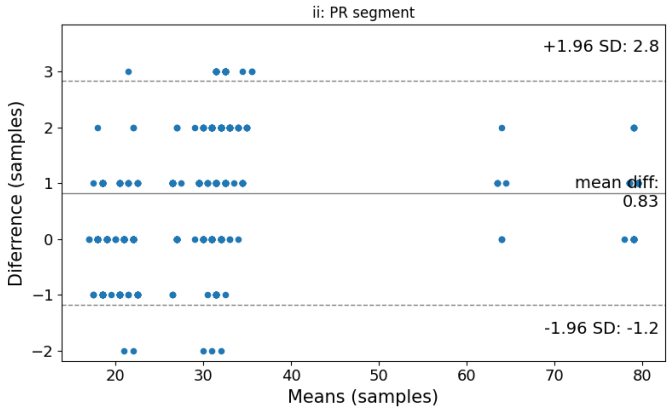

Figure A.112: PR segment Bland-Altman plot for Lead II.

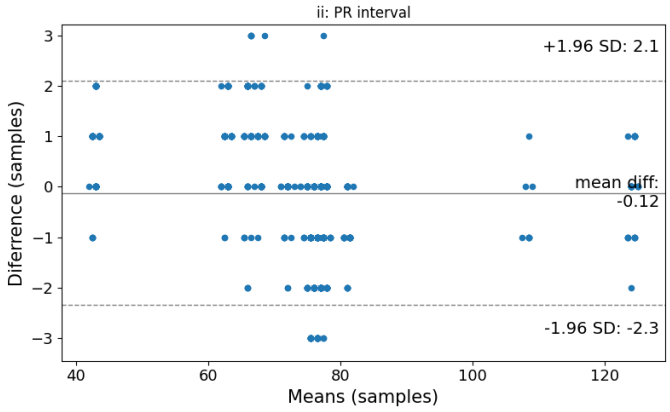

Figure A.113: PR interval Bland-Altman plot for Lead II.

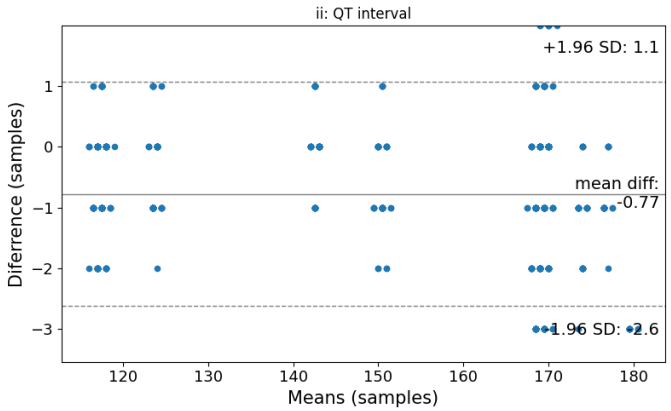

Figure A.114: QT interval Bland-Altman plot for Lead II.

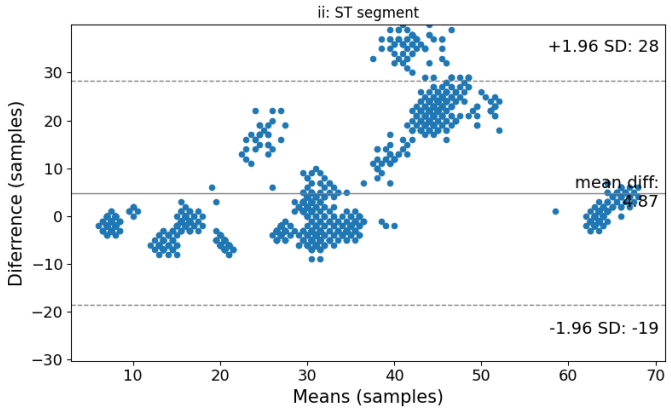

Figure A.115: ST segment Bland-Altman plot for Lead II.

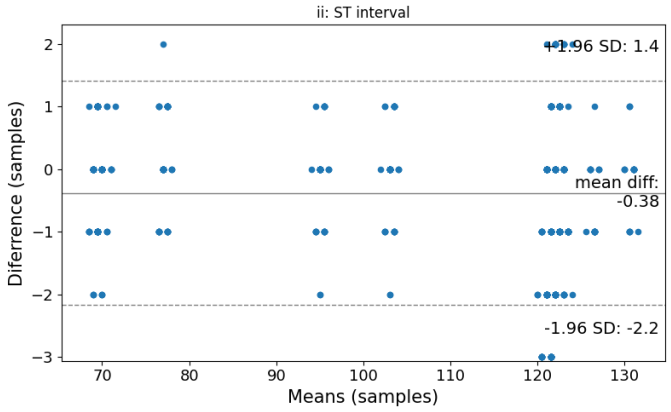

Figure A.116: ST interval Bland-Altman plot for Lead II.

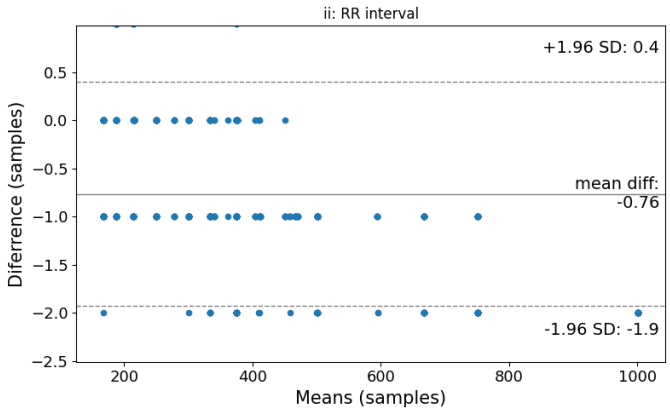

Figure A.117: RR interval Bland-Altman plot for Lead II.

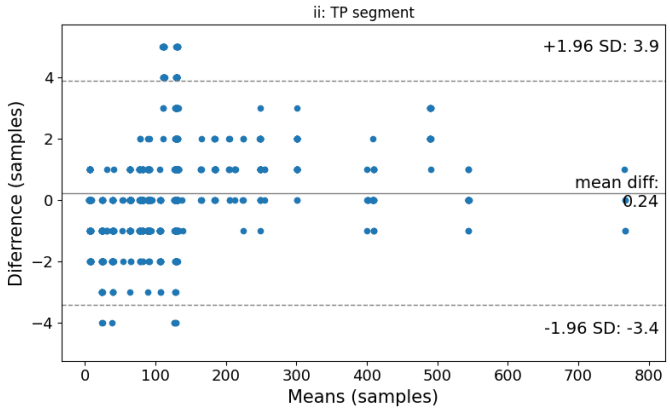

Figure A.118: TP segment Bland-Altman plot for Lead II.

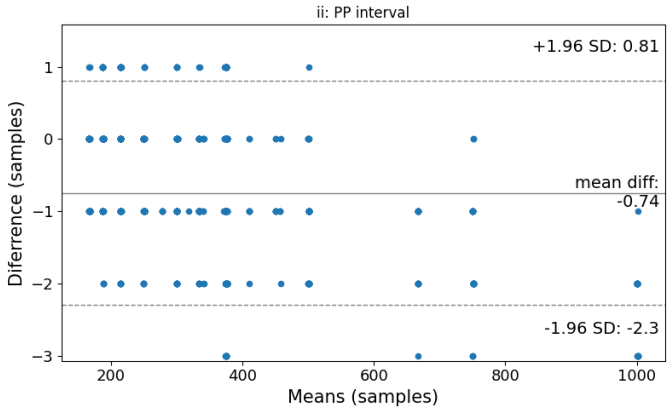

Figure A.119: PP interval Bland-Altman plot for Lead II.

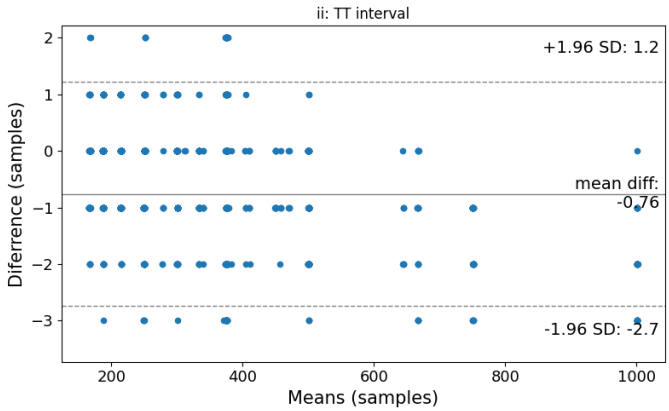

Figure A.120: TT interval Bland-Altman plot for Lead II.

A.2.3 Lead V1

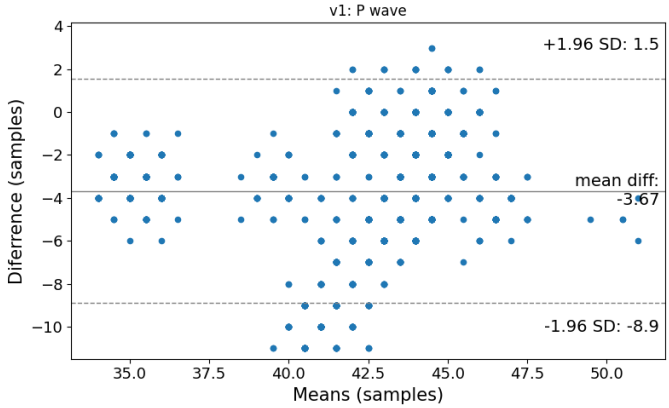

Figure A.121: P wave Bland-Altman plot for Lead V1.

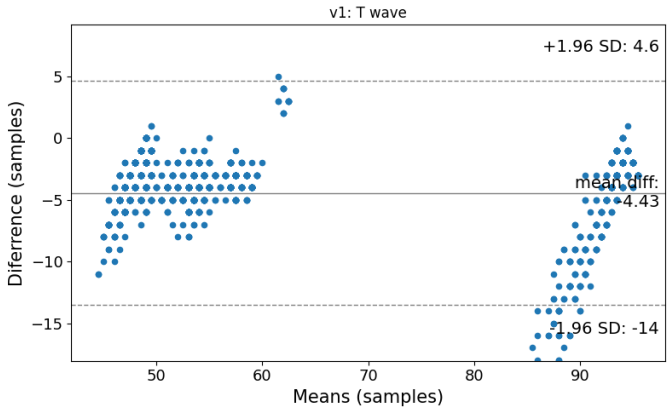

Figure A.122: T wave Bland-Altman plot for Lead V1.

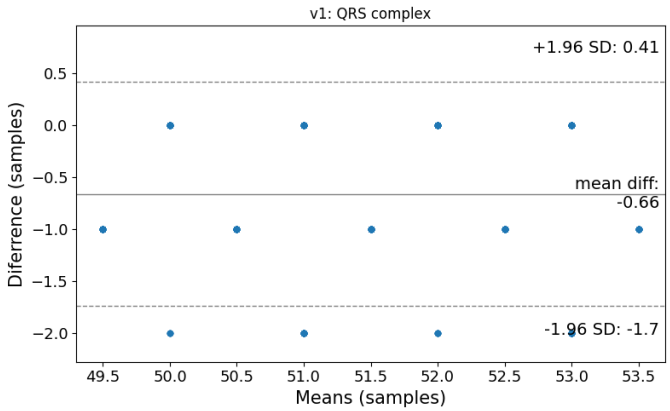

Figure A.123: QRS interval Bland-Altman plot for Lead V1.

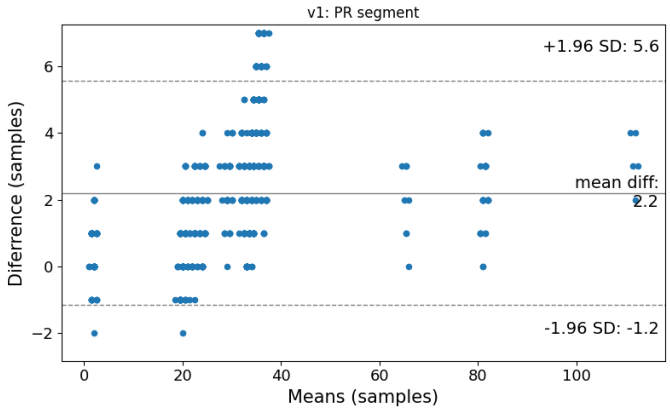

Figure A.124: PR segment Bland-Altman plot for Lead V1.

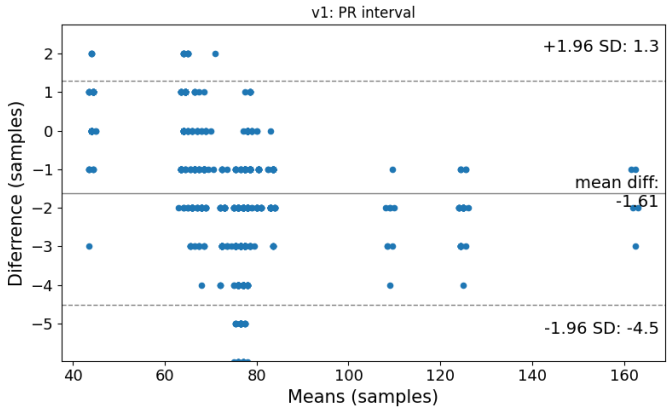

Figure A.125: PR interval Bland-Altman plot for Lead V1.

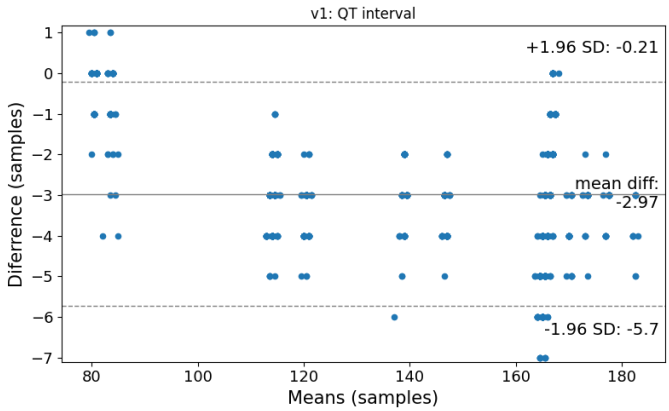

Figure A.126: QT interval Bland-Altman plot for Lead V1.

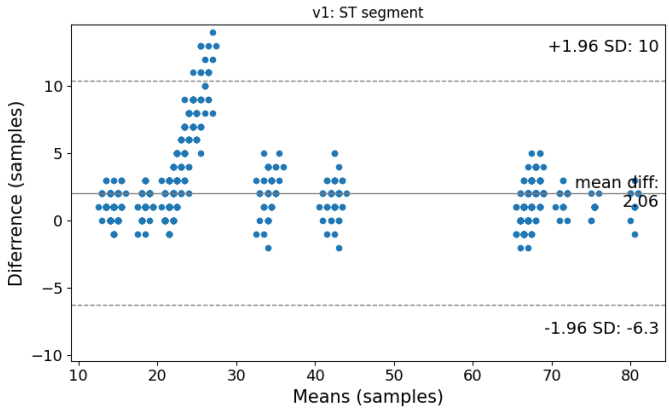

Figure A.127: ST segment Bland-Altman plot for Lead V1.

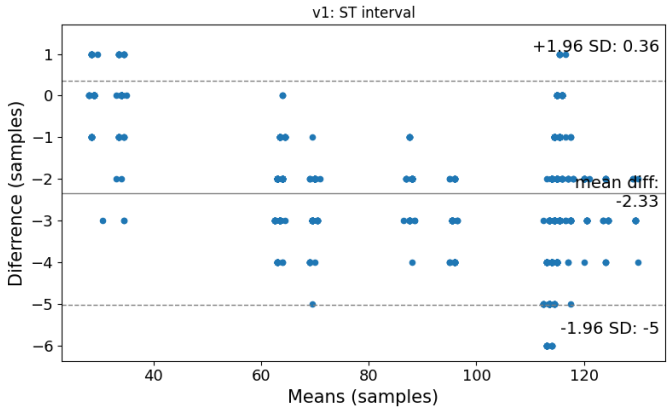

Figure A.128: ST interval Bland-Altman plot for Lead V1.

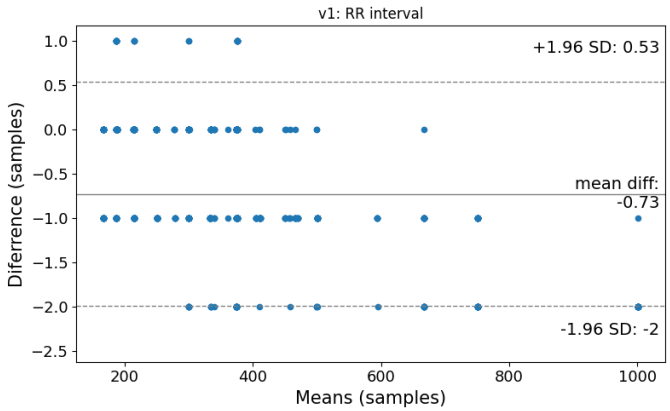

Figure A.129: RR interval Bland-Altman plot for Lead V1.

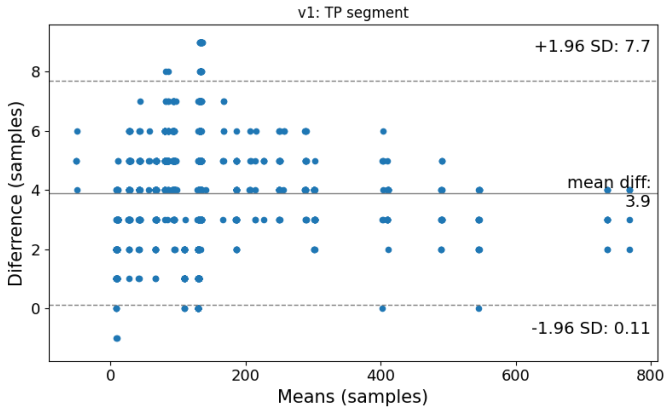

Figure A.130: TP segment Bland-Altman plot for Lead V1.

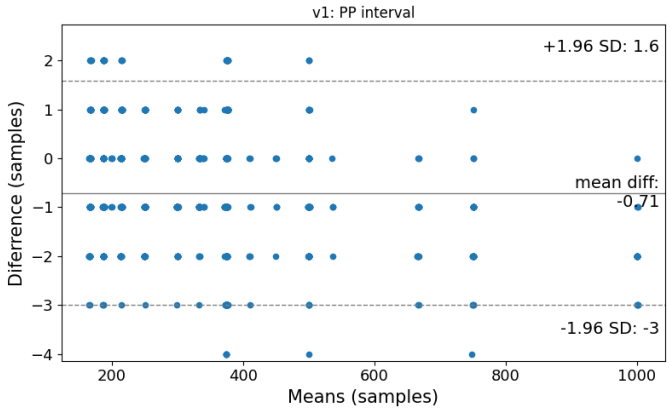

Figure A.131: PP interval Bland-Altman plot for Lead V1.

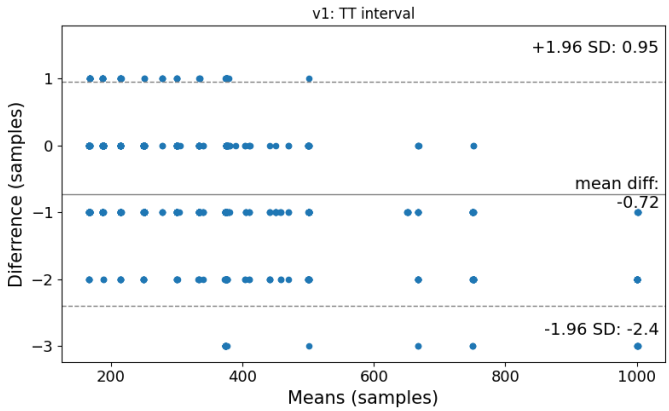

Figure A.132: TT interval Bland-Altman plot for Lead V1.

A.2.4 Lead V2

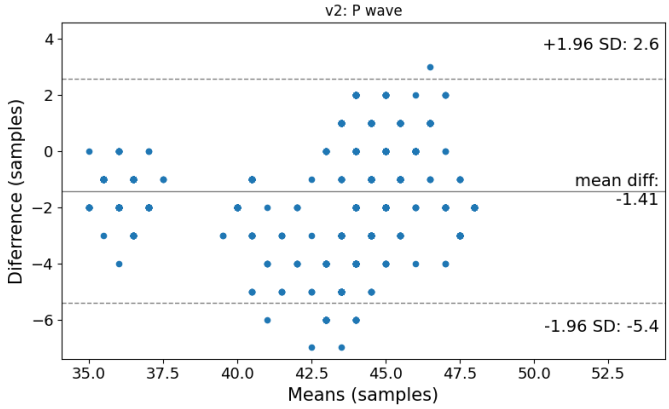

Figure A.133: P wave Bland-Altman plot for Lead V2.

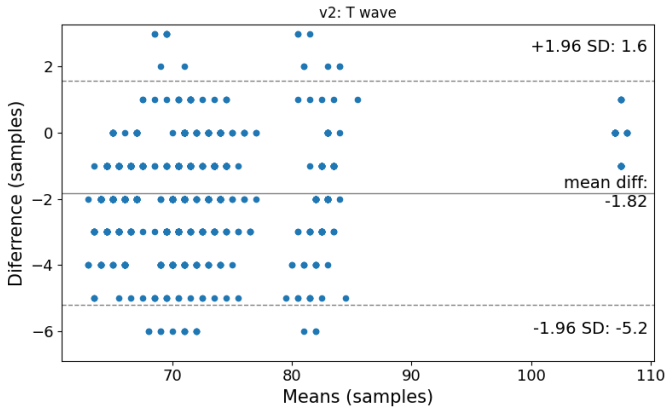

Figure A.134: T wave Bland-Altman plot for Lead V2.

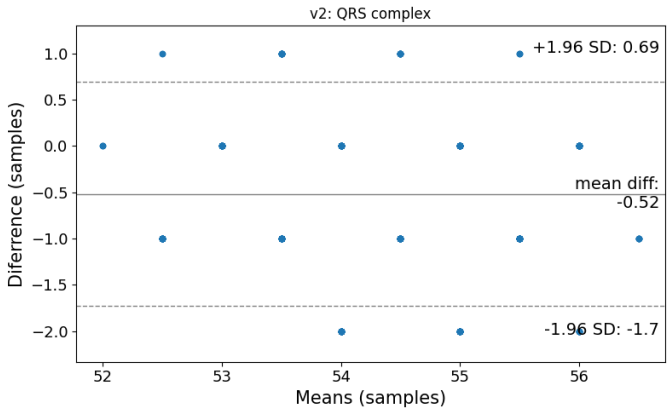

Figure A.135: QRS interval Bland-Altman plot for Lead V2.

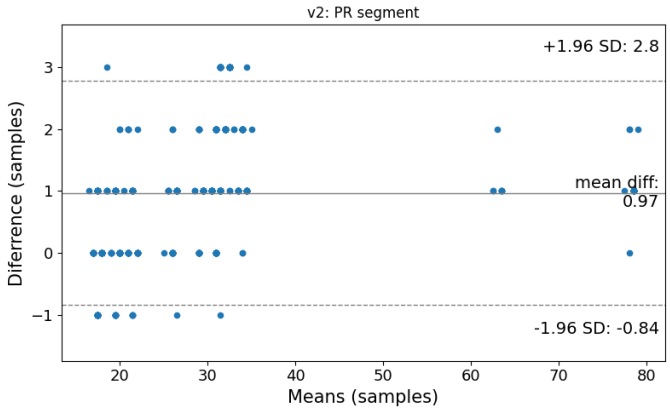

Figure A.136: PR segment Bland-Altman plot for Lead V2.

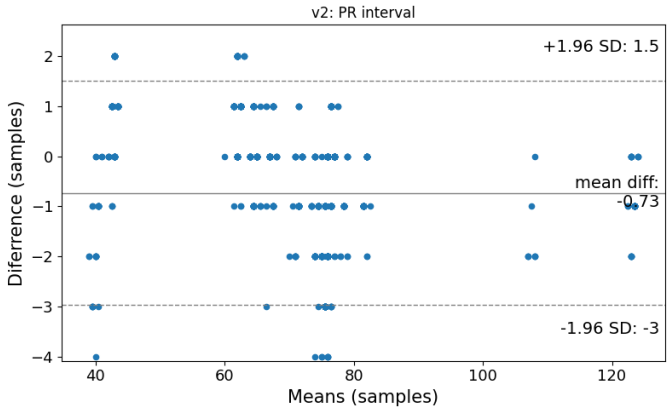

Figure A.137: PR interval Bland-Altman plot for Lead V2.

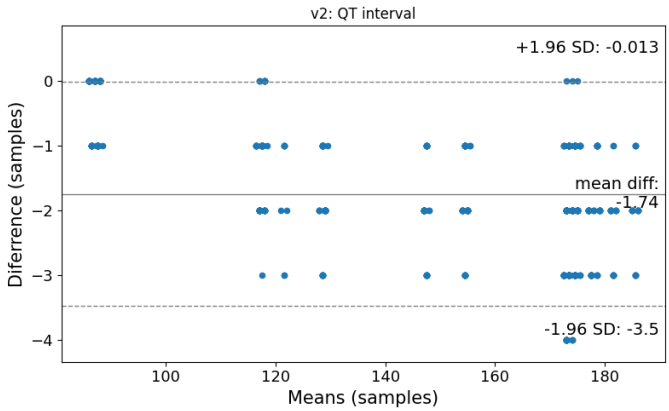

Figure A.138: QT interval Bland-Altman plot for Lead V2.

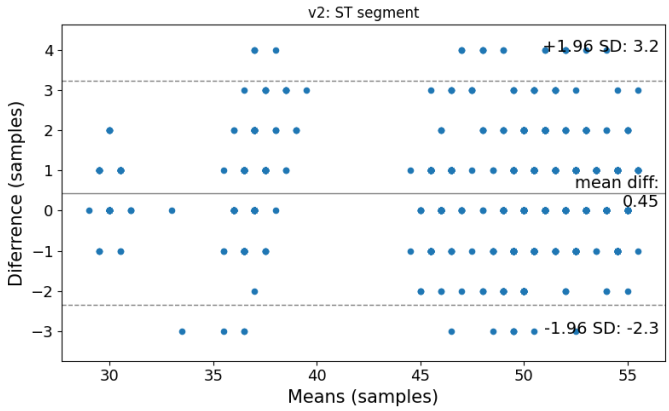

Figure A.139: ST segment Bland-Altman plot for Lead V2.

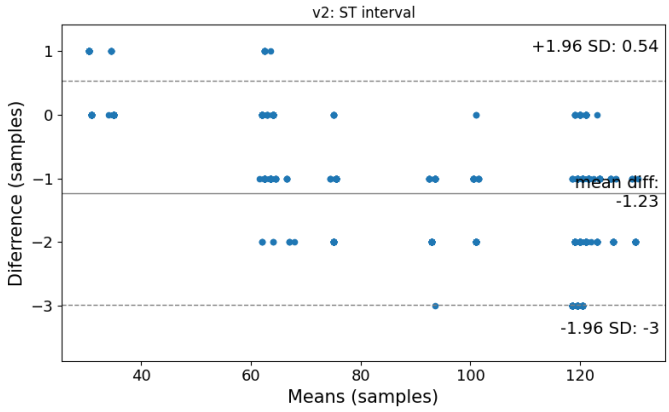

Figure A.140: ST interval Bland-Altman plot for Lead V2.

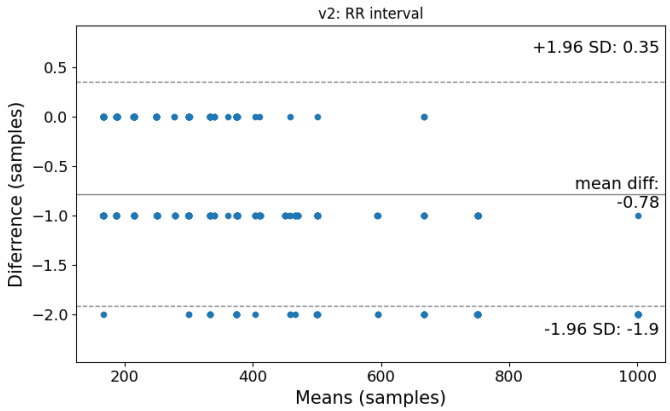

Figure A.141: RR interval Bland-Altman plot for Lead V2.

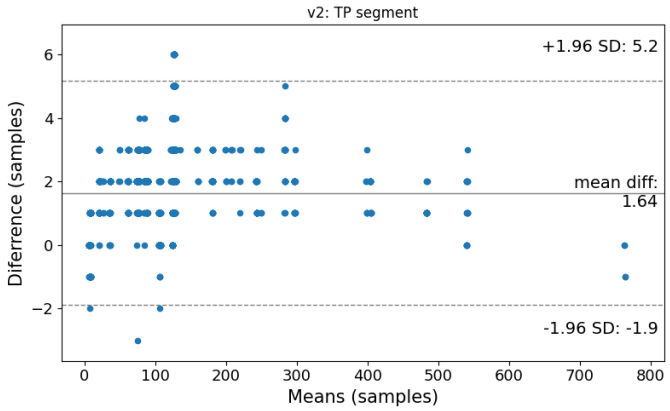

Figure A.142: TP segment Bland-Altman plot for Lead V2.

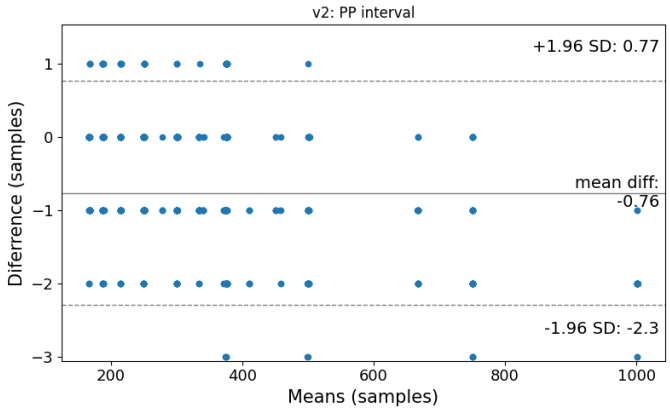

Figure A.143: PP interval Bland-Altman plot for Lead V2.

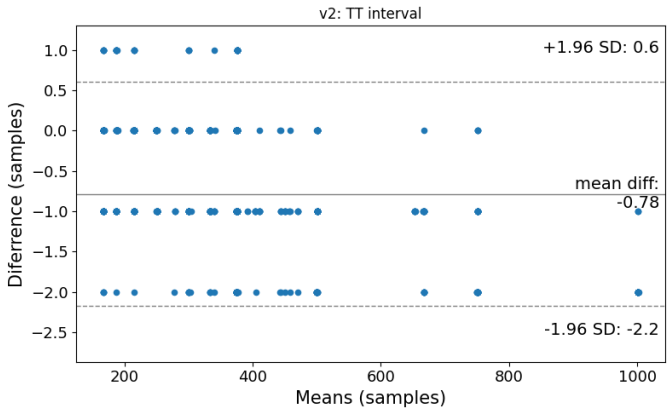

Figure A.144: TT interval Bland-Altman plot for Lead V2.

A.2.5 Lead V3

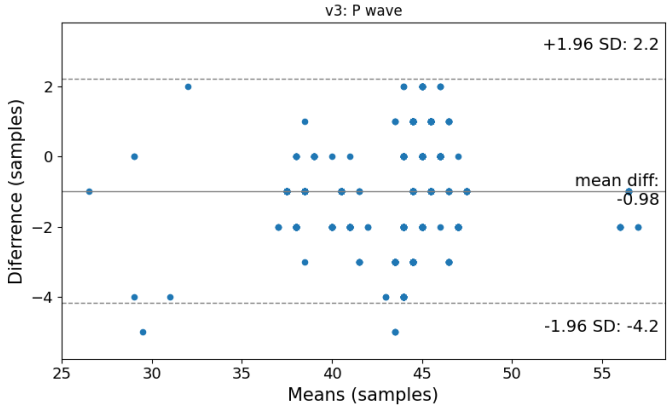

Figure A.145: P wave Bland-Altman plot for Lead V3.

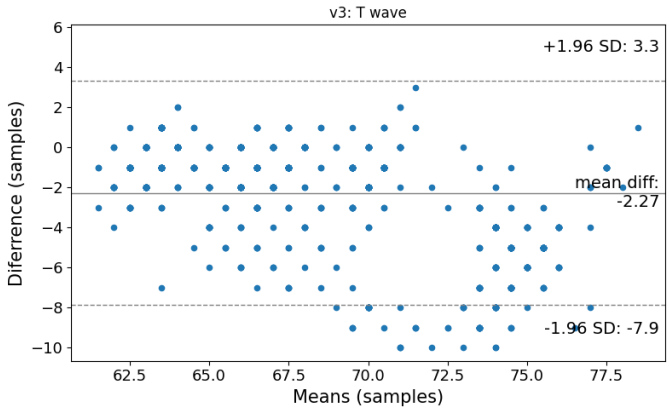

Figure A.146: T wave Bland-Altman plot for Lead V3.

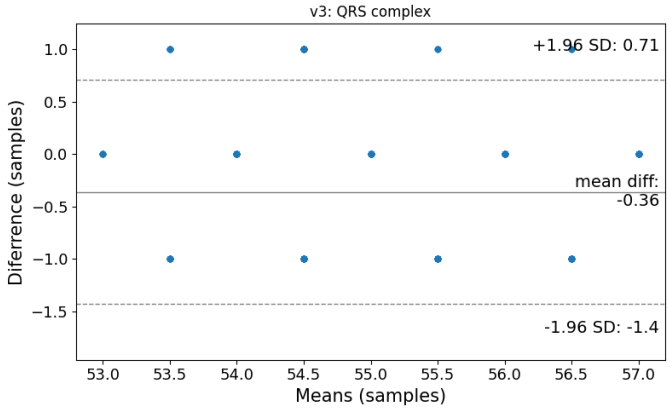

Figure A.147: QRS interval Bland-Altman plot for Lead V3.

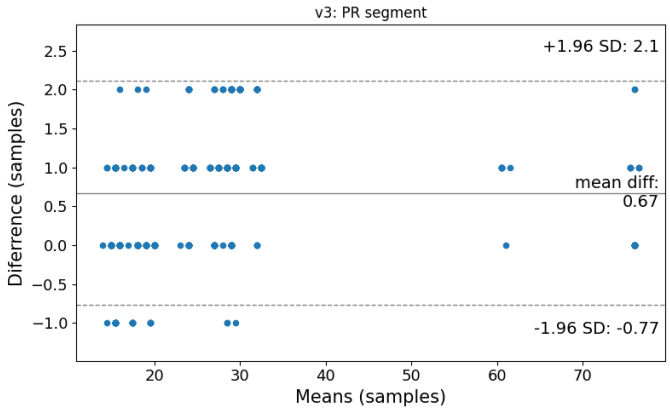

Figure A.148: PR segment Bland-Altman plot for Lead V3.

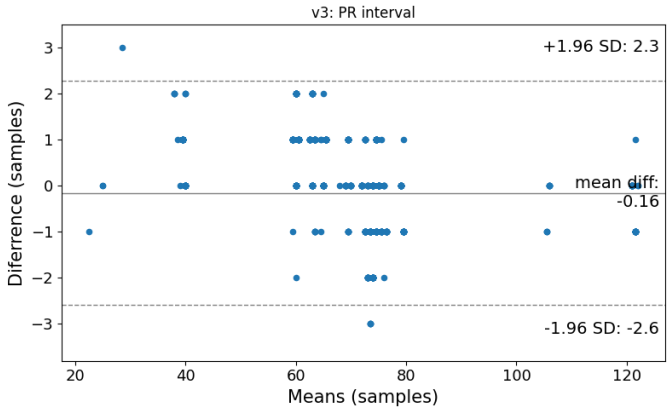

Figure A.149: PR interval Bland-Altman plot for Lead V3.

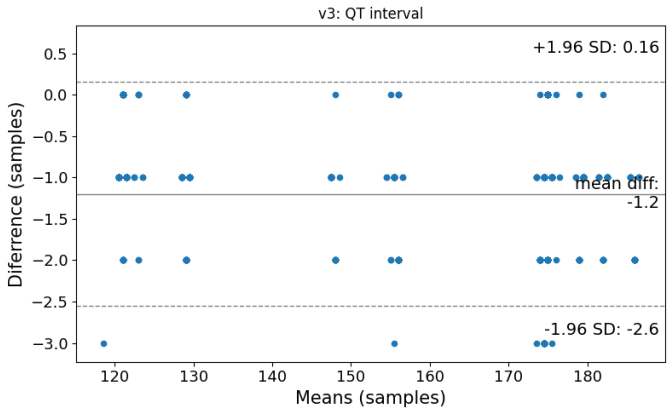

Figure A.150: QT interval Bland-Altman plot for Lead V3.

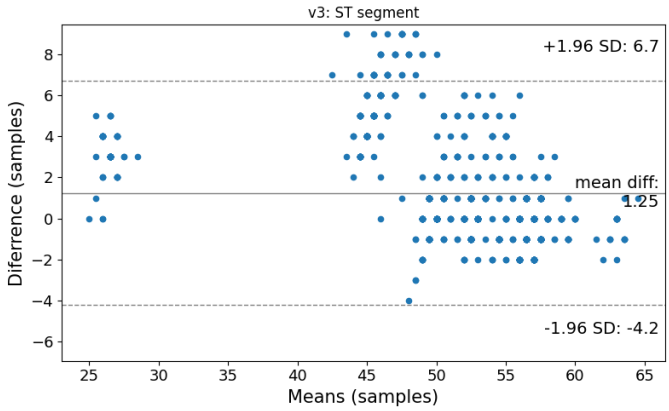

Figure A.151: ST segment Bland-Altman plot for Lead V3.

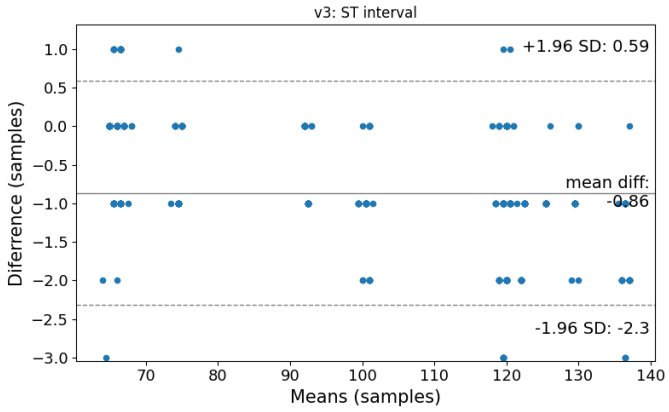

Figure A.152: ST interval Bland-Altman plot for Lead V3.

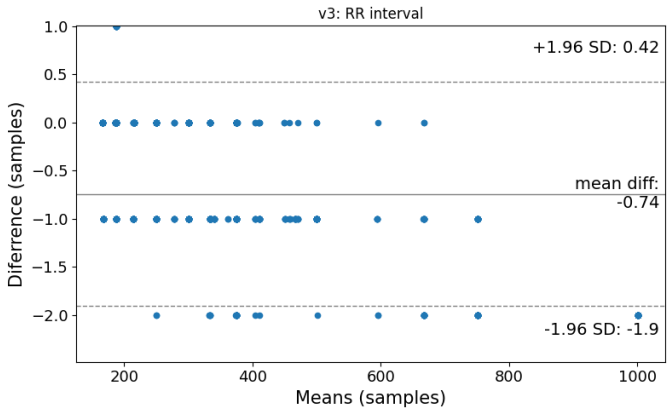

Figure A.153: RR interval Bland-Altman plot for Lead V3.

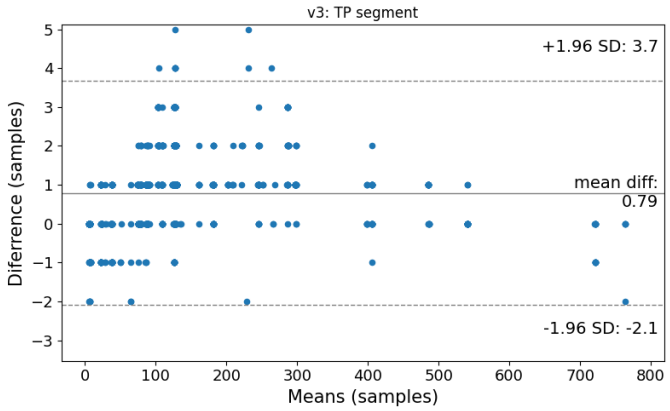

Figure A.154: TP segment Bland-Altman plot for Lead V3.

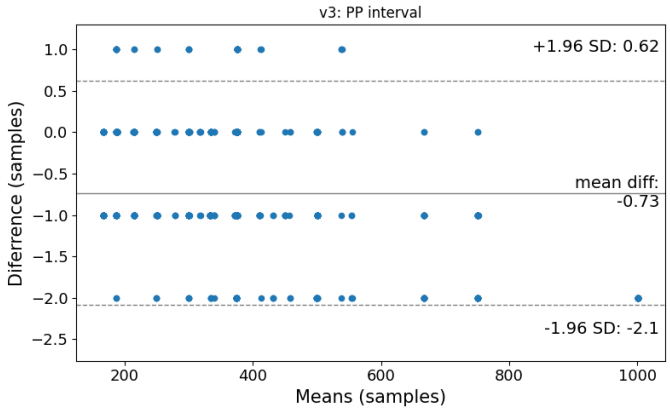

Figure A.155: PP interval Bland-Altman plot for Lead V3.

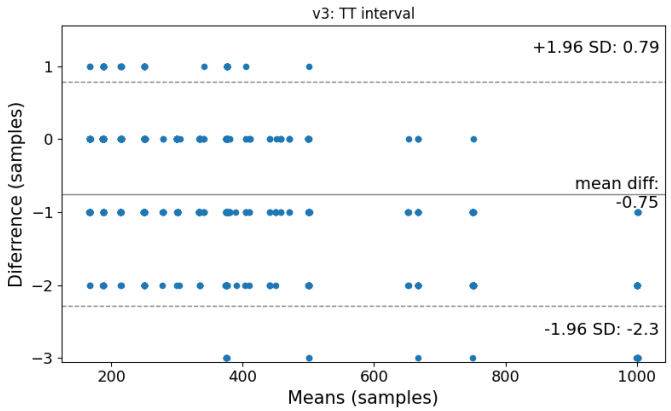

Figure A.156: TT interval Bland-Altman plot for Lead V3.

A.2.6 Lead V4

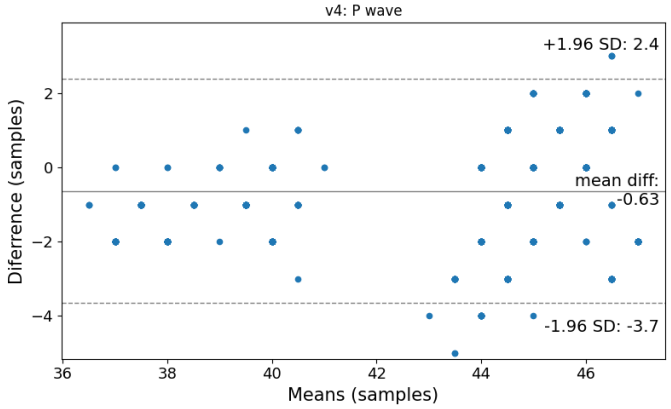

Figure A.157: P wave Bland-Altman plot for Lead V4.

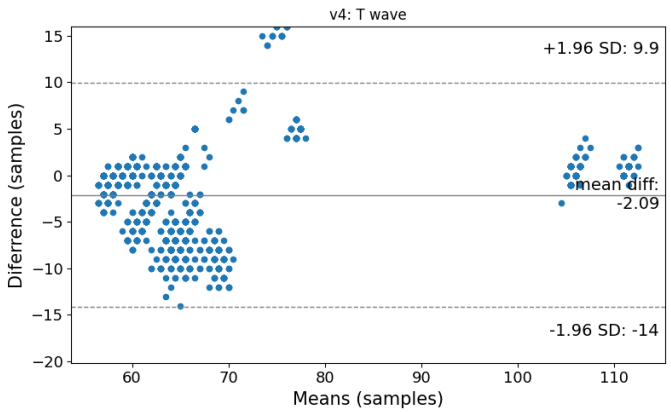

Figure A.158: T wave Bland-Altman plot for Lead V4.

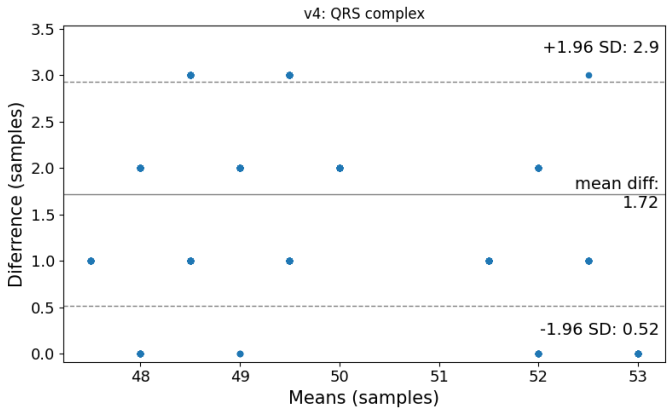

Figure A.159: QRS interval Bland-Altman plot for Lead V4.

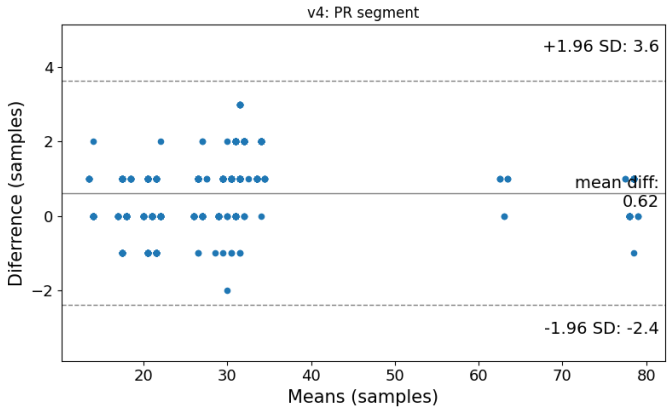

Figure A.160: PR segment Bland-Altman plot for Lead V4.

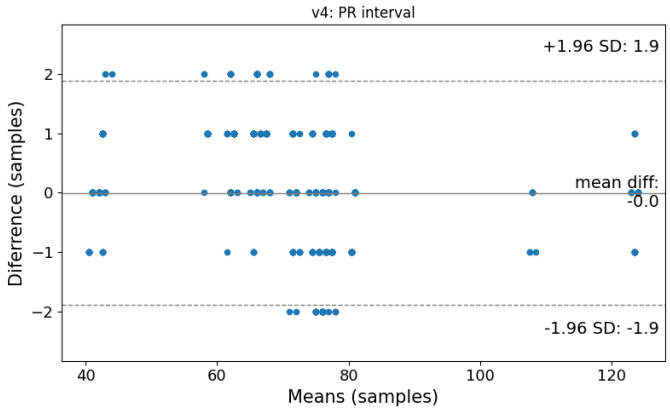

Figure A.161: PR interval Bland-Altman plot for Lead V4.

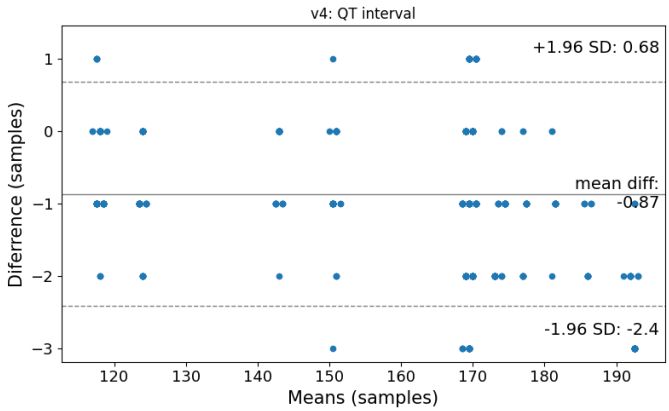

Figure A.162: QT interval Bland-Altman plot for Lead V4.

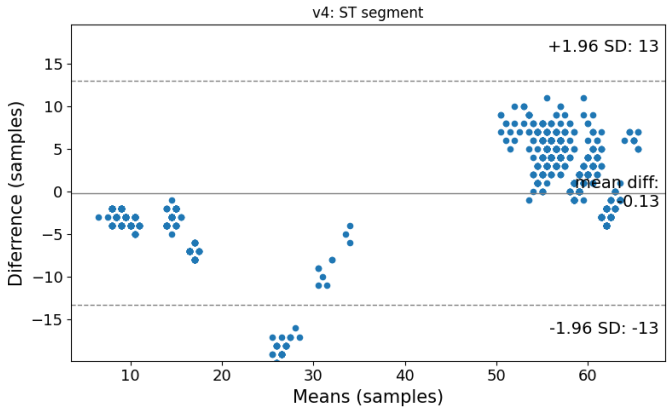

Figure A.163: ST segment Bland-Altman plot for Lead V4.

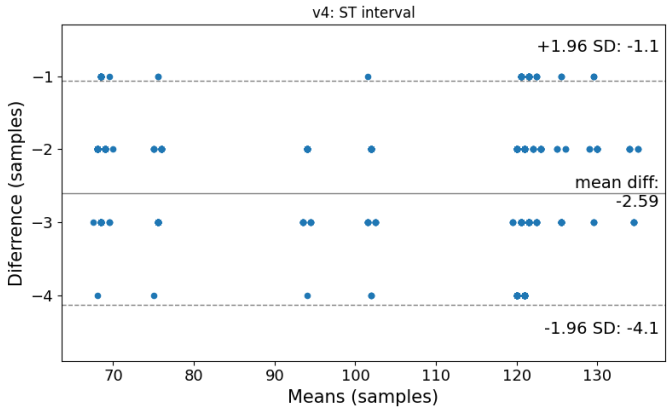

Figure A.164: ST interval Bland-Altman plot for Lead V4.

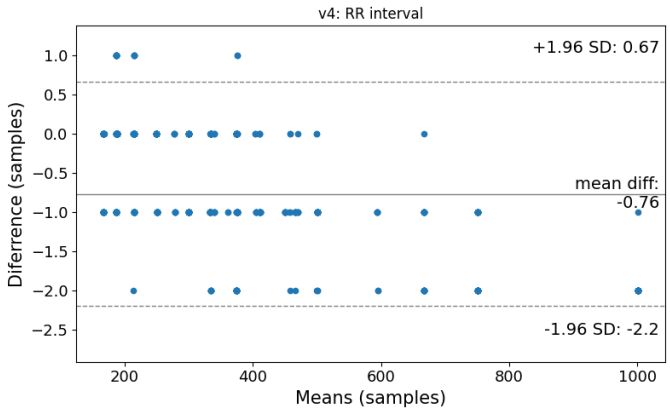

Figure A.165: RR interval Bland-Altman plot for Lead V4.

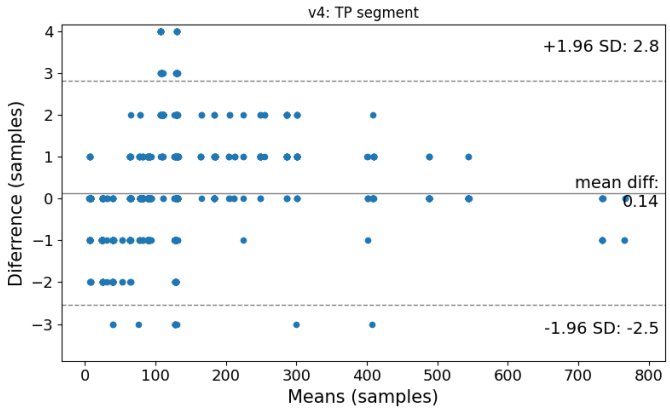

Figure A.166: TP segment Bland-Altman plot for Lead V4.

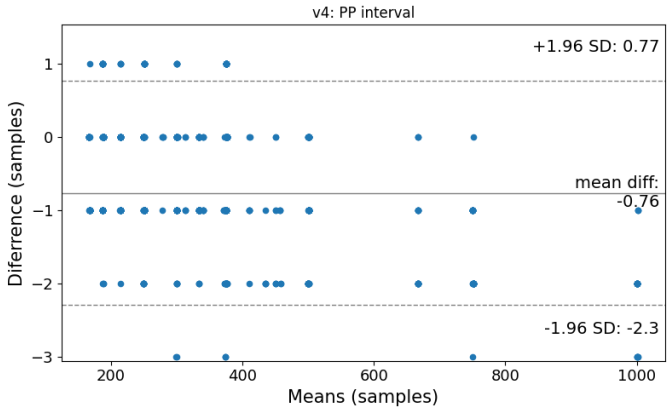

Figure A.167: PP interval Bland-Altman plot for Lead V4.

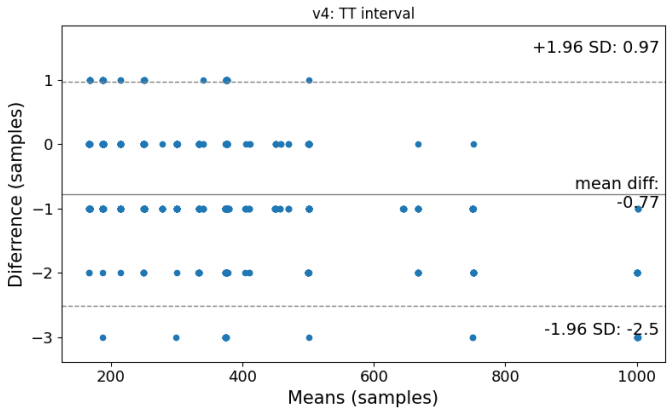

Figure A.168: TT interval Bland-Altman plot for Lead V4.

A.2.7 Lead V5

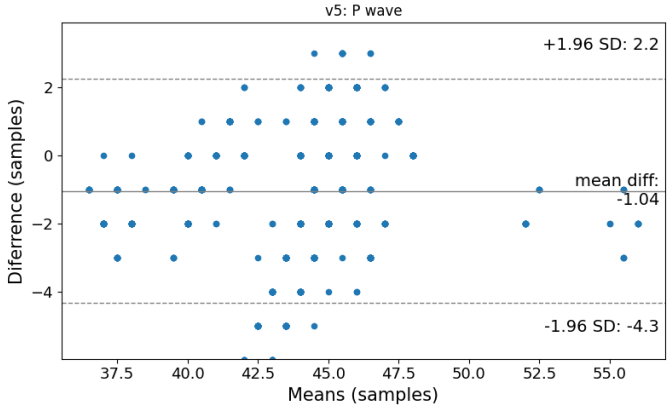

Figure A.169: P wave Bland-Altman plot for Lead V5.

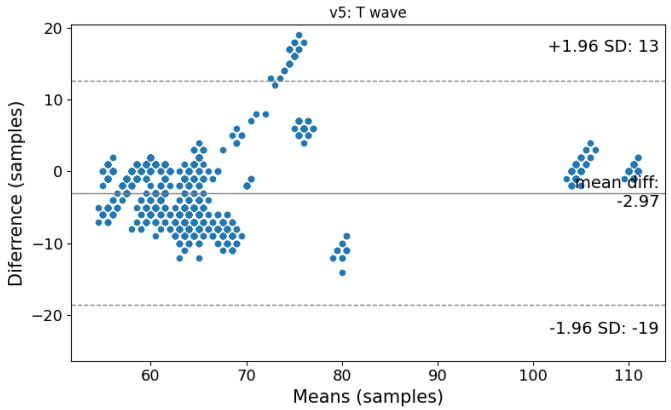

Figure A.170: T wave Bland-Altman plot for Lead V5.

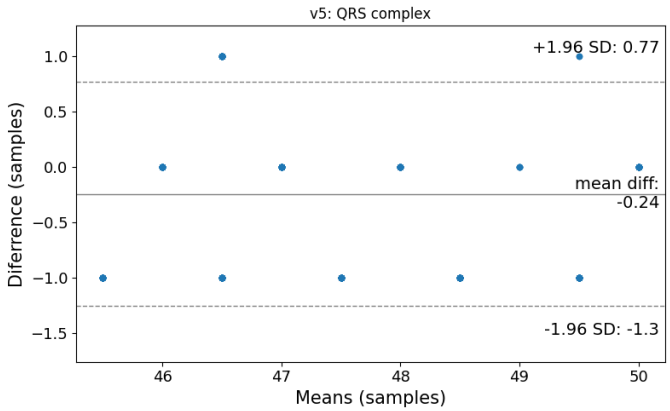

Figure A.171: QRS interval Bland-Altman plot for Lead V5.

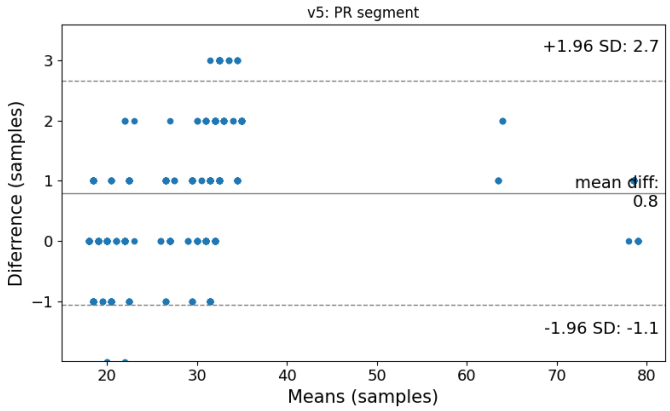

Figure A.172: PR segment Bland-Altman plot for Lead V5.

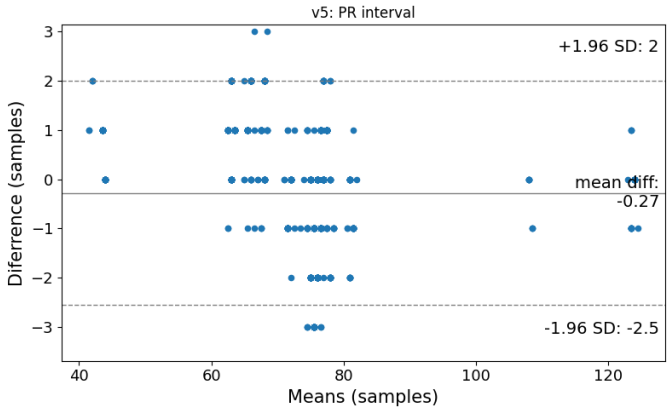

Figure A.173: PR interval Bland-Altman plot for Lead V5.

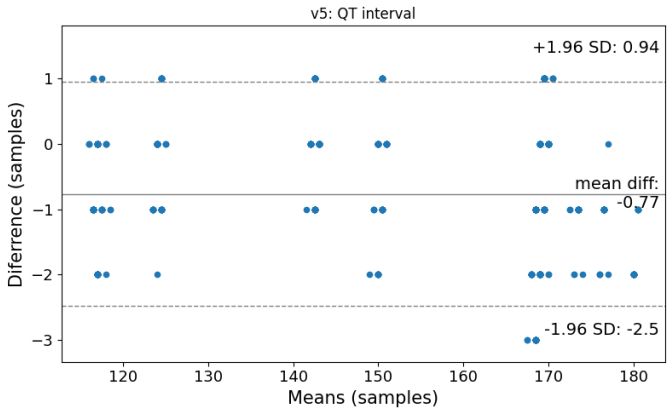

Figure A.174: QT interval Bland-Altman plot for Lead V5.

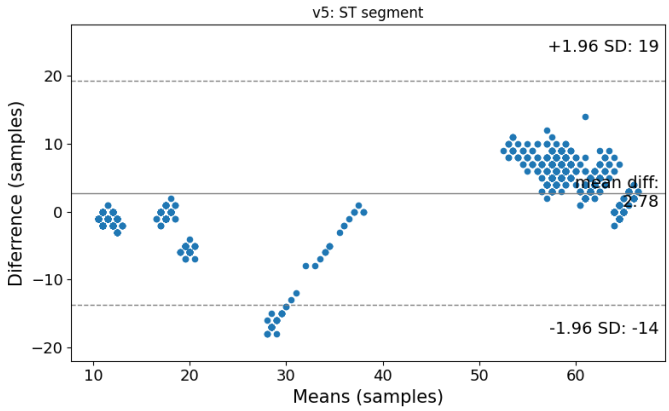

Figure A.175: ST segment Bland-Altman plot for Lead V5.

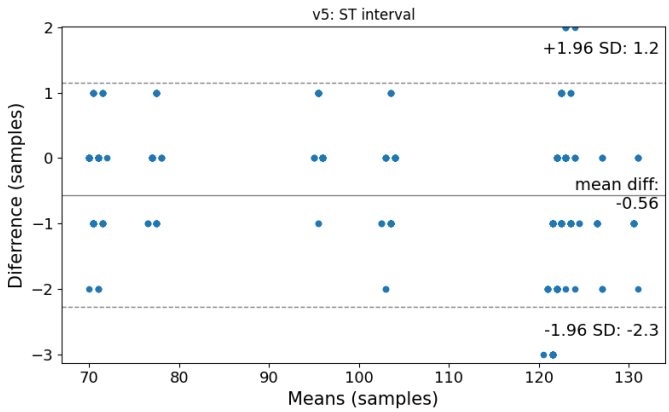

Figure A.176: ST interval Bland-Altman plot for Lead V5.

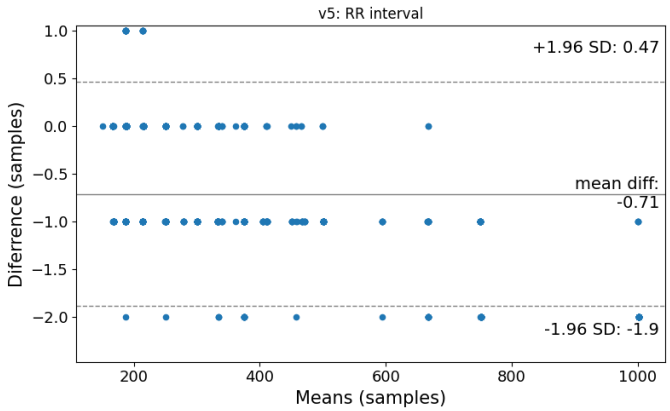

Figure A.177: RR interval Bland-Altman plot for Lead V5.

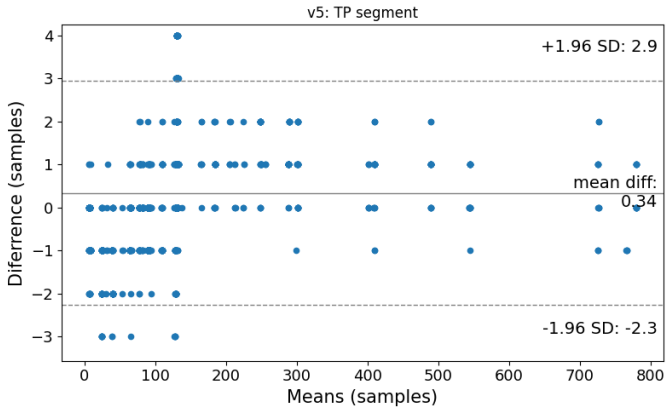

Figure A.178: TP segment Bland-Altman plot for Lead V5.

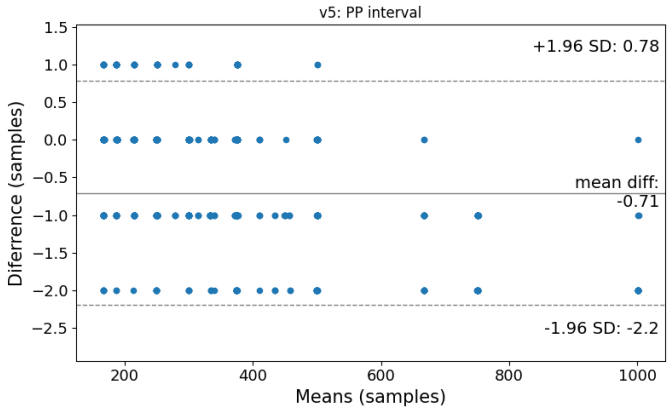

Figure A.179: PP interval Bland-Altman plot for Lead V5.

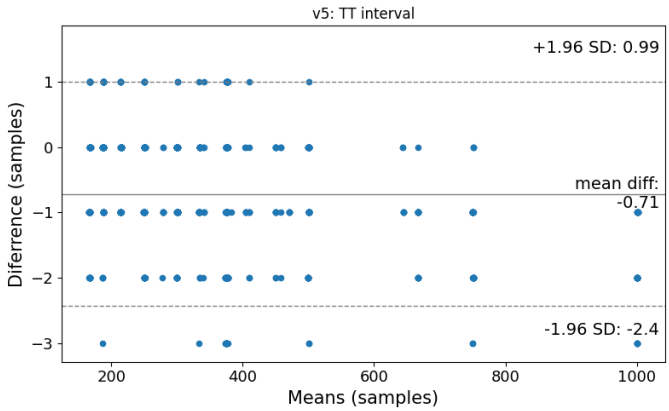

Figure A.180: TT interval Bland-Altman plot for Lead V5.

A.2.8 Lead V6

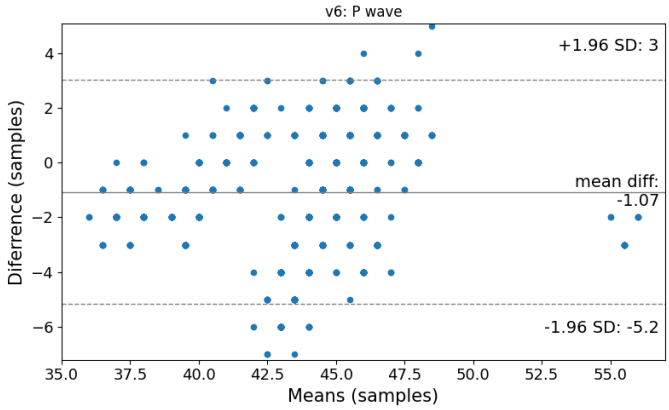

Figure A.181: P wave Bland-Altman plot for Lead V6.

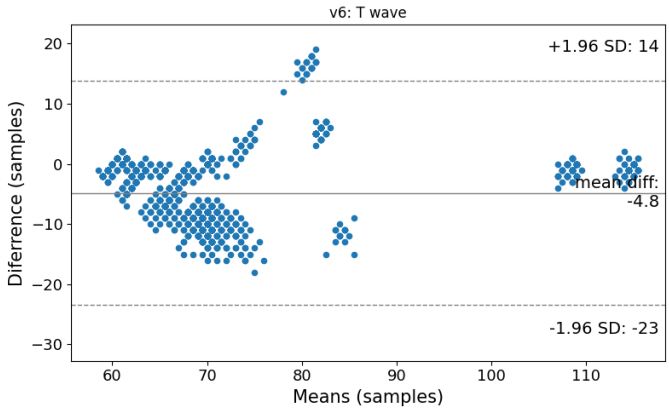

Figure A.182: T wave Bland-Altman plot for Lead V6.

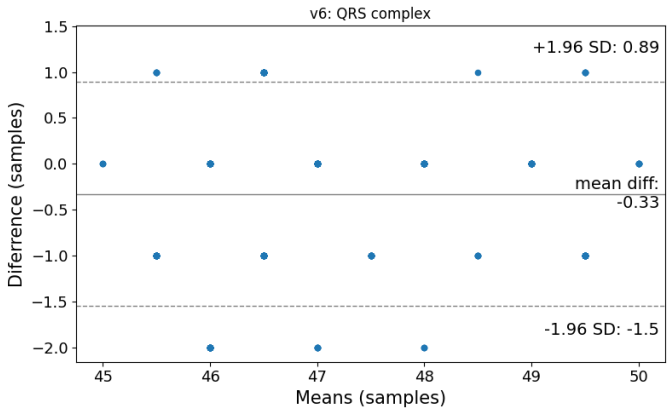

Figure A.183: QRS interval Bland-Altman plot for Lead V6.

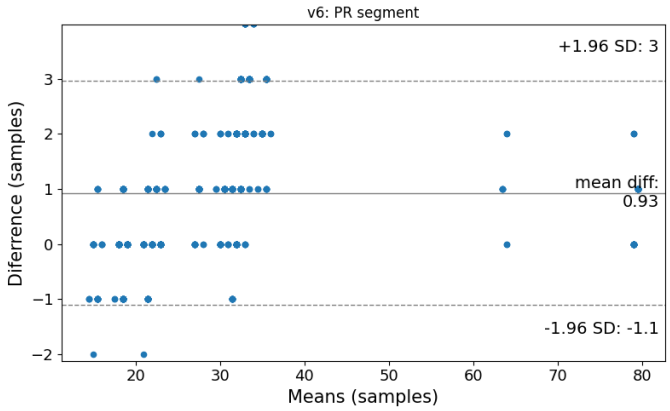

Figure A.184: PR segment Bland-Altman plot for Lead V6.

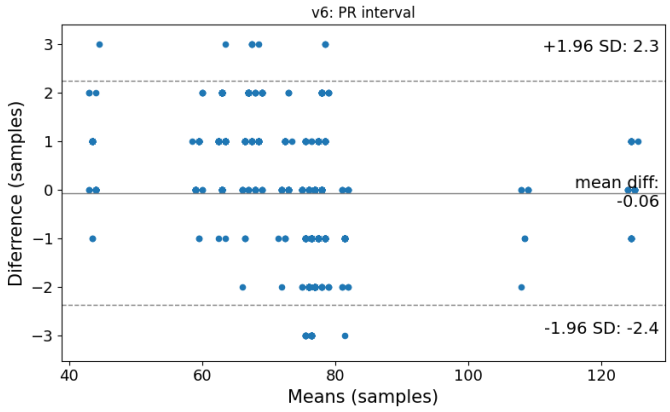

Figure A.185: PR interval Bland-Altman plot for Lead V6.

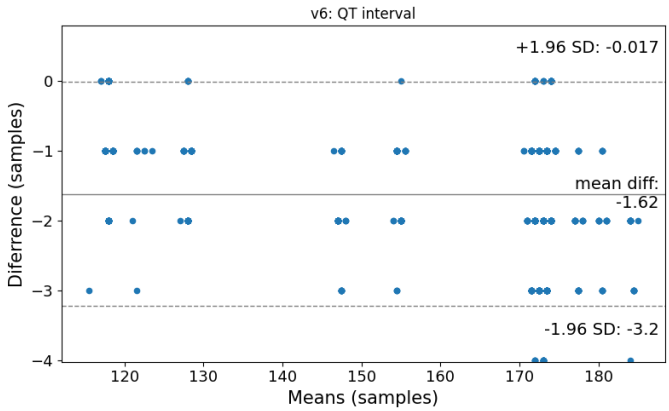

Figure A.186: QT interval Bland-Altman plot for Lead V6.

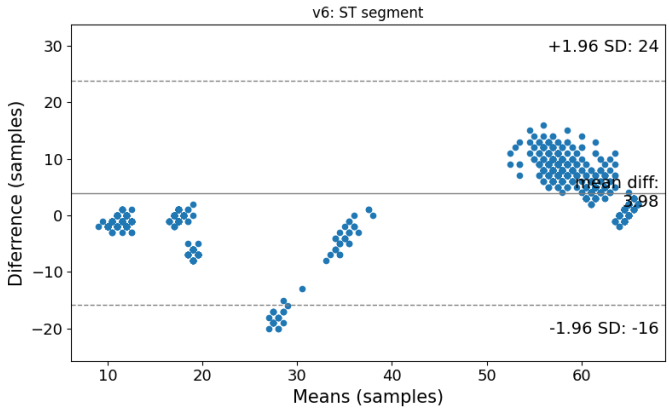

Figure A.187: ST segment Bland-Altman plot for Lead V6.

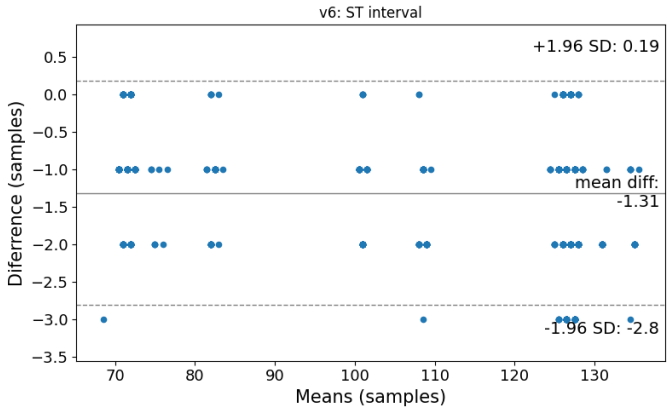

Figure A.188: ST interval Bland-Altman plot for Lead V6.

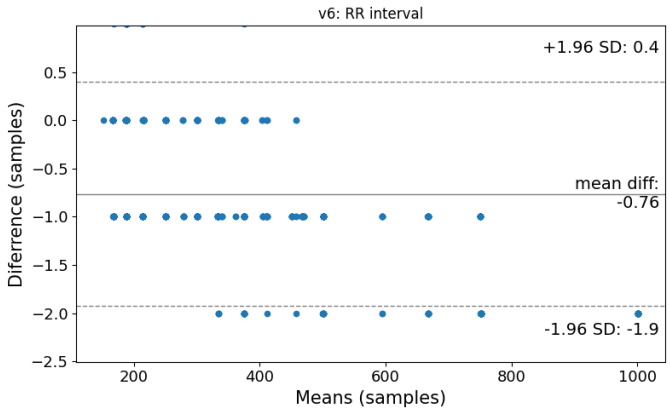

Figure A.189: RR interval Bland-Altman plot for Lead V6.

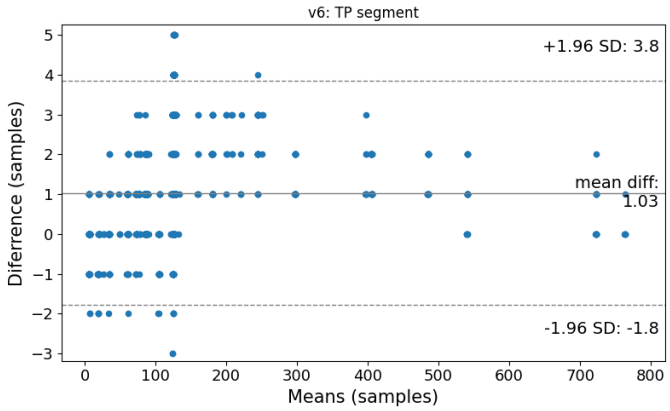

Figure A.190: TP segment Bland-Altman plot for Lead V6.

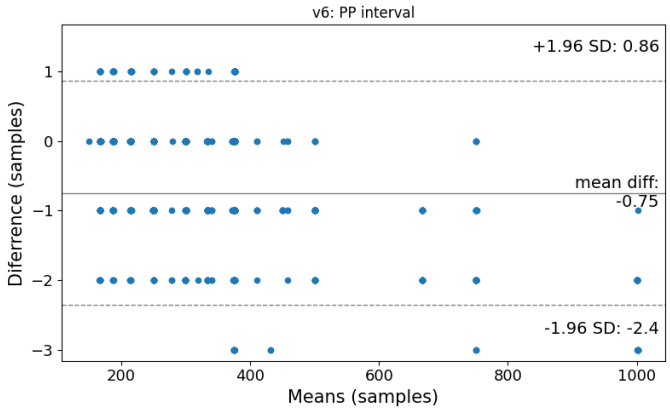

Figure A.191: PP interval Bland-Altman plot for Lead V6.

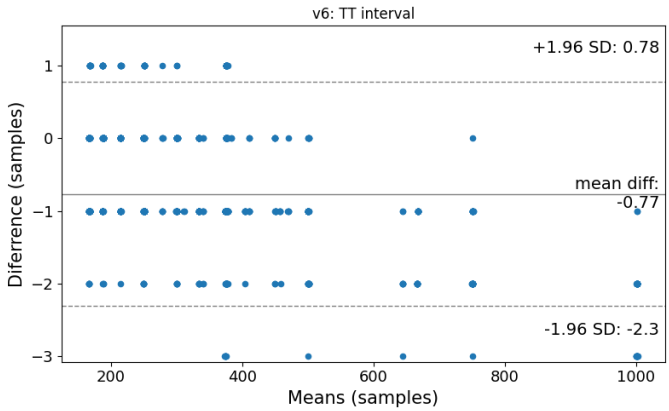

Figure A.192: TT interval Bland-Altman plot for Lead V6.

A.3 Simulator certificate

Certificado de calibración

Certificate of calibration

Número ESTEM-MAD-CI-23016459

Number

Página 1 de 5 páginas

Page __ of __ pages

TRESCAL ESPAÑA DE METROLOGÍA, S.L
Laboratorio de Madrid
Arrastaria, 21 - 28022 MADRID (Spain)

✉ laboratorio.madrid@trescal.com

www.trescal.com

Trescal

| LA METROLOGÍA QUE MEJORA SUS RESULTADOS |

OBJETO *Item*	CALIBRADOR / CALIBRATOR
FABRICANTE *Manufacturer*	GOSSEN METRAWTT
MARCA/MODELO *Trademark/ Type*	SECULIFE PS300
IDENTIFICACIÓN *Identification*	734729911376
SOLICITANTE *Applicant*	DYNASYS - ELECTRÓNICA E TELECOMUNICAÇÕES S.A. Centro Emp. Sado Int. Ed. 4E - Est Nac. 10 2910- 83 Vale Da Rosa-
FECHA/S DE CALIBRACIÓN *Date/s of Calibration*	10 de marzo de 2023

PERSONA QUE AUTORIZA / FECHA DE EMISIÓN

Person authorizing / Date of Issue

Calibración

Calibration

Previo a la calibración, el instrumento permaneció en condiciones ambientales de (23 +/- 2) ºC y humedad relativa <70% h.r. hasta alcanzar su estabilidad térmica. Estas condiciones se mantuvieron durante la calibración.

Prior to calibration, the instrument was maintained in stable environment conditions of (23 +/- 2) ºC and relative humidity below 70%hr up to its stability was reached. These conditions were maintained during the calibration.

Lugar de calibración: Instalaciones del laboratorio de calibración de TRESCAL Madrid.
Calibration site: TRESCAL Madrid calibration laboratory facilities.

Procedimientos de calibración: PC-LC-E/53.R6, E/64.R6
Calibration Procedures

Patrones empleados: E-100, E-86, E-94, E-382
Reference Standards

Dichos patrones tienen garantizada su trazabilidad a través de laboratorios reconocidos por EA e ILAC.
These reference standards have measuring traceability assured through laboratories acknowledged by EA and ILAC.

Incertidumbres

Uncertainties

La incertidumbre expandida declarada se ha obtenido multiplicando la incertidumbre típica de medida por un factor de cobertura k tal que la probabilidad de cobertura sea de aproximadamente el 95%. La incertidumbre típica de medida se ha determinado conforme al documento EA-4/02 M:2022

Los resultados mostrados se refieren al objeto referido en la primera página de este certificado y al momento y condiciones en que se realizaron las medidas, no considerándose su estabilidad a más largo plazo.

Declared expanded uncertainty has been obtained by multiplying the standard measurement uncertainty by a coverage factor k such that the coverage probability is approximately 95%. Uncertainty evaluation is according with EA-4/02 M:2022 document.
Results correspond to the calibration moment. Stability of the calibrated instrument on a longer term basis has not been considered. All the calibration results are only valid for the instrument whose data appear in the first page of this certificate.

Otros datos

Other data

El instrumento se ha calibrado alimentado medidante baterias

The instrument has been calibrated powered by batteries

Generador de tensión (Amplitud ECG) / *Voltage generator (ECG Amplitude)* (*)

Salida seleccionada *Selected output*	**Tensión esperada** *Expected voltage* (**Unid**/*Unit*)	**Unid** *Unit*	**Frec** *Freq* (**kHz**)	**Tensión medida** *Measured voltage* (**Unid**/*Unit*)	**Error** (**Unid**/*Unit*)	**Incert** *Uncert* (***k*=2**) (**Unid**/*Unit*)
LEAD II (LL-RA)	0,5	mV	DC	0,4970	0,0030	0,0028
	1,0	mV	DC	1,0010	-0,0010	0,0028
	1,5	mV	DC	1,5060	-0,0060	0,0028
	2,0	mV	DC	2,0080	-0,0080	0,0029
	3,0	mV	DC	3,0180	-0,0180	0,0029
	4,0	mV	DC	4,0260	-0,0260	0,0030
	5,0	mV	DC	5,0370	-0,0370	0,0030

(*) Forma de onda seleccionada cuadrada 4 s
(*) Selected waveform 4s square

Simulador de frecuencia (ECG) / *Frequency simulator (ECG)* (Lead II)

Indicación seleccionada *Selected indication*	**Valor esperado** *Expected value* (**Unid**/*Unit*)	**Unid** *Unit*	**Frecuencia medida** *Measured frequency* (**Hz**)	**Frecuencia medida** *Measured frequency* (**Unid**/*Unit*)	**Error** (**Unid**/*Unit*)	**Incert** *Uncert* (***k*=2**) (**Unid**/*Unit*)
Cuadrada 0,125 Hz	0,125	BPM (1)	0,124983	0,12498	0,00002	0,00002
Cuadrada 2 Hz	2	BPM	1,99982	1,9998	0,0002	0,0002
Triangular 2 Hz	2	BPM	1,9986	1,9986	0,0014	0,0002
Triangular 2,5 Hz	2,5	BPM	2,5005	2,5005	-0,0005	0,0002
Senoidal 10 Hz	10	BPM	10,0007	10,001	-0,001	0,002
Senoidal 50 Hz	50	BPM	50,0006	50,001	-0,001	0,002
Senoidal 100 Hz	100	BPM	99,997	100,00	0,00	0,02
PULSE 30	30	BPM (1)	0,50001	30,001	0,00	0,07
PULSE 60	60	BPM	1,00003	60,002	0,00	0,07
PULSE 120	120	BPM	2,00005	120,003	0,00	0,07

(1) Las medidas de BPM son medidas de frecuencia multiplicadas por 60 para expresarlas en eventos por minuto. (1 BPM = 1/60 Hz).
(1) BPM measures are frequency measures multiplied by 60 to express them in events per minute. (1 BPM = 1/60 Hz).

Simulador de frecuencia (Respiración) / *Frequency simulator (Respiration)* (Lead II)

Configuración *Settings*	**Indicación seleccionada** *selected indication* (**Unid**/*Unit*)	**Unid** *Unit*	**Frecuencia medida** *Measured frequency* (**Hz**)	**Frecuencia medida** *Measured frequency* (**Unid**/*Unit*)	**Error** (**Unid**/*Unit*)	**Incert** *Uncert* (***k*=2**) (**Unid**/*Unit*)
Baseline 500	15	BrPM (2)	0,25001	15,001	-0,001	0,070
Delta ohms 3	60	BrPM	1,0001	60,006	-0,006	0,070
	120		2,0010	120,060	-0,060	0,070
Control RESP. LEAD (LA-LL)				OK		

(2) Las medidas de BrPM son medidas de frecuencia multiplicadas por 60 para expresarlas en eventos por minuto.
(2) BrPM measures are measures of frequency multiplied by 60 to express them in events per minute.

.

Resistencia de la función Temperatura / *Temperature Function Resistance*

Temperatura seleccionada *Temperature setting* (**Unid**/*Unit*)	**Resistencia esperada** *Expected resistance* *(*)* (**Unid**/*Unit*)	**Unid** *Unit*	**Frec** *Freq* (**kHz**)	**Resistencia medida** *Measured resistance* (**Unid**/*Unit*)	**Error** (**Unid**/*Unit*)	**Incert** *Uncert* (***k*=2**) (**Unid**/*Unit*)
YSI 700 Ohm T1						
30ºC	4832	ohm		4834,9	-2,9	0,2
37ºC	3609	ohm		3608,3	0,7	0,2
40ºC	3196	ohm		3184,6	11,4	0,2
YSI 700 kOhm T2						
30ºC	24,30	kohm		24,275	0,025	0,002
37ºC	18,20	kohm		18,200	0,000	0,002
40ºC	16,16	kohm		16,153	0,007	0,002
Series 400 Ohm						
30ºC	1816	ohm		1813,2	2,8	0,2
37ºC	1355	ohm		1353,0	2,0	0,2
40ºC	1200	ohm		1199,0	1,0	0,2

(*) Según tabla de referencia de resistencia para YSI 400 e YSI 700
(*) According to resistance reference table for YSI 400 and YSI 700

Línea base de impedancia / *Impedance Baseline*

Bornas de medida *Measuring leads*	**Resistencia seleccionada** *Selected resistance* (**Unid**/*Unit*)	**Unid** *Unit*	**Frec** *Freq* (**kHz**)	**Resistencia medida** *Measured resistance* (**Unid**/*Unit*)	**Error** (**Unid**/*Unit*)	**Incert** *Uncert* (***k*=2**) (**Unid**/*Unit*)
LA-RA (Lead I)	500	ohm		488,1	11,9	0,2
	1000	ohm		985,7	14,3	0,2
	1500	ohm		1485,3	14,7	0,2
	2000	ohm		1982,5	17,5	0,2
LL-RA (Lead II)	500	ohm		488,3	11,7	0,2
	1000	ohm		985,6	14,4	0,2
	1500	ohm		1486,3	13,7	0,2
	2000	ohm		1985,5	14,5	0,2
LL-LA (Lead III)	500	ohm		488,7	11,3	0,2
	1000	ohm		987,8	12,2	0,2
	1500	ohm		1486,5	13,5	0,2
	2000	ohm		1985,4	14,6	0,2

Generador de tensión en C.C. (simulador de presión arterial estática) (mmHg)
D.C. voltage generator (static blood pressure simulation) (mmHg)

Canal / *Channel:* **CH1**

Sensibilidad *Sensibility*	**Valor seleccionado** *Selected value*	**Tensión esperada** *Expected voltage* *(*)* (**Unid**/*Unit*)	**Unid** *Unit*	**Tensión medida** *Measured voltage* (**Unid**/*Unit*)	**Error** (**Unid**/*Unit*)	**Incert** *Uncert* (***k*=2**) (**Unid**/*Unit*)
40 µV/V/mmHg	80 mmHg	32,0	mV	32,101	-0,101	0,005
	160 mmHg	64,0	mV	64,179	-0,179	0,008
	320 mmHg	128,0	mV	128,344	-0,344	0,005
5 µV/V/mmHg	80 mmHg	4,0	mV	4,026	-0,026	0,004
	160 mmHg	8,0	mV	8,045	-0,045	0,004
	320 mmHg	16,0	mV	16,084	-0,084	0,004

(*) Según relación: Tensión excitación (10 V) * Sensibilidad (µV/V/mmHg) * Valor seleccionado (mmHg)
*(*) According to relation: Excitation voltage (10 V) * Sensitivity (µV / V / mmHg) * Selected value (mmHg)*

Canal / *Channel:* **CH2**

Sensibilidad *Sensibility*	**Valor seleccionado** *Selected value*	**Tensión esperada** *Expected voltage* *(*)* (**Unid**/*Unit*)	**Unid** *Unit*	**Tensión medida** *Measured voltage* (**Unid**/*Unit*)	**Error** (**Unid**/*Unit*)	**Incert** *Uncert* (***k*=2**) (**Unid**/*Unit*)
40 µV/V/mmHg	50 mmHg	20,0	mV	20,139	-0,139	0,004
	100 mmHg	40,0	mV	40,178	-0,178	0,006
	240 mmHg	96,0	mV	96,413	-0,413	0,010
5 µV/V/mmHg	50 mmHg	2,5	mV	2,514	-0,014	0,003
	100 mmHg	5,0	mV	5,017	-0,017	0,004
	240 mmHg	12,0	mV	12,039	-0,039	0,003

(*) Según relación: Tensión excitación (10 V) * Sensibilidad (µV/V/mmHg) * Valor seleccionado (mmHg)
*(*) According to relation: Excitation voltage (10 V) * Sensitivity (µV / V / mmHg) * Selected value (mmHg)*

A.4 COMEN certificate

EU Quality Management System Certificate CN23/00001577

The management system of

Shenzhen Comen Medical Instruments Co., Ltd.

Floor 10, Floor 11 and Section C of Floor 12 of Building 1A & Floor 1 to Floor 5 of Building 2, FIYTA Timepiece Building, Nanhuan Avenue, Matian Sub-district, Guangming District, Shenzhen, Guangdong, 518106, P.R.China
SRN: CN-MF-000002236

has been assessed and certified as meeting the requirements of

MDR EU Quality Management System certificate (Annex IX QMS)

For the following products
The Scope of Registration appears on page 2 of this certificate

This certificate is valid from 31 March 2023 until 31 March 2028 and remains valid subject to satisfactory surveillance audits.
Re certification audit due before 31 September 2027
Issue 1. Certified since 31 March 2023
Certified activities performed by additional sites are listed on subsequent pages.

Authorised by
Geofrey De Visscher
Head of Notified Body 1639

SGS Belgium NV
SGS House Noorderlaan 87 2030 Antwerp Belgium
t +32 (0)3 545-48-48 - www.sgs.com

Shenzhen Comen Medical Instruments Co., Ltd.

MDR EU Quality Management System certificate (Annex IX QMS)

Active non-implantable device for monitoring of vital physiological parameters including (but not limited to) ECG, TEMP, SpO2, PR, NIBP, RESP and EtCO2, and associated incorporated software.

Class IIb - MDA0203, MDS1009, MDS1010 - EMDN: Z120302

Multi-parameter Patient Monitor:
- Models 1: C30, C30A (Basic UDI-DI: 69454290PM001PA)
- Models 2: C50, C500, C80, C800, C86, C860, Datalys 750, Datalys 780, OPUSi15 (Basic UDI-DI: 69454290PM002PC)
- Models 3: C70, C90, Datalys 770, Datalys 790, C70A, C90A (Basic UDI-DI: 69454290PM003PE)
- Models 4: K12Pro, K12APro, K15Pro, K15APro, K18Pro, K18APro, K22Pro, K22APro (Basic UDI-DI: 69454290PM007PN)
- Models 5: K1, K1A (Basic UDI-DI: 69454290PM008PQ)
- Models 6: NC8, NC8A, NC10, NC10A, NC12, NC12A, STAR8000A, STAR8000B, STAR8000C, OPUS i8, OPUS i10, OPUS i12, OPUSi10 Expert (Basic UDI-DI:69454290PM005PJ)
- Models 7: NC19, NC19A, STAR8000D (Basic UDI-DI: 69454290PM012PF)
- Models 8: STAR8000, STAR8000E, STAR8000F, STAR8000H, OPUS i12 pro (Basic UDI-DI: 69454290PM004PG)
- Models 9: C100A (Basic UDI-DI: 69454290PM006PL)".

Fetal & Maternal Monitor: STAR5000, STAR5000C, STAR5000D, STAR5000E, STAR5000A, STAR5000B, STAR5000F, STAR5000H (Basic UDI-DI:69454290FM001KU)

Specialized Fetal & Maternal Monitor: C10, C11 (Basic UDI-DI:69454290FM001KU)

Specialized Fetal & Maternal Monitor: C21, C21A, C22, C22A (Basic UDI-DI:69454290FM001KU)

Specialized Fetal & Maternal Monitor: C20, C26, C29 (Basic UDI-DI:69454290FM001KU)

Specialized Cardiovascular Monitor: C100, C100B (Basic UDI-DI:69454290PM010PB)

Central Monitoring System Software: STAR8800 (Basic UDI-DI:69454290MS001PK)

Vital Signs Monitor: NC3, NC3A, NC3B, OPUSi3, NC5, NC5A (Basic UDI-DI:69454290SM001QB)

Specialized Neonatal Monitor: C60, C66, C68, Datalys 760 (Basic UDI-DI:69454290PM009PS)

Conditions for & limitation to the validity of the certificate:
For placing on the market of Class III or class IIb implantable devices (except sutures, staples, dental fillings, dental braces, tooth crowns, screws, wedges, plates, wires, pins, clips and connectors and Annex VIII rule 12 devices) covered by this certificate, a Technical Documentation Assessment Certificate according to Annex IX section 4 and 5 is required.

For Class I devices, audit done by SGS Belgium N.V. is limited to the specific aspect described in Article 52 section 7 of MDR (EU) 2017/745 (sterility, reusability or measurement function).

Limitation: N/A
Certification is based on following reports: CN/SZX/50010 S2A 1.3

List of examinations and tests performed, which may include reference to relevant CS and harmonised standards, as per Annex XII, Chapter II, section 10 is available "on request" per email to NB1639@sgs.com

Authorized representative Name and address (if relevant): Lotus NL B.V., Koningin Julianaplein 10, 1 e Verd, 2595AA, The Hague, Netherlands
Previous certificate number: N/A
Changes between this certificate and previous one: N/A

EU Quality Management System Certificate CN23/00001577, continued

Shenzhen Comen Medical Instruments Co., Ltd.

MDR EU Quality Management System certificate (Annex IX QMS)

Issue 1
Sites
Shenzhen Comen Medical Instruments Co., Ltd. Floor 10, Floor 11 and Section C of Floor 12 of Building 1A & Floor 1 to Floor 5 of Building 2, FIYTA Timepiece Building, Nanhuan Avenue, Matian Sub-district, Guangming District, Shenzhen, Guangdong, 518106, P.R.China
Shenzhen Comen Medical Instruments Co., Ltd. Floor 7 of EBOHR Building A & Floor 5 of EBOHR Building B, Timepieces Base, Guangming District, Shenzhen, Guangdong Province, P. R. China
Shenzhen Comen Medical Instruments Co., Ltd. Floor 2 of Building 108B, 7th Industrial Zone, Mashantou, Matian Street, Guangming District, Shenzhen, Guangdong, P. R. China
Shenzhen Comen Medical Instruments Co., Ltd. Unit 501, West Side of the Fifth Floor of the Machinery Factory (No. 2 Area of Chuangxiang), Yanxiang Technology Industrial Park, No.11 of Gaoxin West Road, Guangming Street, Shenzhen, Guangdong, P. R. China
Shenzhen Comen Medical Instruments Co., Ltd. Floor 3, 4 and 8 of Ruihui Building, Intersection of Fuli South Road and Fangyuan Road, Matian Street, Guangming District, Shenzhen, Guangdong, P.R. China